

# **NOVEL TECHNOLOGIES FOR GASEOUS CONTAMINANTS CONTROL**

## **FINAL REPORT FOR THE BASE PROGRAM**

DOE Contract No. DE-AC26-99FT40675

Period of Performance: October 1, 1999, to September 30, 2001

For

U.S. Department of Energy  
National Energy Technology Laboratory  
3610 Collins Ferry Road  
Morgantown, WV 26505

by

B.S. Turk  
T. Merkel  
A. Lopez-Ortiz  
R.P. Gupta  
J.W. Portzer  
G.N. Krishnan (SRI)  
B.D. Freeman (NCSU)  
G.K. Fleming (MEDAL)

Research Triangle Institute  
Research Triangle Park, NC 27709

September 2001

## DISCLAIMER

This report was prepared as an account of work sponsored by an agency of the United States Government. Neither the United States Government nor any agency thereof, nor any of their employees, makes any warranty, express or implied, or assumes any legal liability or responsibility for the accuracy, completeness, or usefulness of any information, apparatus, product, or process disclosed, or represents that its use would not infringe privately owned rights. Reference herein to any specific commercial product, process, or service by trade name, trademark, manufacturer, or otherwise does not necessarily constitute or imply its endorsement, recommendation, or favoring by the United States Government or any agency thereof. The views and opinions of authors expressed herein do not necessarily state or reflect those of the United States Government or any agency thereof.

## **ACKNOWLEDGMENTS**

This work was sponsored by the National Energy Technology Laboratory (NETL) of the U.S. Department of Energy (DOE), under contract No. DE-AC21-99FT40675. Valuable guidance provided by Daniel C. Cicero and Suresh C. Jain as contracting officer's representatives (CORs) is gratefully acknowledged. Ernest Johnson conducted characterization and bench-scale testing of polymer and monolith samples. Analytical support for this testing was provided by Gary Howe. Monolith samples were prepared by Robert Peterson of Sud-Chemie Prototech. Dr. William J. McMichael assisted in preparing the package for economic assessment and in assembling this report. The economic assessment provided in Chapter 5 was conducted by Sam Tam and Shelly Stanton of Nexant, Inc. Editorial assistance provided by Ms. Kathleen Mohar and Mr. David Belton. Ms. Sharon Davis, Ms. Yvonne Harrison and Ms. Debbie Bond are also acknowledged.

## ABSTRACT

The overall objective of this project is to develop technologies for cleaning/conditioning the syngas from an integrated gasification combined cycle (IGCC) system to meet the tolerance limits for contaminants such as  $\text{H}_2\text{S}$ ,  $\text{COS}$ ,  $\text{NH}_3$ ,  $\text{HCN}$ ,  $\text{HCl}$ , and alkali for fuel cell and chemical production applications. RTI's approach is to develop a modular system that (1) removes reduced sulfur species to sub-ppm levels using a hybrid process consisting of a polymer membrane and a regenerable  $\text{ZnO}$ -coated monolith or a mixed metal oxide sorbent; (2) removes hydrogen chloride vapors to sub-ppm levels using an inexpensive, high-surface area material; and (3) removes  $\text{NH}_3$  with acidic adsorbents.

RTI is working with MEDAL, Inc., and North Carolina State University (NCSU) to develop polymer membrane technology for bulk removal of  $\text{H}_2\text{S}$  from syngas. These membranes are being engineered to remove the acid gas components ( $\text{H}_2\text{S}$ ,  $\text{CO}_2$ ,  $\text{NH}_3$ , and  $\text{H}_2\text{O}$ ) from syngas by focusing on the "solubility selectivity" of the novel polymer compositions. The desirable components of the syngas ( $\text{H}_2$  and  $\text{CO}$ ) are maintained at high-pressure conditions as a non-permeate stream while the impurities are transported across the membrane to the low pressure side. RTI tested commercially available and novel materials from MEDAL using a high-temperature, high-pressure (HTHP) permeation apparatus.  $\text{H}_2\text{S}/\text{H}_2$  selectivities  $>30$  were achieved, although there was a strong negative dependence with temperature. MEDAL believes that all the polymer compositions tested so far can be prepared as hollow fiber membrane modules using the existing manufacturing technology.

For fuel cell and chemical applications, additional sulfur removal (beyond that achievable with the membranes) is required. To overcome limitations of conventional  $\text{ZnO}$  pellets, RTI is testing a monolith with a thin coating of high surface area zinc-oxide based materials. Alternatively, a regenerable sorbent developed by DOE/NETL (RVS-1) is being evaluated for this application. A multi-cycle test of 2-in. (5-cm) diameter monolith samples demonstrated that  $<0.5$  ppm sulfur can be achieved.

Removal of  $\text{HCl}$  vapors is being accomplished by low-cost materials that combine the known effectiveness of sodium carbonate as an active matrix used with enhanced surface area supports for greater reactivity and capacity at the required operating temperatures. RTI is working with SRI International on this task. Sorbents prepared using diatomaceous earth and sepiolite, impregnated with sodium carbonate achieved steady-state  $\text{HCl}$  level  $<100$  ppb (target is 10 ppb). Research is continuing to optimize the impregnation and calcination procedures to provide an optimum pore size distribution and other properties.

RTI and SRI International have established the feasibility of a process to selectively chemisorb  $\text{NH}_3$  from syngas on high surface area molecular sieve adsorbents at high temperatures by conducting a series of temperature-programmed reactions at  $225^\circ\text{C}$  ( $437^\circ\text{F}$ ). Significant levels of  $\text{NH}_3$  were adsorbed on highly acidic adsorbents; the adsorbed  $\text{NH}_3$  was subsequently recovered by heating the adsorbent and the regenerated adsorbent was reused.

A comprehensive technical and economic evaluation of this modular gas cleaning process was conducted by Nexant to compare capital and operating cost with existing amine based processes. Nexant estimated a total installed cost of \$42 million for the RTI process for a 500 MWe IGCC plant based on its current state of development. By comparison, Nexant estimated the installed cost for an equivalent sized plant based on the Rectisol process (which would achieve the same sulfur removal specification) to be \$75 million. Thus the RTI process is economically competitive with a state-of-the-art process for syngas cleanup.

## TABLE OF CONTENTS

Chapter		Page
1	INTRODUCTION .....	1-1
	1.1 BACKGROUND .....	1-1
	1.2 PROCESS CONCEPT .....	1-3
2	BULK SULFUR REMOVAL .....	2-1
	2.1 CURRENT STATE-OF-THE-ART .....	2-1
	2.1.1 High-Temperature Sulfur Removal Using Sorbent Technology .....	2-1
	2.1.2 Conventional Sulfur Removal .....	2-2
	2.2 HYBRID SULFUR REMOVAL PROCESS .....	2-3
	2.2.1 Polymer Membrane System .....	2-5
	2.3 FUNDAMENTALS OF MEMBRANE SEPARATIONS .....	2-8
	2.3.1 Solubility Selective Materials .....	2-10
	2.3.2 Facilitated Transport/Solid Polymer Electrolytes .....	2-13
	2.4 POLYMER SYNTHESIS, FILM PREPARATION, AND CHARACTERIZATION .....	2-13
	2.4.1 North Carolina State University .....	2-13
	2.4.2 Characterization of PEO and PEO/salt blends .....	2-18
	2.4.3 MEDAL Samples .....	2-20
	2.5 HIGH-TEMPERATURE/HIGH-PRESSURE (HTHP) MEMBRANE TESTING .....	2-21
	2.5.1 RTI's Membrane Test Facility .....	2-21
	2.5.2 Characterization of a Baseline Solubility Selective Polymer: Poly(dimethylsiloxane) .....	2-22
	2.5.3 Characterization of MEDAL Polymer Samples .....	2-25
	2.5.4 Characterization of NCSU Polymer Samples .....	2-27
	2.6 MEMBRANE MODULE SIMULATIONS .....	2-29
	2.7 SUMMARY AND FUTURE WORK .....	2-30
3	SULFUR POLISHING THROUGH MONOLITH TECHNOLOGY .....	3-1
	3.1 USE OF MONOLITHS IN HYBRID SULFUR REMOVAL PROCESS (POLISHING) .....	3-2
	3.2 SAMPLE PREPARATION .....	3-4
	3.3 THERMOGRAVIMETRIC TESTING .....	3-4
	3.3.1 Washcoat Screening Tests .....	3-4
	3.3.2 Temperature Screening Tests .....	3-9
	3.3.3 Summary of Thermogravimetric Testing .....	3-11
	3.4 BENCH-SCALE TESTING .....	3-11
	3.4.1 Monolith Preparation .....	3-11
	3.4.2 Multicycle Performance Tests .....	3-12
	3.4.3 Parametric Testing .....	3-16
	3.5 CONCLUSIONS .....	3-21

## TABLE OF CONTENTS (continued)

Chapter		Page
4	CHLORINE AND NITROGEN COMPOUND REMOVAL .....	4-1
4.1	INTRODUCTION .....	4-1
4.1.1	Chlorine and Nitrogen Compounds in Syngas Streams .....	4-1
4.1.2	Need for Removal of HCl and NH <sub>3</sub> .....	4-2
4.1.3	Previous Studies .....	4-2
4.1.4	Project .....	4-3
4.2	REMOVAL OF HYDROGEN CHLORIDE VAPOR .....	4-3
4.2.1	Theoretical Considerations .....	4-3
4.2.2	Sorbent Requirements .....	4-4
4.2.3	Detection of Trace Levels of HCl Vapor .....	4-5
4.2.4	Experimental Determination of Sorbent Reactivities for HCl Vapor ..	4-6
4.2.5	Preliminary Economic Analysis .....	4-7
4.2.6	Bulk HCl Removal Cost .....	4-8
4.2.7	Trace HCl Removal Cost .....	4-9
4.3	REMOVAL OF AMMONIA VAPOR .....	4-12
4.3.1	Theoretical Considerations .....	4-12
4.3.2	Sorbents for Ammonia Removal .....	4-13
4.3.3	Process Considerations .....	4-16
4.3.4	Preliminary Economic Analysis .....	4-17
4.4	SUMMARY AND FUTURE WORK .....	4-19
5	TECHNICAL AND ECONOMIC EVALUATION .....	5-1
5.1	NEXANT'S TECHNICAL AND ECONOMIC EVALUATION OF THE RTI PROCESS .....	5-2
5.1.1	Introduction .....	5-2
5.1.2	Conclusions and Recommendations .....	5-6
5.1.3	Conventional Acid Gas Removal Options .....	5-6
5.1.4	RTI Process Objective .....	5-7
5.1.5	RTI Process Description .....	5-7
5.1.6	Methodology for Estimating Total Installed Price for RTI Process ..	5-10
5.2	CONCLUSIONS .....	5-17
6	SUMMARY, CONCLUSIONS, AND FUTURE WORK .....	6-1
6.1	BULK SULFUR REMOVAL .....	6-1
6.2	POLISHING SULFUR REMOVAL .....	6-3
6.3	HCl and NH <sub>3</sub> REMOVAL .....	6-4
6.4	TECHNICAL/ECONOMIC EVALUATION .....	6-6
6.5	OPTION PROGRAM .....	6-6
6.5.1	Bench-Scale Testing .....	6-7
6.5.2	Market Assessment and Commercial Applicability .....	6-9
7	BIBLIOGRAPHY .....	7-1
	LIST OF ACRONYMS	

## LIST OF FIGURES

Number		Page
1-1.	Modular process approach for the RTI gas cleaning process .....	1-3
2-1.	Conventional Selexol process for removal of H <sub>2</sub> S from syngas .....	2-3
2-2.	Hybrid process for syngas desulfurization .....	2-4
2-3.	Separation of acid gases from syngas in polymer membrane module .....	2-5
2-4.	GA results demonstrating thermal stability of MDA-1/PEG2000 block copolymer in simulated Texaco gas at 250°C (482°F) .....	2-8
2-5.	Effect of penetrant size on diffusion coefficients in a rubber [•, cis-plyisopene, T=50°C] (VanAmerongen, 1964) and a glassy polymer [□, poly (vinyl chloride), T=30°C] (Berens and Hopfenberg, 1982) .....	2-9
2-6.	Diffusion coefficients in rubbery poly(dimethylsiloxane) (PDMS) and glassy polysulfone (PSF) at 35°C as a function of penetrant critical volume .....	2-11
2-7.	Penetrant solubility in polysulfone and poly(dimethylsiloxane) at 35°C (95°F) and infinite dilution .....	2-12
2-8.	Effect of upstream pressure on PEO permeability coefficients at 35°C (95°F) ..	2-18
2-9.	Effect of upstream pressure on PEO permeability coefficients at 35°C (95°F) ..	2-18
2-10.	Sorption isotherms in PEO at 35°C (95°F) .....	2-19
2-11.	Monomers employed in MEDAL-supplied materials .....	2-20
2-12.	Schematic diagram of membrane apparatus .....	2-21
2-13.	Pure gas CO <sub>2</sub> permeability coefficients in PDMS as measured by direct flux (no sweep) and via gas chromatograph analysis of permeate composition (He sweep) .....	2-22
2-14.	Mixed-gas O <sub>2</sub> /N <sub>2</sub> selectivity of PDMS as a function of transmembrane pressure difference .....	2-22
2-15.	Syngas permeability coefficients in PDMS as a function of gas-critical temperature. Experimental conditions: upstream pressure = 20 psig, room temperature .....	2-23
2-16.	Permeability coefficients in PDMS as a function of system temperature .....	2-24
2-17.	Activation energies of permeation in PDMS as a function of gas-critical temperature .....	2-25
2-18.	Mixed-gas H <sub>2</sub> S/H <sub>2</sub> and CO <sub>2</sub> /H <sub>2</sub> selectivity of PDMS as a function of system temperature .....	2-25
2-19.	Mixed-gas H <sub>2</sub> S/H <sub>2</sub> selectivity as a function of system temperature .....	2-27
2-20.	Permeability coefficients in PDMS and AF1600 as a function of gas-critical temperature .....	2-28
2-21.	NCSU simulator's calculated H <sub>2</sub> loss as a function of CO <sub>2</sub> removal .....	2-29
2-22.	NCSU simulator's calculated H <sub>2</sub> loss and H <sub>2</sub> S remaining in the residue as a function of CO <sub>2</sub> removal .....	2-30

## LIST OF FIGURES (continued)

Number		Page
3-1.	Equilibrium H <sub>2</sub> S concentration in syngas as a function of temperature and H <sub>2</sub> O content . . . . .	3-2
3-2.	Breakthrough profiles for selected cycles of a Zn-Ti coated cordierite monolith . . . . .	3-3
3-3.	Sulfur capacity of Zn-Ti coated monolith at breakthrough . . . . .	3-3
3-4.	1.5-cycle TGA tests of monolith samples for washcoat screening tests . . . . .	3-6
3-5.	Comparison of weight profiles for 1.5 cycle TGA test for monoliths with TiO <sub>2</sub> washcoat and high and low ZnO loading . . . . .	3-8
3-6.	TGA tests with ZnO-TiO <sub>2</sub> -washcoated monolith as a function of temperature . . .	3-9
3-7.	4.5-Cycle TGA test of zinc on titania-washcoated 400-cpsi cordierite monolith with sulfidation temperature of 200°C (392°F), regeneration temperature of 650°C (1202°F) . . . . .	3-10
3-8.	Effluent H <sub>2</sub> S concentrations for 5-cycle test as a function of sulfur loading . . . .	3-13
3-9.	Typical regeneration effluent concentration profile of monolith RT11-11-1 . . . .	3-14
3-10.	Effluent H <sub>2</sub> S concentrations for 4-cycle test as function of sulfur loading . . . . .	3-15
3-11.	Effluent H <sub>2</sub> S concentrations for monolith activation during parametric testing . .	3-17
3-12.	Temperature effect on H <sub>2</sub> S leak and sulfur load . . . . .	3-18
3-13.	Sulfur load H <sub>2</sub> S and COS effluent versus temperature using syngas . . . . .	3-19
3-14.	Effluent H <sub>2</sub> S concentrations during monolith testing at a space velocity of 29,000 h <sup>-1</sup> . . . . .	3-20
4-1.	The equilibrium partial pressure of HCl is a function of temperature at 20 atm in a Texaco col gasifier gas stream . . . . .	4-4
4-2.	Detection of trace levels of anions, including chloride in an aqueous solution . . .	4-6
4-3.	HCl breakthrough curves for sepiolite- and earth-based sorbents . . . . .	4-7
4-4.	Process block diagram for removal of HCl vapor from hot syngas streams . . . . .	4-8
4-5.	Schematic diagram of trace HCl removal process using fixed-bed reactors . . . .	4-9
4-6.	The equilibrium partial pressures of NH <sub>3</sub> as a function of temperature at 20 atm in a Texaco coal gasifier gas stream . . . . .	4-12
4-7.	Temperature-programmed desorption of NH <sub>3</sub> adsorbed on various molecular sieves . . . . .	4-15
4-8.	Process block diagram for removal of NH <sub>3</sub> from hot syngas stream . . . . .	4-16
4-9.	Schematic diagram of ammonia removal unit . . . . .	4-17
5-1.	RTI process flow diagram, with Nexant equipment tag numbers and scaled-up duties . . . . .	5-8
5-2.	Rectisol process flow diagram . . . . .	5-15

## LIST OF TABLES

Number		Page
2-1.	Physical Properties of H <sub>2</sub> and CO <sub>2</sub> . . . . .	2-6
2-2.	Permeation Properties of H <sub>2</sub> and CO <sub>2</sub> . . . . .	2-7
2-3.	Permeability of H <sub>2</sub> and CO <sub>2</sub> in Heterophase Block Copolymers at 35°C (95°F) . . . . .	2-7
2-4.	Activation Energies of Permeation, E <sub>p</sub> , in PEO at Infinite Dilution . . . . .	2-19
2-5.	Effect of Salt Additive on Gas Transport at 6.8 Bars . . . . .	2-19
2-6.	Pure Gas Permeabilities of Medal Synthesized Films . . . . .	2-21
2-7.	Activation Energies of Permeation in PDMS . . . . .	2-24
2-8.	Summary of MEDAL Polymers Permeation Properties . . . . .	2-26
2-9.	Summary of Permeability and Selectivity Data for NCSU Samples . . . . .	2-27
2-10.	CO <sub>2</sub> /H <sub>2</sub> S Selectivity of Fluorinated and Nonfluorinated Polymers . . . . .	2-28
3-1.	BET Surface Areas for Various Monolith Samples . . . . .	3-5
3-2.	Summary of Temperatures, Gas Compositions, and Events in a 1.5-Cycle Test . . . . .	3-6
3-3.	Measurements of Zn Content for Cordierite Monolith Samples with Titania Washcoat and Zinc Oxide . . . . .	3-7
3-4.	BET Surface Areas for Various Monolith Samples with High and Low ZnO Loadings . . . . .	3-9
3-5.	Posttest BET Surface Area for ZnO and Titania Washcoated Cordierite Monolith . . . . .	3-10
3-6.	Summary of Operational Conditions During 5-Cycle Performance Test . . . . .	3-13
3-7.	Summary of Operational Conditions During 4-Cycle Performance Test . . . . .	3-15
3-8.	Summary of Operational Conditions for Monolith Activation During Parametric Testing . . . . .	3-17
3-9.	Summary of Operational Conditions for Parametric Temperature Testing . . . . .	3-18
3-10.	Summary of Operational Conditions During Parametric Temperature Testing with Syngas . . . . .	3-19
3-11.	Summary of Operational Conditions During High Space Velocity Testing . . . . .	3-20
4-1.	Results of HCl Vapor Removal Experiments . . . . .	4-7
4-2.	Annual Cost of Bulk HCl Removal Unit (Texaco Entrained-Bed, Oxygen-Blown Gasifier, 400 MWe) . . . . .	4-8
4-3.	Process Design Basis for Trace HCl Removal Unit (Texaco Entrained-Bed, Oxygen-Blown Gasifier, 400 MWe) . . . . .	4-9
4-4.	Capital Cost of Trace HCl Removal System (Texaco Entrained-Bed, Oxygen-Blown Gasifier, 400 MWe) . . . . .	4-10
4-5.	Annual Cost of Trace HCl Removal Unit (Texaco Entrained-Bed, Oxygen-Blown Gasifier, 400 MWe) . . . . .	4-10
4-6.	Economic Sensitivity Analysis of Trace HCl Vapor Removal System . . . . .	4-11
4-7.	Amount of NH <sub>3</sub> Adsorbed and Maximum Desorption Temperatures . . . . .	4-14
4-8.	Properties of Molecular Sieves for NH <sub>3</sub> Adsorption . . . . .	4-15
4-9.	Process Design Basis for Ammonia Removal Unit (Texaco Entrained-Bed, Oxygen-Blown Gasifier, 400 MWe) . . . . .	4-18

## LIST OF TABLES (continued)

Number		Page
4-10.	Capital Cost of NH <sub>3</sub> Removal System (Texaco Entrained-Bed, Oxygen-Blown Gasifier, 400 MWe) .....	4-18
4-11.	Annual Cost of NH <sub>3</sub> Removal Unit (Texaco Entrained-Bed, Oxygen-Blown Gasifier, 400 MWe) .....	4-19
5-1.	Process Sulfur Removal Efficiency .....	5-2
5-2.	Mass and Energy Balance for RTI Process (nominal basis–100 lbmol/hr syngas) .....	5-3
5-3.	Impurity Limits for Chemical and Fuel Cell Use .....	5-7
5-4.	RTI Process Conditions .....	5-7
5-5.	Estimated Capital for RTI Process .....	5-11
5-6.	Polymer Membrane Permeability .....	5-12

## EXECUTIVE SUMMARY

### INTRODUCTION/PROJECT GOALS

The Department of Energy's (DOE) VISION 21 Program conceptualizes energy facilities that use advanced technologies to convert fossil fuels, primarily solid carbonaceous fuels, into electricity plus co-products (transportation fuels, chemicals, etc.) without impacting the environment. The project described in this report addresses one of the "enabling technologies" specified in the VISION 21 Program Plan: "gas stream purification" for removing sulfur-, nitrogen-, chlorine-, and alkali-containing species to near-zero levels from the syngas produced in an integrated gasification combined cycle (IGCC) system. During gasification of a carbonaceous feedstock, fuel-bound contaminants that are naturally present will convert into gaseous impurities, such as H<sub>2</sub>S, COS, NH<sub>3</sub>, HCN, HCl, and alkali (sodium/potassium macromolecules).

The overall objective of this project is to develop technologies for cleaning/conditioning IGCC-generated syngas to meet contaminant tolerance limits for fuel cell and chemical production applications. The specific goals are to develop processes for (1) removal of reduced sulfur species to sub-ppm levels using a hybrid process consisting of a polymer membrane and a regenerable ZnO-coated monolith or a mixed metal oxide sorbent; (2) removal of hydrogen chloride vapors to sub-ppm levels using an inexpensive, high-surface area material; and (3) removal of NH<sub>3</sub> with acidic adsorbents followed by conversion of the NH<sub>3</sub> into nitrogen and water.

### BULK SULFUR REMOVAL BY MEMBRANES

RTI is working with MEDAL (MEmbrane DuPont Air Liquide)—a joint venture between DuPont and Air Liquide (now a wholly owned subsidiary of Air Liquide)—to develop and commercialize gas separation membrane technologies, and with North Carolina State University (NCSU) to develop polymer membrane technology for bulk removal of H<sub>2</sub>S from syngas. These membranes are being engineered to remove the acid gas components (H<sub>2</sub>S, CO<sub>2</sub>, NH<sub>3</sub>, and H<sub>2</sub>O) from syngas by focusing on the "solubility selectivity" of the novel polymer compositions. The result of this approach is that the desirable components of the syngas (H<sub>2</sub> and CO) will be maintained at high-pressure conditions as a non-permeate stream while the impurities are transported across the membrane to the low pressure side. By contrast, conventional polymer membranes for H<sub>2</sub> purification result in a low-pressure hydrogen stream that must be recompressed.

RTI designed and constructed a high-temperature, high-pressure (HTHP) permeation apparatus to measure the selectivity of various candidate polymer compositions. Initial testing was with polydimethylsiloxane (PDMS), a commercially available material. The permeability results from testing CO, H<sub>2</sub>S, COS, and SO<sub>2</sub> indicate that their transport (separation) behavior is consistent with theory based on the penetrants' molecular properties.

Subsequently, RTI tested 15 additional novel materials that MEDAL prepared and supplied. H<sub>2</sub>S/H<sub>2</sub> selectivities >30 were achieved, although there was a strong negative dependence with temperature. Significant effort is being directed toward improving the H<sub>2</sub>S/H<sub>2</sub> selectivity at high temperatures by making chemical structure changes in the polymer materials. Based on

MEDAL's evaluation, all the polymer compositions tested so far can be prepared as hollow fiber membrane modules using the existing manufacturing technology.

## **POLISHING DESULFURIZATION**

The existing technologies for polishing desulfurization—the additional sulfur removal that will be required for fuel cell and chemical applications that cannot be achieved by the membrane process—all have limitations in either operating temperature or regenerability. This part of the project shows that the low reactivity and limited capacity of ZnO pellets (a conventional material) could potentially be overcome by using a monolith with a thin coating of high surface area zinc-oxide based materials. Alternatively, regenerable ZnO-based sorbent pellets are newly available to lower the sulfur content of the syngas to sub-ppm levels.

Building on earlier work with small-scale thermogravimetric testing of ZnO-coated monolith materials, the optimum formulations were used to prepare 2-inch diameter samples for testing in RTI's HTHP bench-scale reactor. A multi-cycle test at 538°C (1000°F), 280 psig, and a space velocity of 2000 h<sup>-1</sup> (at STP) showed that effluent sulfur concentrations <0.5 ppm can readily be achieved, and underscored the importance of achieving optimal regeneration conditions and activation of the material during the first cycle. In a second test sequence, the desulfurization temperature was lowered by 38°C (100°F) during each subsequent cycle. The decreased temperature had little effect on effluent sulfur concentration.

The RVS-1 sorbent was developed by researchers at DOE's National Energy Technology Laboratory (NETL) and has been evaluated for a number of syngas desulfurization cases. A multicycle test at 271°C (520°F), 450 psig, and a space velocity of 2000 h<sup>-1</sup> (at STP) showed that RVS-1 could readily reduce effluent sulfur concentrations to below 1 ppmv even at steam concentrations of >60 vol%. Thus, both monoliths and fixed-bed sorbents have demonstrated the potential for polishing desulfurization service by (1) reducing effluent concentrations to <1 ppmv, (2) maintaining desulfurization performance after multiple regeneration cycles, and (3) operating at lower sulfidation temperatures.

## **REMOVAL OF HCl VAPORS**

Previous work conducted at RTI and SRI International has established that sodium-based compounds are effective at removing HCl vapors to trace levels. By thermodynamic calculations, the syngas stream must be cooled to less than 350°C (662°F) to achieve the goal of 10 ppb chloride vapor. Earlier studies showed that at this temperature, the low-cost, natural mineral form of sodium carbonate had limited reactivity and capacity. Existing synthetic sodium-based sorbents, while effective, are not economical for large gas streams. This project is exploring several low cost, moderate surface area materials as support media for the sodium carbonate active ingredient.

SRI International is using a bench-scale system to determine the performance of pellets made from diatomaceous earth or sepiolite, and impregnated with sodium carbonate. Both candidate materials achieved steady-state HCl levels of less than 100 ppb and greater than 10% sorbent utilization. Research is continuing to optimize the impregnation and calcination procedures to provide an optimum pore size distribution.

## **REMOVAL OF AMMONIA VAPORS**

Catalytic decomposition is a technique that has been proposed for removal of ammonia from syngas. However, SRI International conducted thermodynamic studies showing that achieving a residual  $\text{NH}_3$  level <10 ppmv by catalytic decomposition will require operation at lower than desired temperature. In this project, SRI is investigating an adsorption process to chemisorb  $\text{NH}_3$  on high surface area molecular sieve adsorbents, at high temperatures. The feasibility of this process was established by conducting a series of temperature-programmed reactions at 225°C (437°F) in which significant levels of  $\text{NH}_3$  were adsorbed on highly acidic adsorbents. The adsorbed  $\text{NH}_3$  was subsequently recovered by heating the adsorbent and the regenerated adsorbent was reused.

## **TECHNICAL AND ECONOMIC FEASIBILITY ASSESSMENT**

Based on the background information and the experimental results, RTI conceptualized a process design that incorporated two of the key technologies being developed in this project: (a) a polymeric membrane module for bulk removal (90%) of the  $\text{H}_2\text{S}$ ; and (b) a monolith reactor to remove the remainder of the sulfur down to <50 ppbv in the syngas. The conceptualized process also included a recompression of the membrane permeate stream so that the sulfur species could be converted to elemental sulfur using RTI's Direct Sulfur Recovery Process.

An information package including the process flow diagram, a mass and energy balance generated using the ASPEN PLUS process simulation software, and preliminary guidelines for the design of the key items of process equipment, was sent to Nexant, Inc., for cost estimating and economic assessment. Nexant estimated the size and material of construction for all the major equipment based on the syngas flow of a 500 MWe IGCC plant. A factored approach was used to arrive at an estimate of \$42 million (2001 US\$) for the installed cost. For comparison purposes, Nexant estimated the installed cost for an equivalent sized plant based on the Rectisol process (which would achieve the same sulfur removal specification) to be \$75 million. On the other hand, the total installed cost of an MDEA system would be \$18 million, except that MDEA does not remove the  $\text{H}_2\text{S}$  below 50 ppmv and requires additional equipment to remove COS from the syngas. Thus the RTI process was shown to be economically very competitive with a state-of-the-art process for syngas cleanup.

## **CONCLUSIONS AND FUTURE WORK**

The favorable economic assessment of the technology suggests that further development effort is warranted. In bulk desulfurization, work will continue on screening the polymer membrane samples, and with scale-up to bench-scale membrane modules. Polishing desulfurization research and development work will continue by optimizing the regeneration conditions and sorbent compositions for both monoliths and fixed-bed pellets. For HCl removal, a two-stage system will be investigated as a practical way to achieve the required removal efficiency. For the  $\text{NH}_3$  removal system studies, a high-pressure fluidized-bed reactor is being set up to study adsorbent compositions under simulated syngas conditions. The technical and economic evaluation by Nexant, Inc. will be updated to incorporate process improvements.

# CHAPTER 1

## INTRODUCTION

In October 1999, Research Triangle Institute (RTI) initiated a research program titled “Novel Technologies for Gaseous Contaminants Control” under the sponsorship of the U.S. Department of Energy (DOE). This research effort has been directed at developing novel technologies for controlling sulfur-, nitrogen-, and chlorine-species found in syngas generated by gasification of carbonaceous fuels in an integrated gasification combined cycle (IGCC) system. The research carried out in this program has been conducted under DOE Contract Number DE-AC26-99FT40675 and has been the cooperative research effort of RTI; MEDAL, L.P., a wholly owned subsidiary of Air Liquide of America; North Carolina State University (NCSU); SRI International; and Süd-Chemie Prototech, Inc., a wholly owned subsidiary of Süd-Chemie, Inc.

The research work in this project was divided into two programs: Base and Option. The focus of the Base Program was to demonstrate the feasibility of various contaminant control processes. A comprehensive technical and economic evaluation of sulfur control processes was conducted by Nexant, Inc., based on the laboratory results obtained by RTI and its project partners. This report describes details of experimental testing and process simulations, as well as technical and economic assessment conducted by Nexant, Inc.

### 1.1 BACKGROUND

An important goal of the DOE’s VISION 21 Program Plan (DOE, 1999) is to develop enabling technologies to convert fossil fuels into electricity and other value-added chemicals. Current and growing reliance on oil and natural gas to meet our electricity and transportation fuel needs can potentially endanger our economic future. DOE’s VISION 21 Program conceptualizes energy facilities that use advanced technologies to convert fossil fuels, primarily solid carbonaceous fuels, into electricity and other coproducts (transportation fuels, chemicals, etc.) without impacting the environment. In these advanced energy facilities, conventional pollutants (such as sulfur, nitrogen, chlorine, and heavy metals) would be captured and either disposed of or converted to marketable co-products (such as elemental sulfur, NH<sub>3</sub>, and NaCl). Furthermore, these advanced technologies must reduce emissions of CO<sub>2</sub> and other greenhouse gases with no solid or liquid discharges from these energy facilities.

One of the enabling technologies specified in the VISION 21 Program Plan is “gas stream purification” for removing sulfur-, nitrogen-, chlorine-, and alkali-containing species to near-zero levels. In IGCC systems, during gasification of a carbonaceous feedstock, fuel-bound constituents naturally present in carbonaceous materials convert to gaseous impurities, such as H<sub>2</sub>S, COS, NH<sub>3</sub>, HCN, HCl, and alkali (sodium/potassium macromolecules). Depending on the

temperature and pressure in various IGCC subsystems (syngas cooler, particulate control, gas and steam turbines, etc.), these gaseous species can pass directly through the particulate and sulfur control subsystems. For example, at temperatures above 675°C (1250°F), ceramic barrier filters will not capture alkali species. These alkali species are known precursors of corrosion-inducing condensates formed on gas turbine blades (Bachovchin et al., 1986). Similarly, if reduced sulfur species (e.g., H<sub>2</sub>S, COS) in syngas are not controlled, they can poison NH<sub>3</sub> decomposition catalysts downstream (Jothimurugesan and Gangwal, 1998). Both sulfur and nitrogen species entering the gas turbine will be converted to SO<sub>x</sub> and NO<sub>x</sub>, which are known precursors of acid rain and whose emission into the atmosphere is regulated by federal, state, and local laws. Uncontrolled chlorine species might damage the sulfur control systems (by reacting with desulfurization materials) and can potentially induce corrosion of the turbine blades in an IGCC system.

In today's market-driven electric power production environment, the current high capital cost of IGCC systems (\$1,200 to \$1,500/kW) precludes their commercial deployment in the near future. The current low cost of natural gas in conjunction with the low capital cost of gas turbines (\$400 to \$600/kW) makes natural gas combined cycle (GCC) a more attractive option for power production than an IGCC system or even a conventional coal-fired boiler. Furthermore, concerns over global climate change resulting from emissions of greenhouse gases (especially CO<sub>2</sub> from the use of solid carbonaceous fuels with high carbon intensity) have further decreased the merits of coal-fired systems. Although IGCC systems are significantly more efficient than coal combustion boilers, the amount of CO<sub>2</sub> formed per kilowatt-hour of electricity produced is much higher than that formed in a GCC system. This scenario of declining interest in coal-based power production, which may continue until there is a sharp increase in oil and natural gas prices, has led to alternative applications of the IGCC technology in fuel cell systems and the production of value-added chemicals.

Traditionally, natural gas (predominantly methane) has been used as a primary building block for producing H<sub>2</sub>, methanol, Fischer-Tropsch liquids, and other value-added chemicals and as the feed to fuel cells (molten carbonate, phosphoric acid, etc.). However, natural gas needs to be reformed into syngas (containing CO and H<sub>2</sub>) before it can be used for these applications. In an IGCC system, syngas is the product of gasification of carbonaceous fuels, but the IGCC syngas needs deep cleaning to remove various contaminants before it can be used for production of H<sub>2</sub> and value-added chemicals and in fuel cells.

The specific objective of this effort was to develop an integrated syngas cleaning system based on novel modular processes to

- Remove reduced sulfur species (H<sub>2</sub>S, COS, and CS<sub>2</sub>) to sub-ppm levels using a hybrid process consisting of a polymer membrane and a monolith desulfurizer in series

- Remove HCl vapors to sub-ppm levels using inexpensive disposable alkali carbonate sorbents supported on an agriculture waste material
- Remove NH<sub>3</sub> by selective adsorption on highly acidic adsorbents.

## 1.2 PROCESS CONCEPT

A simplified flow diagram of the RTI's modular process to clean up syngas produced in an IGCC process to generate value-added products is shown in Figure 1-1. This approach consists of a number of different modular processes that can be integrated as needed for the different syngas conditioning requirements for fuel cell, chemical production, or power generation applications. The temperature range investigated for contaminant removal processes in this project was fairly broad to permit adaptation of many technologies novel to syngas conditioning. These include specific component-selective membranes, regenerable polishing sulfur removal monoliths, regenerable acidic adsorbents for NH<sub>3</sub>, and inexpensive high-surface-area materials for removal of hydrogen chloride (HCl) vapors.

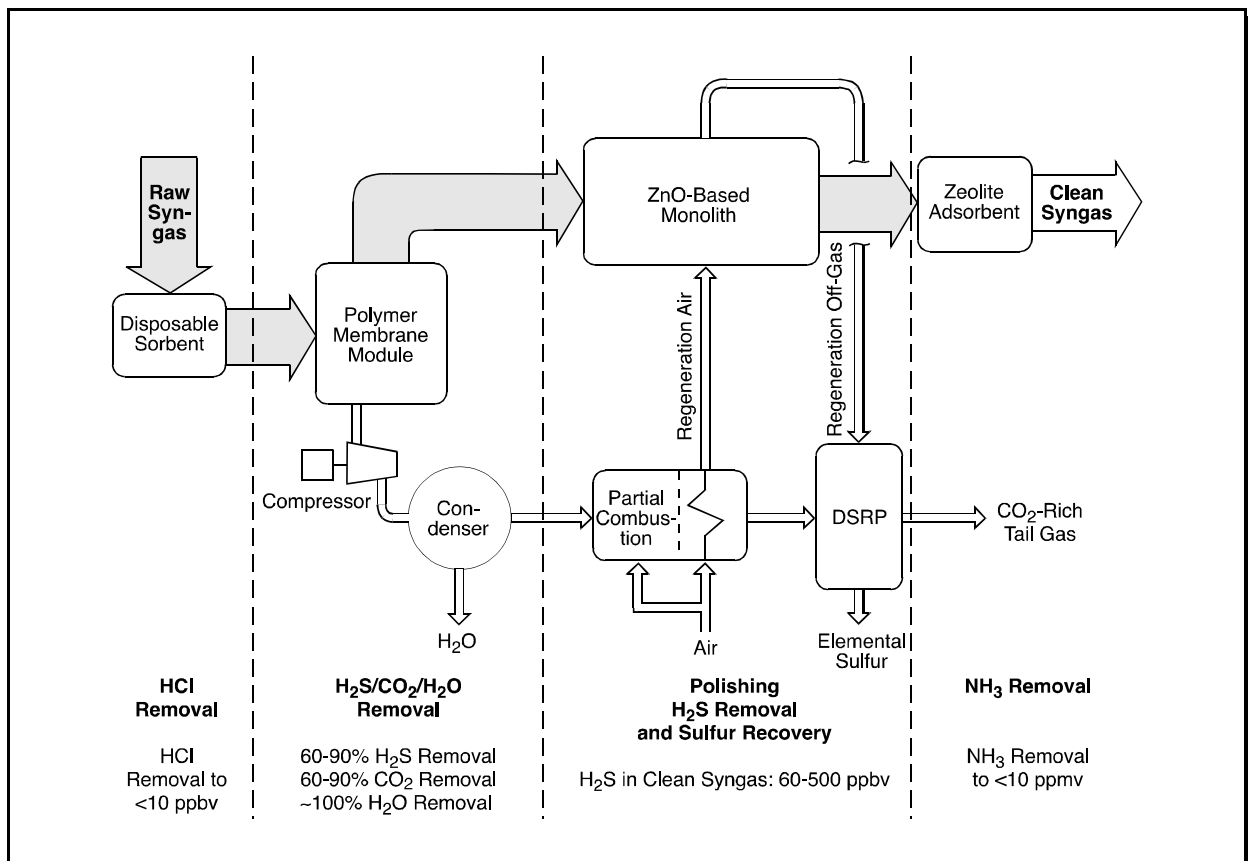


Figure 1-1. Modular process approach for the RTI gas cleaning process.

As shown in Figure 1-1, the hybrid process for sulfur removal consists of a bulk sulfur removal (60 to 90% removal) process and a polishing sulfur removal (down to sub-ppm levels) process. Team members (MEDAL, NCSU, and RTI) have been actively involved in the bulk sulfur removal research. Bulk sulfur removal using polymer membranes engineered to specifically remove the acid gas components ( $\text{H}_2\text{S}$ ,  $\text{CO}_2$ ,  $\text{NH}_3$ , and  $\text{H}_2\text{O}$ ) from syngas was proposed. By focusing on “solubility selectivity” of the novel polymer compositions—an area that has received little attention in conventional commercial membrane development focused on diffusivity-selective  $\text{H}_2$  separation membranes—acid gas selective membranes can be optimized. Leveraging the existing commercial membrane production technology and increasing thermal stability require copolymerization of a polymer that was acid-gas-selective with another polymer that provides the mechanical integrity and thermal stability required in the process. The scope of development in the Base Program was to demonstrate the technical feasibility of engineering these copolymers in which both the acid gas selectivity and the mechanical and thermal stability could be modified. In the Option Program, the effort will be to optimize membrane properties of acid gas to hydrogen selectivity and thermal stability, scale up to commercial membrane production, and prepare a prototype of a commercial membrane module. A detailed description of project activities carried out under this task is provided in Chapter 2.

In the polishing sulfur removal process, RTI collaborated with Süd-Chemie Prototech, Inc., to develop regenerable ZnO-coated monoliths for removing any remaining sulfur to sub-ppm levels. These monoliths can achieve the same sub-ppm-level sulfur removal available with disposable commercial ZnO-based materials, but, unlike these materials, the monolith can be regenerated for repeated use. In the Base Program, Prototech and RTI demonstrated the technical feasibility of achieving both sub-ppm levels of sulfur removal and the ability to regenerate the monolith. In the Option Program, the monolith properties and process conditions will be optimized to reduce the sulfur removal temperature as much as possible. This optimization activity will be followed by the testing of prototype commercial monoliths. In addition to testing monolith materials advanced fixed-bed sorbent will also be tested in the Option Program. Project activities conducted under this task are described in detail in Chapter 3.

For chloride removal, SRI and RTI collaborated on the development of an inexpensive disposable sorbent. To accomplish this, SRI and RTI extended their previous work with nahcolite minerals into preparation of supported sorbent materials. The main advantage of this material over available commercial technologies is a significant decrease in the price of a disposable material. The unique aspect of this research was the use of low cost support materials such as sepiolite, diatomaceous earth and rice hulls as high-surface-area supports. During the Base Program, samples of these supported sorbents were prepared and tested to demonstrate technical and economic feasibility. During the Option Program, these supported sorbents will be optimized in terms of chemical and physical properties and cost of production.

Ammonia present in syngas was removed by adsorption on to high-surface-area acidic supports and subsequent desorption by temperature and/or pressure swings to generate a small NH<sub>3</sub> tail gas stream. This NH<sub>3</sub> tail gas stream could be converted to nitrogen and water with commercially available catalytic oxidation processes, if desired. Commercial technologies for NH<sub>3</sub> removal are not directly applicable at the temperature range examined. One potential advantage of this process is that it has no liquid or solid discharges. In the Base Program, SRI and RTI collaborated to screen commercially available molecular sieves and hydrodenitrogenation catalysts for their NH<sub>3</sub> adsorption and desorption potential and to demonstrate technical and economic feasibility with limited bench-scale reactor testing. In the Option Program, both the material properties and process conditions will be optimized with bench-scale testing. Additional bench-scale testing will include extended 10-cycle testing. SRI International's report submitted on this task is enclosed as Chapter 4 which describes the research work conducted on both HCl and NH<sub>3</sub> removal.

Nexant, Inc., conducted a comprehensive technical and economic evaluation of RTI's gas cleaning process and found that RTI technology (based its current state of development) costs about 45% less than the Rectisol technology for obtaining a syngas containing <1 ppm sulfur. Further reductions in cost in the RTI process can be achieved by lowering the maximum operating temperatures for the monolith and partial oxidation reactor, thus allowing the metallurgy to be changed to carbon steel. Also, further improvements in membrane selectivity and sorbent kinetics as a result research in the option program are expected to lead to further significant savings in capital and operating costs. Details of this economic evaluation is described in Chapter 5.

## CHAPTER 2

### BULK SULFUR REMOVAL

As described in Chapter 1, RTI proposed to carry out bulk sulfur removal (up to 90% removal) from syngas using advanced membrane technology. This chapter briefly discusses the current state-of-the-art on sulfur removal processes for both bulk and polishing applications, the application of membranes to bulk sulfur removal from syngas, the fundamentals of membrane separations, and the results obtained by NCSU, MEDAL and RTI on membrane preparation, characterization and testing. Process simulation results obtained using a membrane-simulator are also discussed in this chapter.

#### 2.1 CURRENT STATE-OF-THE-ART

Over the past two decades, primarily under DOE/National Energy Technology Laboratory (NETL) leadership, a significant research and development (R&D) effort has been expended to develop removal processes for sulfur,  $\text{NH}_3$ , and HCl found in IGCC-generated syngas. This section briefly describes the current status of the sulfur removal technology.

##### 2.1.1 High-Temperature Sulfur Removal Using Sorbent Technology

Of all the chemical contaminants in syngas, sulfur has received the most attention. Most of this research work has focused on the development of regenerable sorbents based on mixed metal oxide compositions for high-temperature 427 to 649°C (800 to 1200°F) sulfur removal. It has been reported that removal of gaseous contaminants (primarily sulfur) at high temperatures results in a 2 to 3% increase in thermal efficiency of an IGCC plant (DOE, 1998). The extensive research and development work on the sorbent technology in this decade has culminated in a number of sorbent compositions that are near commercialization. A number of review articles and detailed reports on sorbent research for removal of sulfur at high-temperature, high-pressure (HTHP) conditions have been published (Gangwal, 1991; Gupta and Gangwal, 1992; Swisher and Schwerdtfeger, 1992a,b). A recent publication by Cicero et al. (1999) summarizes the status of hot-gas desulfurization technology worldwide. RTI has been on the forefront of the sorbent technology development for the past 15 years.

Among various metal oxides, ZnO-based sorbents have received the most attention because of their favorable thermodynamics, their favorable kinetics for desulfurization and regeneration reactions, and their stability under reducing and oxidizing conditions. Mixed-metal-oxide sorbents combining zinc oxide and a secondary oxide (e.g., iron, titanium, or nickel oxide) have also been investigated. A number of ZnO-based sorbents, including zinc titanate (containing ZnO and  $\text{TiO}_2$ ), Z-Sorb (ZnO and NiO on a proprietary matrix), and RVS-1 (ZnO on a patented matrix) have reached the pilot- to demonstration-scale-testing stage.

Following sorbent composition selection, the next most critical feature of a hot-gas desulfurization process is reactor design. A two-reactor system is necessary because of the cyclic nature of the process. Early reactor systems used fixed beds; however, the highly exothermic regeneration and formation of undesirable metal sulfides during regeneration promoted testing of alternative reactor designs, such as moving beds and fluidized beds. Kellogg, Brown, and Root (KBR), formerly the M.W. Kellogg Company, developed a transport reactor system (essentially fluid catalytic cracker design) for hot-gas desulfurization. KBR designed, constructed, and installed a commercial unit at Sierra Pacific Power Company's Tracy Station power plant in Reno, Nevada. This IGCC plant, known as Piñon Pine IGCC, is a 107-MWe (gross) plant and is based on a KBR air-blown pressurized fluidized-bed coal gasification system. In this system, in-bed limestone captures most of the sulfur, and the remaining sulfur is removed in the KBR transport reactor system using a ZnO-based sorbent. During startup in December 1997, Sierra used a spray-dried Z-Sorb material developed by Phillips Petroleum Company. However, because of excessive sorbent attrition, Sierra needed an alternative material. RTI, working with DOE and Intercat, coordinated production and delivery of a 50,000-lb batch of zinc titanate sorbent (EX-S03) that was loaded in the desulfurizer and circulated without any attrition problems. Besides zinc titanate and Z-Sorb, a sorbent developed by in-house DOE/NETL researchers and tested by RTI has exhibited excellent potential for a variety of sulfur cleanup applications (Turk and Gupta, 2001).

Currently, the limitations of sorbent-based gas desulfurization processes may be summarized as follows:

- Inability to reduce H<sub>2</sub>S concentration of syngas to sub-ppm (parts per million) levels
- Relatively slow kinetics at temperatures below 427°C (800°F)
- Relatively low sulfur capacity at low temperatures 204 to 427°C (400 to 800°F)
- Poor regenerability at temperatures below 538°C (1000°F).

### **2.1.2 Conventional Sulfur Removal**

Conventional commercial methods for removing sulfur from syngas for fuel cell and chemical production applications involve scrubbing H<sub>2</sub>S with an amine-based system (e.g., methyl di-ethyl-amine [MDEA]) and removing any remaining H<sub>2</sub>S traces with a disposable ZnO-guard bed. These amine absorption processes are subject to process equipment corrosion, foaming, amine-solution degradation, and amine solution evaporation (Kohl and Nielson, 1997). A fraction of the complexity of these processes can be seen in Figure 2-1 (Kubek et al., 1997). Figure 2-1 does not include the Claus process for sulfur recovery for the acid gas tail gas generated by the H<sub>2</sub>S absorption process. Although the disposable ZnO-guard beds are very effective, their sulfur capacity at low temperatures is limited, and they cost between \$200 and \$300/ft<sup>3</sup>.

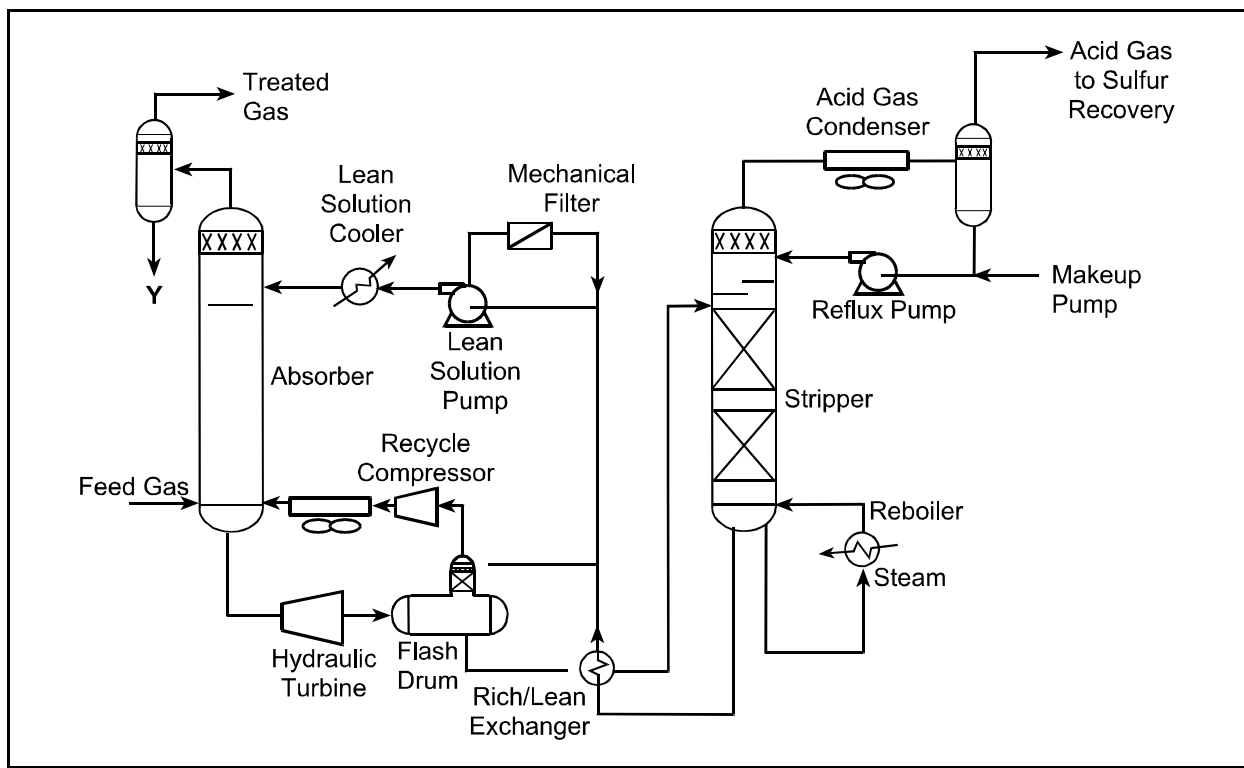


**Figure 2-1. Conventional Selexol process for removal of H<sub>2</sub>S from syngas.**

Based on the above considerations, commercially available syngas conditioning for fuel cell and chemical production applications is complex, capital-intensive, and operationally expensive. For sulfur conditioning of IGCC-generated syngas, conventional amine-based desulfurization only adds additional cost to an already economically disadvantaged process. Alternatively, the technical limitations associated with regenerable metal-oxide sorbents, particularly for low-temperature sulfur removal, do not meet the sub-ppm level requirements for fuel cell and chemical production applications. Hence, development of a simple, relatively inexpensive and effective process for sulfur removal is necessary to make IGCC systems an economically competitive means of producing clean syngas in the fuel cell and chemical production markets.

## 2.2 HYBRID SULFUR REMOVAL PROCESS

In the hybrid sulfur removal system investigated in this study, a polymer membrane module removes between 60 and 90% of the reduced sulfur species in the dirty syngas. Additional sulfur removal to reduce the syngas concentration to sub-ppm levels is performed by a regenerable ZnO-coated monolith. The hybrid approach seeks to capitalize on the relative strengths of each technology and limit any potential disadvantages. The objective of the hybrid sulfur removal process is to remove sulfur compounds to less than 60 ppb.

Commercial polymer membrane modules are noted for their simplicity, reliability, and effectiveness of operation. The disadvantage of membrane systems is that all gas components permeate the membrane to some extent (i.e., finite selectivity). For some components, such as H<sub>2</sub>O and CO<sub>2</sub>, this results in the effective removal of inert components of the syngas enriching the H<sub>2</sub> and CO content of the clean syngas, thus increasing its Btu value. Alternatively, for components such as H<sub>2</sub> and CO, their removal from the clean syngas represents a significant loss. Polymer membrane modules can be designed to achieve sub-ppm sulfur levels in the clean syngas, but H<sub>2</sub> and CO loss in the permeate stream may make the process economically prohibitive.

In commercial applications, particularly in automotive exhaust treatment, and volatile organic compound (VOC) abatement, monolith-based catalysts are known for their ability to handle high space velocities while simultaneously reducing pollutants to very low levels. Monolith-based solvents could not effectively reduce the typical H<sub>2</sub>S levels in dirty syngas, particularly from oxygen-blown gasifiers, to sub-ppm levels because of their relatively small sulfur capacity. However, they are ideal for removing the small amount of H<sub>2</sub>S which would be present in the syngas after treatment by a membrane.

The technical challenges facing development of each of these technologies for the hybrid desulfurization process are discussed in detail in subsequent sections. One common technical challenge these technologies face is expanding their typical operating temperatures to permit integration in the hybrid process, as shown in Figure 2-2.

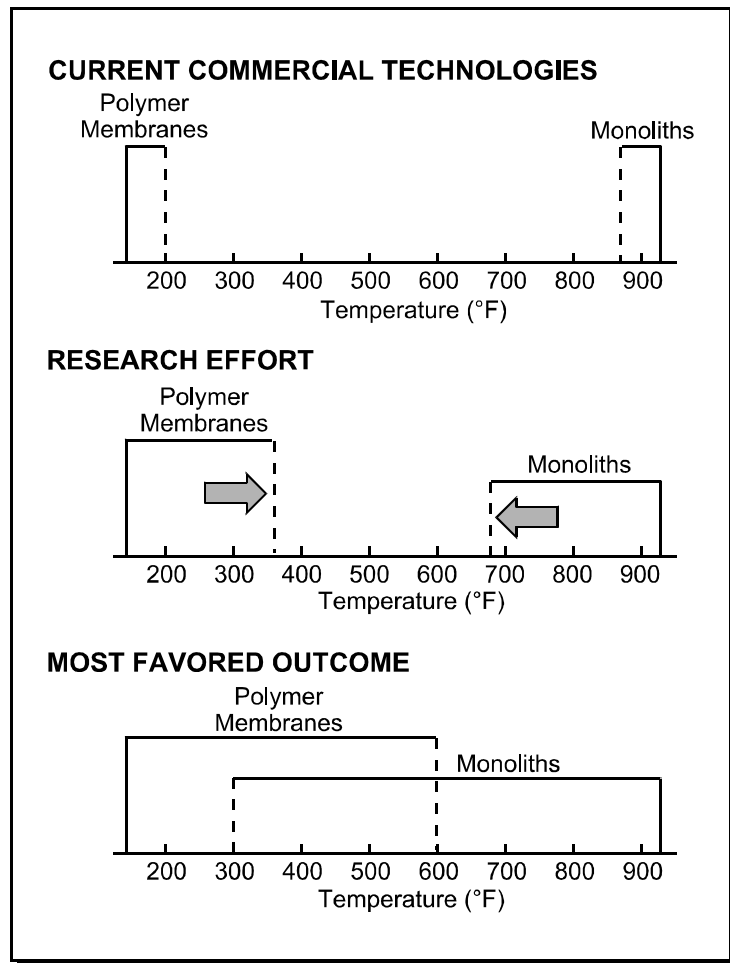
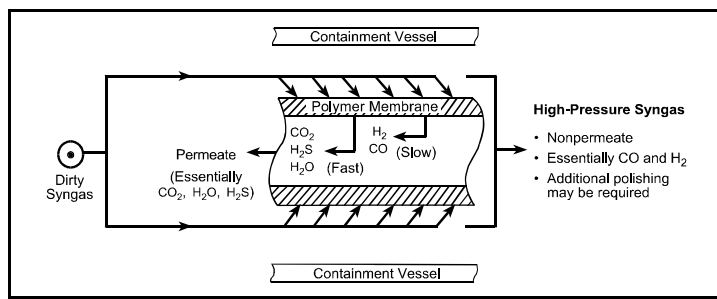


Figure 2-2. Hybrid process for syngas desulfurization.

### 2.2.1 Polymer Membrane System

The first component of this hybrid process for sulfur removal is a polymer membrane system. This membrane technology development work was performed in collaboration with NCSU and MEDAL, L.P., a leader in the membrane industry possessing the production facilities, technical expertise, and marketing infrastructure to commercialize this technology.

Membrane separation is a relatively new technology wherein polymer membrane modules separate gases by selective permeation of one or more gaseous components from one side of a membrane barrier to the other side, as shown in Figure 2-3. Gas components are transported across the membrane as a result of a concentration gradient. The concentration gradient is maintained by a relatively high partial pressure of gas components on the feed (or upstream) side of the membrane barrier and a low partial pressure on the permeate (or downstream) side.



**Figure 2-3. Separation of acid gases from syngas in polymer membrane module.**

Typical commercial membrane systems (e.g., air separation, H<sub>2</sub> recovery from NH<sub>3</sub> purge gas, and CO<sub>2</sub> removal from natural gas) are based on stiff-chain rigid glassy polymers, which exhibit high size (or diffusion) selectivity. In these membranes, small penetrants permeate through the membrane faster than larger penetrants (Stern, 1994; Freeman and Pinnau, 1997). If this type of polymer were used for syngas conditioning, H<sub>2</sub> would easily pass through the membrane and collect in large concentrations on the low pressure side of the membrane (permeate). Recompression of this H<sub>2</sub>-rich stream to feed pressure is economically prohibitive. Consequently, conventional membrane technology is not appropriate for syngas conditioning.

If suitable polymeric membrane materials can be developed that selectively permeate H<sub>2</sub>S, CO<sub>2</sub>, and other acid or polar gases (such as NH<sub>3</sub> and H<sub>2</sub>O) in mixtures with light gases (such as H<sub>2</sub>, CO, or N<sub>2</sub>) at high temperatures, membrane technology can become an attractive option for a host of applications requiring the removal of H<sub>2</sub>S and CO<sub>2</sub>. These applications include CO<sub>2</sub> removal from flue gas, CO<sub>2</sub> removal from mixtures with H<sub>2</sub> in reformer gas for fuel cells, and removal of CO<sub>2</sub> and H<sub>2</sub>S from sour natural gas (Bhide and Stern, 1993a,b).

Research efforts driving the improvement of commercial membranes, particularly H<sub>2</sub> separation membranes, have focused almost exclusively on size selective glassy polymers. For this reason, conventional membrane research may never generate materials suitable for syngas conditioning. Besides size (or diffusion) selectivity, the other component that contributes to the overall membrane selectivity, and has generally been overlooked by this research effort, is

solubility selectivity. Gas flux through a membrane barrier depends not only on the rate of penetrant diffusion, but also on the solubility of the penetrant in the polymer. Generally, larger, more condensable penetrants are more soluble in polymers than smaller, permanent gases. In some polymers, these highly soluble penetrants are also more permeable than permanent gases.

In the absence of strong polymer-penetrant interactions, the most important factor affecting solubility selectivity is relative penetrant condensability. Critical temperature is a property directly related to condensability and is frequently used as a scaling factor for penetrant solubility in polymer materials. As shown in Table 2-1, H<sub>2</sub>S and CO<sub>2</sub> have much higher critical temperatures than H<sub>2</sub>, indicating these compounds are more soluble in polymers than H<sub>2</sub>. This fact suggests that in polymers where solubility selectivity is more important than diffusion selectivity, H<sub>2</sub>S and CO<sub>2</sub> will be more permeable than H<sub>2</sub> and could be selectively stripped from syngas by a polymer membrane. Similarly, other acid gases such as HCl, NH<sub>3</sub>, and H<sub>2</sub>O should also be more permeable than H<sub>2</sub> in these polymers.

**Table 2-1. Physical Properties of H<sub>2</sub> and CO<sub>2</sub>**

	Size		Condensability
	Critical Volume (cm <sup>3</sup> /mol) <sup>a</sup>	d <sub>k</sub> <sup>b</sup> (Å)	Critical Temperature (K) <sup>a</sup>
H <sub>2</sub>	65.1	2.89	33.2
CO <sub>2</sub>	93.9	3.30	304.2
H <sub>2</sub> S	98.6	Not available	373.2

<sup>a</sup> Data from Reid et al. (1987). Critical temperature is a common measure of penetrant condensability. Penetrant solubility in polymers typically increases with increasing penetrant condensability (Stannett, 1968).

<sup>b</sup> Data from Koros et al. (1989). Critical volume and kinetic diameter, d<sub>k</sub>, are common measures of penetrant size and are useful indicators, therefore, of penetrant diffusivity in a polymer matrix.

Polymers where solubility selectivity dominates over diffusivity selectivity are typically rubbery materials. Alternatively, polymers for which diffusivity selectivity is greater than solubility selectivity are frequently glassy materials. Conventional commercial H<sub>2</sub> separation membranes are glassy polymers. Table 2-2 shows the permeation properties of H<sub>2</sub> and CO<sub>2</sub> for both glassy and rubbery polymers. For rubbery polyisoprene, CO<sub>2</sub>/H<sub>2</sub> selectivity is more than five times greater than that of the glassy polymers. Consequently, materials having transport properties useful for syngas conditioning are likely to be rubbery polymers.

As would be expected, the physical properties of rubbery polymers differ considerably from glassy polymers. Since commercial processes for preparation of polymer membrane modules depend on the rigidity of the glassy polymers to produce reliable and functional membrane modules for real-world applications, rigidity must also be incorporated into the proposed rubbery

**Table 2-2. Permeation Properties of H<sub>2</sub> and CO<sub>2</sub>**

Type	Polymer	Permeability <sup>a</sup>		Selectivity
	Name	H <sub>2</sub> <sup>b</sup>	CO <sub>2</sub>	CO <sub>2</sub> /H <sub>2</sub>
Glassy	Polysulfone (PSF)	14.0	5.6	0.40
	Polycarbonate (PC)	14.0	6.5	0.46
	Cellulose acetate (CA)	13.6	5.5	0.40
Rubbery	cis-Polyisoprene (PI)	49	134	2.7

<sup>a</sup> Pure gas permeability coefficients reported at 95°F. All data are from Zolandz and Fleming (1992). Permeability values are reported in barrers, where 1 barrer = 10<sup>-10</sup> cm<sup>3</sup> (STP) cm/(cm<sup>2</sup> s cm Hg).

<sup>b</sup> When H<sub>2</sub> permeability coefficients were not available, He was used as a surrogate. He and H<sub>2</sub> typically have similar permeation properties (Zolandz and Fleming, 1992).

polymers to leverage this available commercial processing technology. Because the desired operating temperature range for the proposed process is above the dewpoint of syngas (>150°C [>300°F]), these rubbery polymers must also be thermally stable.

These rather conflicting simultaneous physical requirements for rigidity, thermal stability, and rubberiness can be achieved with heterophase block copolymers. Hard (glassy) blocks, providing the mechanical strength and thermal stability, are coupled with soft (rubbery) blocks, controlling the gas transport properties. With block copolymers, the transport and separation efficacy can be manipulated independent of the mechanical strength and thermal stability. Polymer materials produced under the Pebax trademark by ELF-Atochem are examples of commercially produced heterophase block copolymers. Table 2-3 shows H<sub>2</sub> and CO<sub>2</sub> permeabilities of several commercially available Pebax heterophase block copolymers. Microstructured heterophase polymers with high concentrations of soft ether blocks prepared at NCSU exhibit high permeability to CO<sub>2</sub> and the highest CO<sub>2</sub>/N<sub>2</sub> and CO<sub>2</sub>/H<sub>2</sub> separation factors reported for nonfacilitated transport polymer membranes (Bondar et al., 1997).

**Table 2-3. Permeability of H<sub>2</sub> and CO<sub>2</sub> in Heterophase Block Copolymers at 35°C (95°F)**

Polyether Type/ Composition <sup>a</sup>	Polyamide Type	Permeability (Barrers) <sup>b</sup>		Selectivity
		H <sub>2</sub> <sup>b</sup>	CO <sub>2</sub>	CO <sub>2</sub> /H <sub>2</sub>
PTMEO/80	PA12	46	225	4.9
PTMEO/53	PA12	30	110	3.7
PEO/57	PA6	9	65	7.2

<sup>a</sup> Polyether composition is the weight percent polyether in the copolymer.

<sup>b</sup> Pure gas permeability coefficients reported at 35°C (95°F) and 10 atm upstream pressure.

The permeability and selectivity results for the block copolymers described in the preceding paragraphs were obtained at essentially ambient temperature. In the syngas desulfurization application, the membranes would be required to demonstrate thermal stability above the dewpoint of syngas. To determine the thermal stability, a series of these polymer materials

were exposed to a Texaco composition syngas at temperatures as high as 260°C (500°F) in a thermogravimetric analyzer (TGA) at RTI. Figure 2-4 shows the TGA profile of the MDA-1/PEG2000 film sample tested at 250°C (482°F) in Texaco coal gas. As can be seen, after an initial weight loss of 2% due to the evaporation of surface moisture, the weight of the film did not show any effects of the high-temperature exposure or the presence of Texaco coal gas. This provided evidence that these polymers possess high-temperature stability.

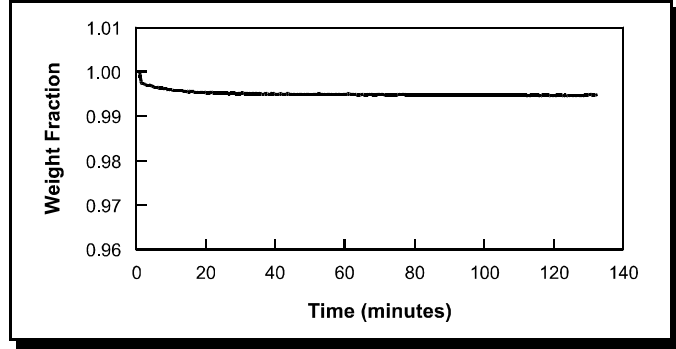


**Figure 2-4. GA results demonstrating thermal stability of MDA-1/PEG2000 block copolymer in simulated Texaco gas at 250°C (482°F).**

Thus, in contrast to conventional material design rules currently used for membranes in O<sub>2</sub>/N<sub>2</sub>, H<sub>2</sub>/N<sub>2</sub>, H<sub>2</sub>/hydrocarbon, and CO<sub>2</sub>/CH<sub>4</sub> separation, tailoring the solubility selectivity of soft blocks in heterophase block copolymers to specifically remove acid gas components of syngas and, in particular, H<sub>2</sub>S, was conducted for preparing a new generation of membrane materials. Optimization of the hard block properties in these block copolymers would allow the leveraging of available commercial membrane processing technology and increasing of the thermal stability of the membranes.

### 2.3 FUNDAMENTALS OF MEMBRANE SEPARATIONS

The permeability of a gas A, P<sub>A</sub>, through a membrane of thickness  $\ell$  is:

$$P_A \equiv \frac{N_a \ell}{(p_2 - p_1)} \quad (1)$$

where N<sub>a</sub> is the steady-state gas flux through the membrane,  $\ell$  is the membrane thickness, and p<sub>2</sub> and p<sub>1</sub> are the feed (i.e., high) pressure and permeate (i.e., low) pressure, respectively (Ghosal and Freeman, 1994). In a gas mixture, p<sub>2</sub> and p<sub>1</sub> denote the partial pressures of component A on the high- and low-pressure sides of the membrane, respectively. When the downstream pressure, p<sub>1</sub>, is much lower than the upstream pressure, p<sub>2</sub>, the permeability is often expressed as follows:

$$P_A = D_A \times S_A \quad (2)$$

where D<sub>A</sub> is the effective concentration-averaged diffusivity (Ghosal and Freeman, 1994). The solubility coefficient, S<sub>A</sub>, is defined as C<sub>2</sub>/p<sub>2</sub>, where C<sub>2</sub> is the gas concentration in the polymer at the upstream face of the membrane. The ability of a membrane to separate two components is

often characterized in terms of the ideal selectivity,  $\alpha_{A/B}$ , which is the ratio of permeabilities of the two components (Ghosal and Freeman, 1994):

$$\alpha_{A/B} \equiv \frac{P_A}{P_B} = \frac{[D_A]}{[D_B]} \times \frac{[S_A]}{[S_B]} \quad (3)$$

Here,  $D_A/D_B$  is the diffusivity selectivity, which is the ratio of diffusion coefficients of components A and B. The ratio of solubility coefficients of components A and B,  $S_A/S_B$ , is the solubility selectivity. Solubility selectivity is controlled by the relative condensability of the penetrants and the relative affinity of the penetrants for the polymer matrix, whereas diffusivity selectivity is governed primarily by the size difference between the penetrant molecules and the size-sieving ability of the polymer matrix (Stern, 1994; Petropoulos et al., 1994).

Commercial membranes used for gas separation (e.g., air separation, hydrogen recovery from ammonia purge gas, and carbon dioxide removal from natural gas) are based on stiff chain, rigid, glassy materials. Smaller penetrants are more permeable than larger penetrants because these polymers have more restricted backbone torsional mobility and, therefore, exhibit higher diffusivity selectivity than rubbery polymers (Stern, 1994; Freeman and Pinnau, 1997). This point is illustrated in Figure 2-5, which presents the effect of penetrant size on diffusion coefficients for a series of penetrants in *cis*-polyisoprene, an amorphous rubber, and poly(vinyl chloride) (PVC), a glassy polymer. In this figure, critical volume is used as a convenient measure of penetrant size. Diffusion coefficients are higher in rubbery polyisoprene; however, the effect of penetrant size on diffusivity is far greater for glassy PVC. Therefore, to achieve high diffusivity selectivity, glassy polymers are clearly more useful than rubbery polymers. Hence, glassy polymeric membranes have been commercialized for the separation of gas pairs such as  $O_2/N_2$ ,  $H_2/CH_4$ , and  $CO_2/CH_4$ .

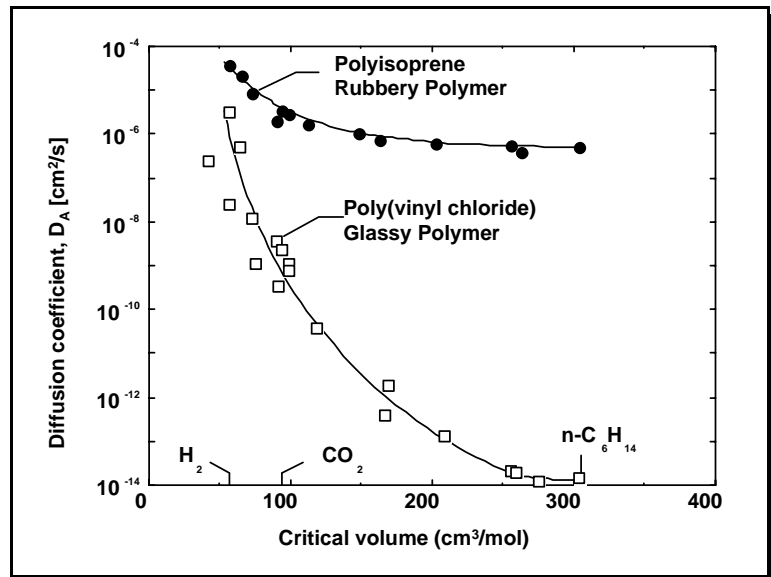


**Figure 2-5. Effect of penetrant size on diffusion coefficients in a rubber [ $\bullet$ , *cis*-polyisoprene,  $T=50^\circ C$ ] (VanAmerongen, 1964) and a glassy polymer [ $\square$ , poly(vinyl chloride),  $T=30^\circ C$ ] (Berens and Hopfenberg, 1982).**

### 2.3.1 Solubility Selective Materials

There are classes of separations for which strongly size-sieving polymers (i.e., those with very high diffusivity selectivity) are not appropriate. The separation of organic vapors and other condensable from supercritical gases is also an application of considerable industrial importance and is performed economically using membranes (Freeman and Pinnau, 1997; Baker et al., 1987; Baker and Wijmans, 1994; Morisato et al., 1996a,b; Pinnau and Toy, 1996; Pinnau et al., 1996; Singh et al., 1998). The removal of volatile organic compounds (e.g., vinyl chloride monomer [Lahiere et al., 1993], propylene, ethylene, gasoline, and freons [Baker and Wijmans, 1994]) from mixtures with air or nitrogen is practiced commercially. The removal of higher hydrocarbons from refinery hydrogen purge streams or from methane in natural gas represents promising future applications (Freeman and Pinnau, 1997; Baker et al., 1987). Removal of acid gas components (e.g., H<sub>2</sub>S and CO<sub>2</sub>) from synthesis gas is not practiced commercially, but could be another viable example of such a separation. Because organic vapors or acid gases are typically the minor components in these streams and because it is often desirable to keep the supercritical gas components at high pressure (e.g., methane in natural gas or CO + H<sub>2</sub> in synthesis gas), membranes with high organic vapor or acid gas/supercritical gas selectivity and high organic vapor or acid gas flux are required for economical processes (Freeman and Pinnau, 1997; Baker et al., 1987; Baker and Wijmans, 1994). Such membranes sieve penetrant molecules based primarily on relative penetrant solubility in the polymer since larger penetrants are usually more soluble than smaller penetrants.

Conventional glassy polymers, such as polysulfone (which is widely used as an air separation membrane), are not suitable for such separations because they are more permeable to the light gas components than to larger, more condensable species in a gas mixture (Pauly, 1989; Anonymous, 1995). If a conventional glassy polymer membrane were used, the bulk of the light gas (i.e., H<sub>2</sub> + CO in synthesis gas) would have to permeate through the membrane. Not only would this require a very large membrane area, but the product gas would be produced at low pressure. Recompressing the entire treated stream to process pressure would be economically impractical. Thus, optimized materials for this separation should have high acid gas permeability and high acid gas/supercritical gas selectivity. Because acid gas components in these separations are larger than the supercritical gas components, membrane materials that sieve molecules strictly based on size are not useful.

As shown in Figure 2-6, diffusion coefficients decrease with increasing penetrant size in both conventional glassy polymers, such as polysulfone, and in rubbery, solubility selective polymers such as poly(dimethylsiloxane). Therefore, for an acid gas/supercritical gas membrane separation, diffusivity selectivity is always less than 1:

$$\frac{D_{\text{acid gas}}}{D_{\text{supercritical gas}}} < 1 \quad (4)$$

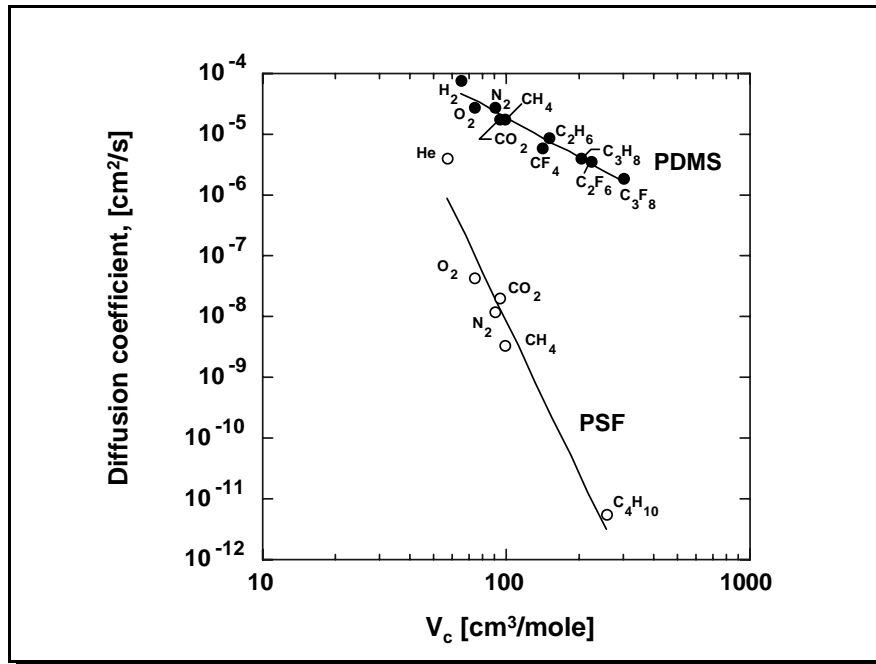


Figure 2-6. Diffusion coefficients in rubbery poly(dimethylsiloxane) (PDMS) and glassy polysulfone (PSF) at 35°C (95°F) as a function of penetrant critical volume.

For overall organic vapor/supercritical gas selectivity to be greater than 1, solubility selectivity must be sufficiently greater than 1 to offset the unfavorable diffusivity selectivity. As indicated in Figure 2-7, larger penetrant molecules are, in general, more soluble than smaller penetrants. Thus, for acid gas/supercritical gas separations, solubility selectivity generally favors the larger acid gas components:

$$\frac{S_{\text{acid gas}}}{S_{\text{supercritical gas}}} > 1 \quad (5)$$

At present, there are two classes of polymers that have sufficiently low diffusivity selectivity to permit:

$$\frac{P_{\text{acid gas}}}{P_{\text{supercritical gas}}} > 1 \quad (6)$$

They are rubbery polymers and ultra-high free-volume glassy materials (Freeman and Pinnau, 1997). Polydimethylsiloxane (PDMS) is an example of the first class, and poly(1-trimethylsilyl-1-propyne) (PTMSP) is an example of the second class. PDMS has the lowest diffusivity selectivity of any rubbery polymer. It has a very flexible polymer backbone as indicated by its extremely low glass transition temperature. As a result, PDMS has a very weak ability to sieve penetrant molecules based on size and can, therefore, achieve the criterion of Equation 6. Because of its good balance of permeability and selectivity for a wide range of organic vapor/supercritical gas separations, PDMS is used commercially for the separation of organic compounds from air (Baker et al., 1987; Baker and Wijmans, 1994).

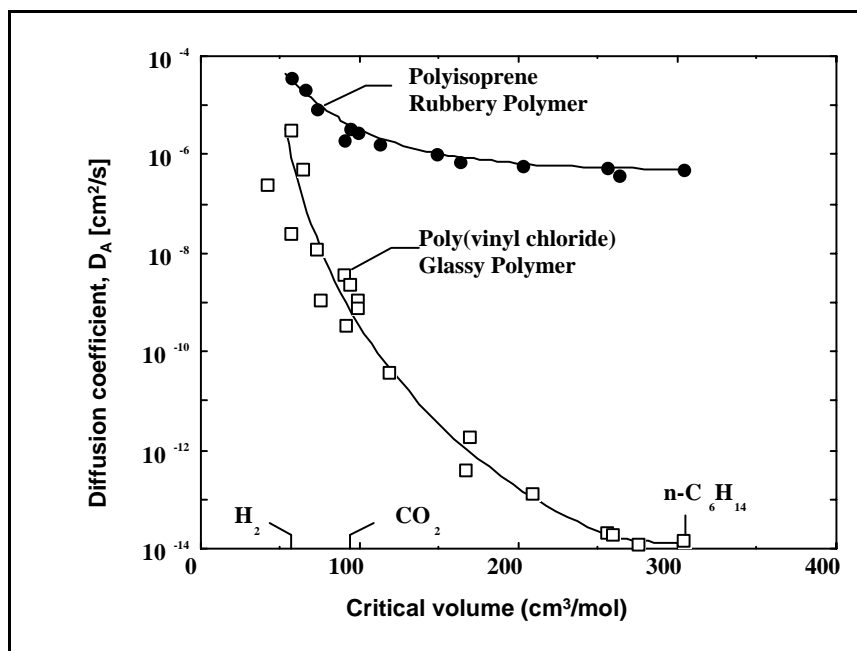
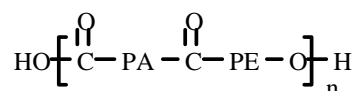


**Figure 2-7. Penetrant solubility in polysulfone and poly(dimethylsiloxane) at 35°C (95°F) and infinite dilution.**

For acid gas separations, there is also the possibility of using polymers that have an affinity for the acid gas component to further boost the solubility and, in turn, permeability of acid gas components. In this regard, it was recently discovered that microstructured block copolymers with high concentrations of flexible, polar ether linkages exhibit high permeability to CO<sub>2</sub> and the highest CO<sub>2</sub>/N<sub>2</sub> and CO<sub>2</sub>/H<sub>2</sub> separation factors reported for nonfacilitated transport polymeric membrane materials (Bondar et al., 1997). For example, CO<sub>2</sub>/H<sub>2</sub> separation factors at low feed pressure (1 bar) of 6.6 have been measured, and selectivity values increase with increasing CO<sub>2</sub> partial pressure up to values of almost 9 at a CO<sub>2</sub> partial pressure of 15 bar (Bondar et al., 1997). These high factors are accompanied by CO<sub>2</sub> permeability coefficients as high as 60 barrers. These commercial poly(ether-*b*-amide) (PE-*b*-PA) multiblock copolymers have the following general chemical structure:



where PA is an aliphatic polyamide “hard” block (nylon 6 [PA6] or nylon 12 [PA12]), and PE denotes a polyether “soft” block, either poly(ethylene oxide) [PEO] or poly(tetramethylene oxide) [PTMEO]. The soft polyether blocks are the locus of most of the gas transport and are therefore responsible for the separation efficacy of these materials. However, the mechanical properties of these wax-like, rubbery polyethers are not suitable for direct incorporation into robust, thin membranes such as those used industrially. The hard nylon blocks provide mechanical strength and can be used to tailor polymer rheological properties and solubility in the spinning dope used to prepare hollow fiber membranes on a commercial scale. Such

heterophase materials provide independent control of transport and separation efficacy (by tailoring soft block chemical structure, chain length, phase continuity, and the extent of block demixing) and solution processing characteristics via systematic manipulation of hard block composition and chain length. Based on pilot studies, the gas sorption and permeation properties of PE-*b*-PA block copolymers suggest strong favorable interactions between CO<sub>2</sub> and the ether linkages in the PE phase, resulting in unusually high CO<sub>2</sub> solubility and solubility selectivity in these polymers. These materials are sold commercially under the Pebax trademark by Elf-Atochem. One of the objectives of this research was to test the gas permeation properties of PEO and of new block copolymers based on PEO as the soft block.

### **2.3.2 Facilitated Transport/Solid Polymer Electrolytes**

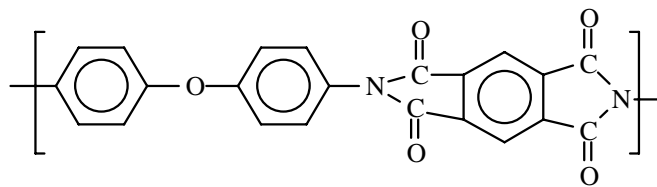
One method of strongly enhancing acid gas separations using membranes is to incorporate additives into polymers that interact specifically with the acid gas component (i.e., CO<sub>2</sub> or H<sub>2</sub>S) but not with light gas components (i.e., CO or H<sub>2</sub>). Solid polymer electrolytes, an entirely new class of hybrid inorganic/organic materials, are being studied for the separations of interest to this program. These materials consist of solid solutions of salts dissolved in hydrophilic rubbery polymer matrices such as PEO. The salts are selected to provide excellent solubility of acid gas or polar components such as CO<sub>2</sub> and H<sub>2</sub>S and, through enhanced solubility of these components, to achieve very high separation factors for CO<sub>2</sub>/H<sub>2</sub> or H<sub>2</sub>S/H<sub>2</sub>.

The scientific literature contains hints that this approach could be very useful. For example, Quinn et al. (1994, 1995a,b, 1997) showed that composite membranes prepared from PVBTAF (poly(vinylbenzyltrimethyl ammonium fluoride)) exhibited a CO<sub>2</sub>/H<sub>2</sub> selectivity value of 87. Also, a composite membrane of PDMS/PDADMAF/PDMS has an H<sub>2</sub>S/H<sub>2</sub> selectivity of 260. Blends of low molecular weight, liquid poly(ethylene glycol) (PEG) with salts containing a basic anion (Kawakami et al., 1983) (e.g., KF or CaF<sub>2</sub>) have been studied as immobilized liquid membranes and exhibit CO<sub>2</sub>/N<sub>2</sub> selectivity values as high as 110. This approach to materials design had never been tried for synthesis gas separation; this research effort explored the possibility of using such materials for sulfur removal from synthesis gas.

## **2.4 POLYMER SYNTHESIS, FILM PREPARATION, AND CHARACTERIZATION**

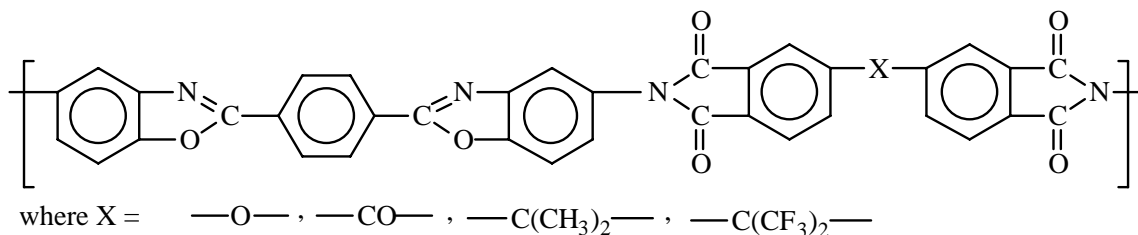
### **2.4.1 North Carolina State University**

A sample of Kapton polyimide film was provided to RTI for testing. The structure of Kapton polyimide is



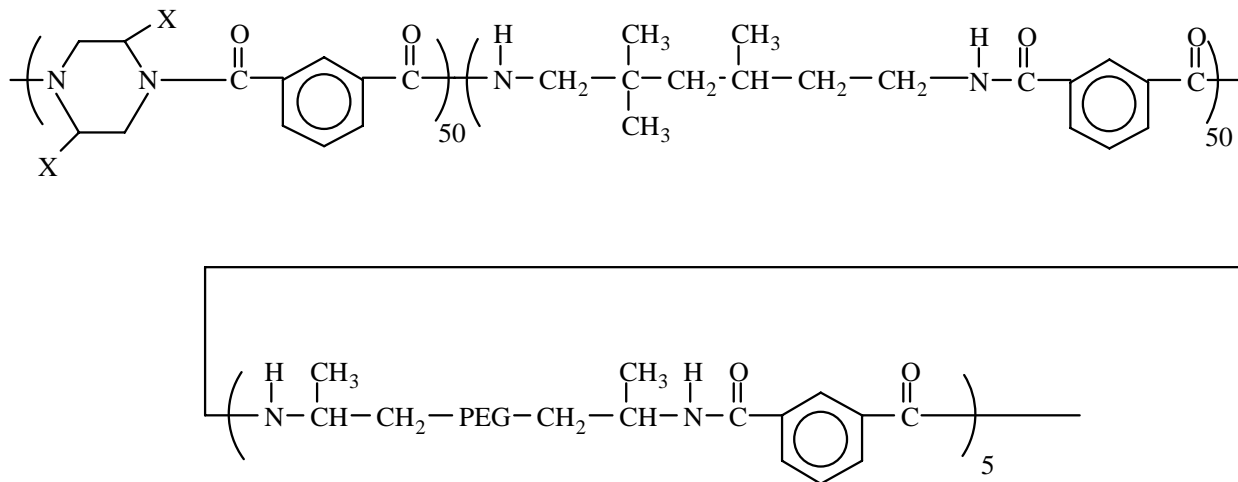
Kapton is a commercially available, high-glass-transition-temperature, thermally stable polyimide. While it was not expected to be acid-gas-selective at low temperature, it was hoped that Kapton might become acid-gas-selective at sufficiently high temperature. However, the permeability of this material was so low that it was impossible to characterize, and no further studies were conducted.

NCSU supplied representatives of benzoxazole-imide samples for testing at RTI. These materials have the following chemical structure:

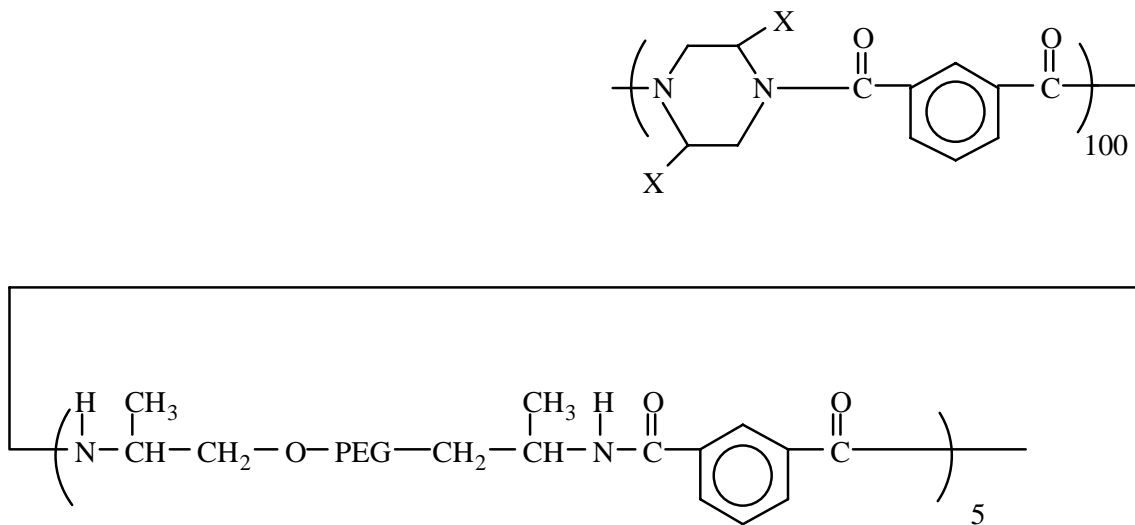


These materials are the most thermally stable polymers known and were thought to have excellent chemical resistance as well. These materials turned out to have extremely low permeability, difficult film formation characteristics, and no further work was undertaken.

Some of the most promising materials from the pilot studies were polyamide-polyether block copolymers. These materials had very high selectivity for acid gases in mixtures with permanent gases. Therefore, materials were prepared similar to the one shown below, which is based on the same design concept as the polyamide-polyether block copolymers:

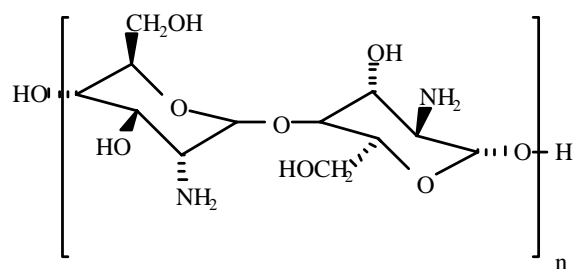


and



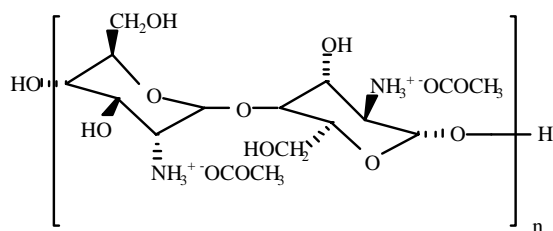
where X is either H or methyl, and PEG is poly(ethylene glycol) units with a nominal molecular weight of 2,000 g/mol. The advantage of these materials relative to the block copolymers is that they may be prepared with a wide range of acid-gas loving PEG units, providing a systematic series of materials for inclusion in the program. It was not possible to form strong defect-free films from these materials, so no further characterization was pursued.

Previous studies indicate that chitosan and chitin-based materials have extremely high water uptake and water permeability, two good indicators for highly selective polar/nonpolar gas separation membranes. Therefore, NCSU prepared several samples for characterization at RTI. The chemical structure of chitosan is:



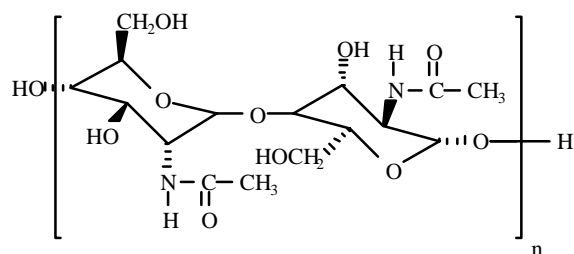
**Chitosan**

Chitin, the precursor to this naturally occurring polymer, is produced in the shells of crabs, shrimp, etc. Chitosan was also modified to increase its utility for acid gas separations. The chemical modification of chitosan is accomplished by contacting chitosan with an acid, such as acetic acid to form a salt:



**Water-Soluble Salt**

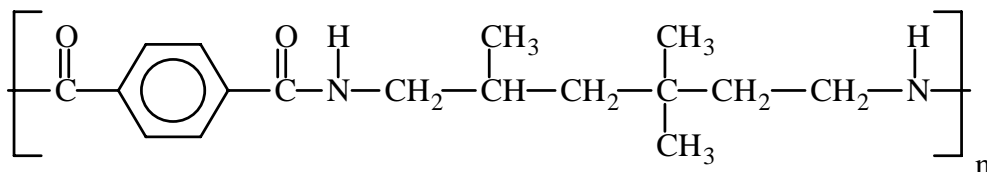
This salt can then be heated at rather mild conditions to convert the salt to the corresponding amide:



**Water-Insoluble Chitin**

However, preliminary gas permeation testing revealed that all samples were hydrogen selective rather than acid-gas-selective. So no further work was pursued with these materials.

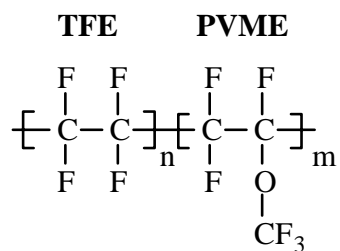
Compatible blends of Trogamide-T (TA) and poly(2-ethyl-2-oxazoline) (PEOXA) also offer high water uptake and high water permeability, which were expected to be a signature of strongly acid-gas-philic behavior. However, blended samples of this type were always hydrogen-selective, so further testing was not pursued. For reference, the chemical structure of TA is as follows:



**Trogamide-T [TA]**

An industrial source of novel triblock copolymers of the type PS-PEO-PS polystyrene was identified. The architecture of the chain backbone of these polymers is very different from that of the random segmented copolymers considered elsewhere in this research program. In this regard, these materials will provide an excellent test bed to evaluate the effect of chain architecture on acid gas/hydrogen separation performance. In general, there is no fundamental information in the literature to guide the selection of block copolymer architectures. Because PEO crystallizes, will be added to reduce the degree of PEO crystallinity. PS-PEO-PS is readily available from commercial sources with different molecular weights of PEO and PS blocks.

Based on some pilot test results during permeation system calibration at RTI, fluoropolymers were discovered to have unusually high CO<sub>2</sub>/H<sub>2</sub>S selectivity. Therefore, RTI was supplied a rubbery, random fluorocopolymer (DuPont 9918). This fluorinated rubbery copolymer is prepared from tetrafluoroethylene (TFE) and perfluoromethyl vinyl ether (PVME) and has the following chemical structure:



The composition of the sample supplied to RTI was 38.2 wt% (50.7 mole%) TFE and 61.8 wt% (49.3 mol%) PVME.

### 2.4.2 Characterization of PEO and PEO/salt blends

PEO films prepared by solution casting have a density of 1.21 g/cm<sup>3</sup>. DSC results showed that the crystallinity of these samples is 65 wt%, and the melting point is 66°C (151°F). Permeability coefficients at 35°C (95°F) are presented in Figure 2-8. CO<sub>2</sub> is much more permeable than the other gases considered, including H<sub>2</sub>. The CO<sub>2</sub>/H<sub>2</sub> pure gas selectivity is 7.4 at zero pressure and increases to 9.9 at 13 atm. Permeability coefficients of the other penetrants are essentially independent of pressure, which is consistent with their behavior in other polymers (Petropoulos, 1994).

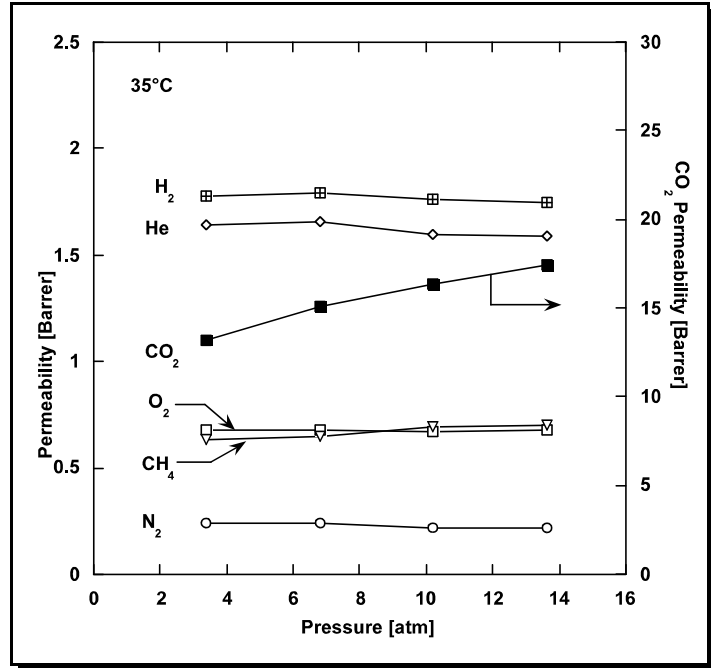


Figure 2-8. Effect of upstream pressure on PEO permeability coefficients at 35°C (95°F).

To provide some perspective of the CO<sub>2</sub>/H<sub>2</sub> separation properties of PEO, Figure 2-9 presents a so-called tradeoff curve for CO<sub>2</sub>/H<sub>2</sub> separation, where the ratio of CO<sub>2</sub>/H<sub>2</sub> permeability for a wide variety of polymers is presented as a function of the CO<sub>2</sub> permeability. All of the data points, except the two for PEO and a blend of PEO and salt, fall below the solid line, which provides a reference upper limit of performance for conventional polymers. Consistent with other separations that achieve high selectivity via high solubility selectivity, polymers that are more permeable to CO<sub>2</sub> generally have higher CO<sub>2</sub>/H<sub>2</sub> selectivity (Singh et al., 1998).

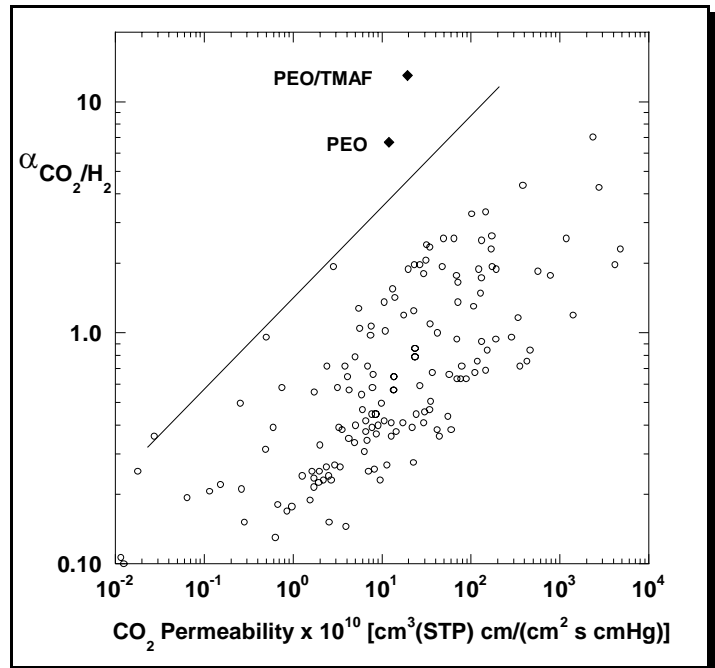


Figure 2-9. Effect of upstream pressure on PEO permeability coefficients at 35°C (95°F).

The effect of temperature on gas transport in pure PEO was studied. CO<sub>2</sub>/H<sub>2</sub> selectivity decreases with increasing temperature. The pure

gas selectivity at zero upstream pressure decreases from 8 at 25°C (77°F) to 6.2 at 45°C (113°F). The activation energy of permeation,  $E_p$ , was calculated, and the results are reported in Table 2-4.  $\text{CO}_2$  has the lowest  $E_p$ , 66 kJ/mol, while that of  $\text{H}_2$  is 75 kJ/mol.

**Table 2-4. Activation Energies of Permeation,  $E_p$ , in PEO at Infinite Dilution**

Gas	$\text{N}_2$	$\text{O}_2$	He	$\text{H}_2$	$\text{CH}_4$	$\text{CO}_2$
$E_p$ (kJ/mol)	105	84	73	75	114	66

Figure 2-10 presents sorption isotherms in PEO. The isotherms are linear ( $\text{O}_2$ ,  $\text{N}_2$ , and  $\text{CH}_4$ ) or nearly linear ( $\text{CO}_2$ ), which is consistent with sorption results in other rubbery polymers (Stern, 1994). Gas concentration increases with penetrant critical temperature. For example  $\text{CO}_2$  is much more soluble than the other gases.  $\text{CO}_2$  solubility selectivity is higher in PEO than in other less polar rubber polymers. For example, in PEO,  $\text{CO}_2/\text{CH}_4$  infinite dilution solubility selectivity is 6.7, while in PDMS, selectivity is only 3, which suggests that the polar nature of PEO enhances  $\text{CO}_2$  sorption (Ghosal and Freeman, 1994).

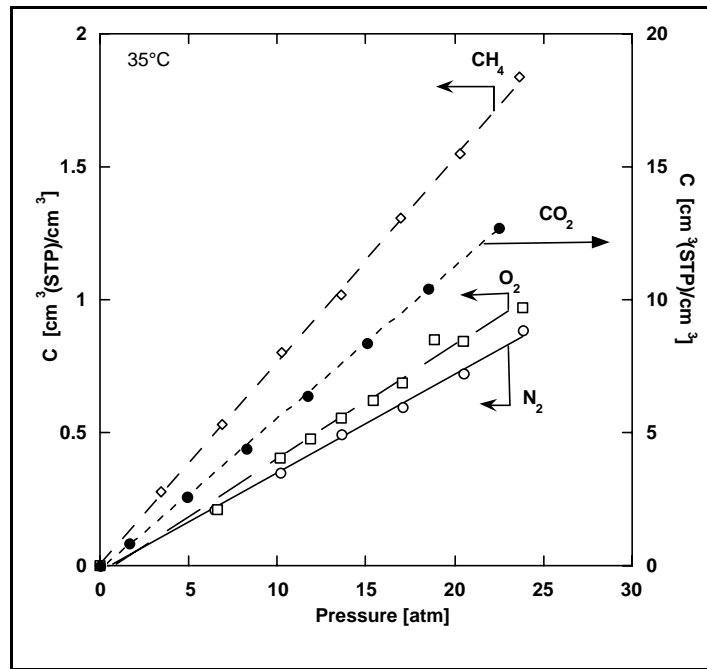


**Figure 2-10. Sorption isotherms in PEO at 35°C (95°F).**

Blends of PEO and salts containing basic anions were studied. Preliminary results are presented in Table 2-5. The film containing KF was measured at 35°C (95°F), while the film with  $(\text{CH}_3)_4\text{NF}$  was studied at 25°C (77°F). The addition of KF to the polymer matrix decreased  $\text{CO}_2/\text{H}_2$  selectivity. Further addition of KF causes phase separation in the blend sample and the film becomes brittle. The addition of 22 wt% TMAF ( $(\text{CH}_3)_4\text{NF}$ ) increases both  $\text{CO}_2$  permeability and  $\text{CO}_2/\text{H}_2$  pure

**Table 2-5. Effect of Salt Additive on Gas Transport at 6.8 Bars**

Salt	Loading (wt%)	$\text{CO}_2$ Permeability (Barrer)	$\text{CO}_2/\text{H}_2$ Selectivity
None (25°C [77°F])		12	9.3
None (35°C [95°F])		15	8.4
KF	20	21	7.7
$(\text{CH}_3)_4\text{NF}$	22	19	13

gas selectivity. This result suggests that such salt/polymer blends may be a promising future avenue of exploration in the research for highly CO<sub>2</sub> selective membranes.

### 2.4.3 MEDAL Samples

Numerous novel thermoplastic elastomers were synthesized with potential for enhanced acid gas (CO<sub>2</sub>, H<sub>2</sub>S) permeability versus H<sub>2</sub> at MEDAL. The primary focus was on hard-soft segment block copolymers incorporating a high degree of polar groups thought to promote affinity with polar penetrants. The ability to quickly synthesize materials for this study was aided significantly by research chemists from DuPont who have a wealth of experience with similar materials (e.g., Lycra®, Hytrel®).

Figure 2-11 shows a partial list of soft and hard segment monomers employed in this study. These monomers, while not exotic or expensive, provide a means to examine multiple complex factors such as soft segment polarity, soft segment chain length, hard segment polarity, and hard segment crystallinity. It should be noted that virtually all of the materials synthesized are not easily dissolved in common solvents. Also, it is well known that materials made from the monomers shown in Figure 2-11 are likely to exhibit strong sensitivity to moisture. That is,

they often swell and become gel-like and tacky in high relative humidity. Thus, a major objective in this study was to make materials with an affinity to polar gases while limiting moisture sensitivity. A material with “balance” hydrophilicity may be key to providing a means for the processing and handling necessary in commercial fabrication. The thermoplastic elastomers supplied for this study were primarily block copolymers, consisting of roughly 60 to 80% polyether soft segment. The remainder consisted of a variety of hard segments. The hard segments were polyimides (PI), polyamides (PA), polyesters (PE), polyurethanes (PU), and polyureas (Pur). Both aromatic and aliphatic hard segments were examined. Of the numerous films synthesized and that exhibited sufficient molecular weight, flat films were formed via solvent casting or melt press 200-250°C (392 to 482°F). These films were then tested at MEDAL using a pure gas permeability apparatus with 8 atm CO<sub>2</sub> and H<sub>2</sub> feed with vacuum permeate at approximately 25°C (77°F). Films showing good permeation and selectivity were

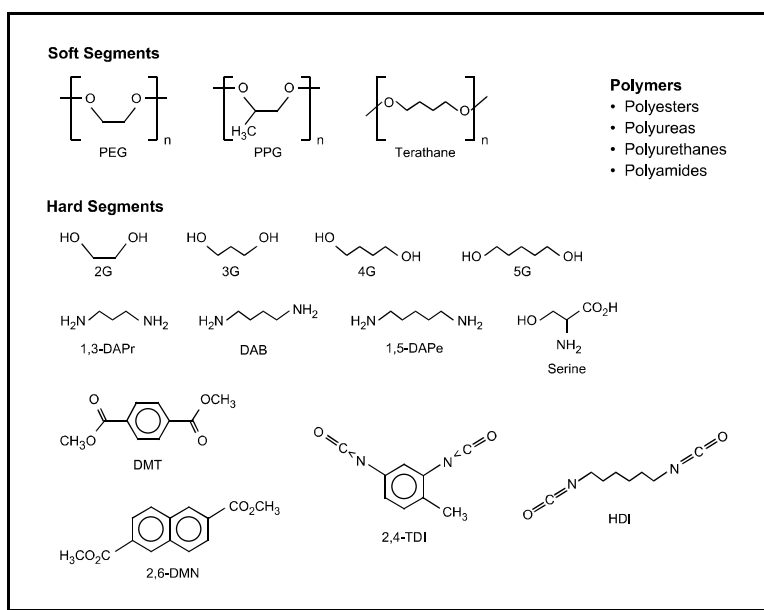


**Figure 2-11. Monomers employed in MEDAL-supplied materials.**

then passed on to RTI for mixed gas testing. Table 2-6 shows the films provided to RTI for testing. Note that, as the program progressed, pure gas selectivities increased steadily.

## 2.5 HIGH-TEMPERATURE/HIGH-PRESSURE (HTHP) MEMBRANE TESTING

### 2.5.1 RTI's Membrane Test Facility

A mixed-gas, high-temperature, permeation apparatus was designed and constructed at RTI in order to screen candidate polymer materials for their ability to separate acid gases ( $H_2S$  and  $CO_2$ ) from syngas at the proposed process conditions. A schematic representation of this system is provided in Figure 2-12. The pertinent features of this test apparatus include a membrane cell that contains the polymer sample to be tested, mass flow controllers to regulate the flow rate of feed and sweep gases, gas chromatographs for measuring the compositions of permeate and/or residue streams, and an insulated, leak-proof housing for temperature and hazardous emissions control. This system has the ability to measure pure or mixed-gas permeability coefficients in polymer materials at various upstream pressures from room temperature up to  $220^\circ C$  ( $428^\circ F$ ).

**Table 2-6. Pure Gas Permeabilities of MEDAL Synthesized Films**

Pure Gas Measures		
Film No.	$PCO_2(b)$	$P(CO_2)/P(H_2)$
1	59	2.66
2	13.6	2.83
3	532	3.04
4	301	3.18
5	336	2.9
6	450	5.5
7	330	5.5
8	33	6.71
8	264	6.52
10	373	5.54
11	190	5.27
12	660	6.38
13	974	7.42
14	1082	7.42
15	586	7.66
16	242	6.85
17	303	6.73
18	222	7.02
19	--	--
20	--	--
21	249	8.28
22	--	--

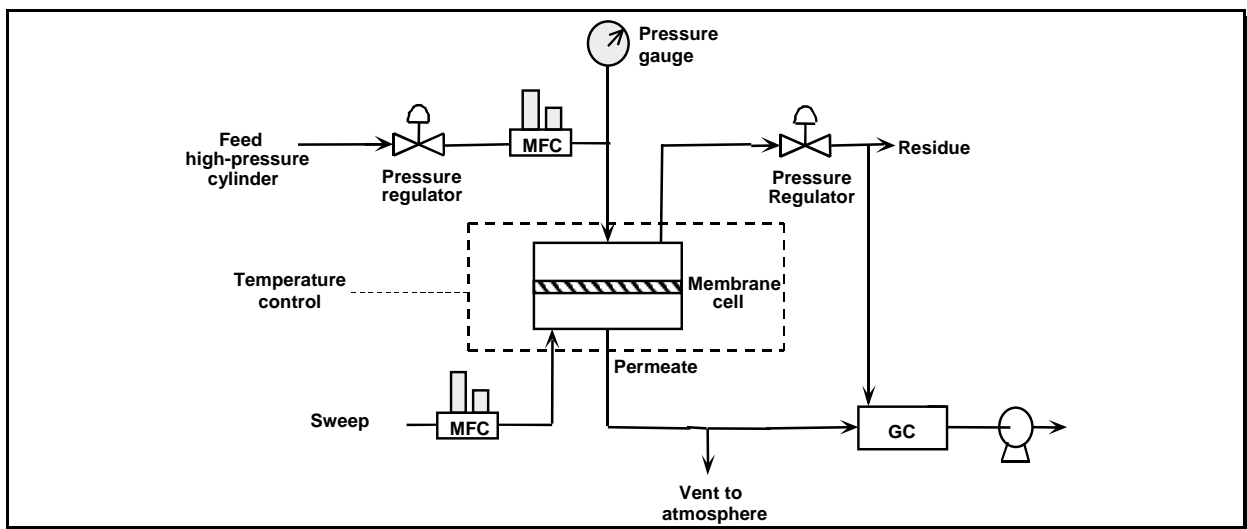


**Figure 2-12. Schematic diagram of membrane apparatus.**

The system was initially calibrated by measuring pure and mixed-gas permeabilities in PDMS, a standard solubility selective polymer whose transport properties near room temperature are well documented (Merkel et al., 2000). The results of these tests are presented in Figures 2-13 and 2-14. CO<sub>2</sub> permeability coefficients in PDMS, calculated via two different methods, are compared in Figure 2-13 as a function of the pressure difference across the polymer membrane,  $\Delta p$ . The points labeled “no sweep” were obtained by directly measuring gas flux through PDMS, while those labeled “He sweep” were calculated by using a gas chromatograph (GC) to measure permeate composition. Values obtained by the two methods are equivalent within experimental uncertainty and are consistent with literature CO<sub>2</sub> permeability coefficients (Merkel et al., 2000). This result demonstrates the validity of using a helium sweep in conjunction with an inline GC to measure permeability coefficients. Figure 2-14 presents the mixed-gas O<sub>2</sub>/N<sub>2</sub> selectivity (i.e., ratio of mixed gas permeability coefficients) of PDMS at room temperature as a function of  $\Delta p$ . The measured value of ~2 is consistent with literature values for this polymer (Merkel et al., 2000) and, together with the CO<sub>2</sub> data, provides strong evidence that the system is producing reliable data.

### 2.5.2 Characterization of a Baseline Solubility Selective Polymer: Poly(dimethylsiloxane)

As mentioned previously, PDMS is a standard solubility selective polymer used commercially for removing large condensable vapors from permanent gases (Baker et al., 1987; Baker and Wijmans, 1994). As such, it is known to be more permeable to CO<sub>2</sub> than to H<sub>2</sub> at room temperature. Because the transport of common gases (N<sub>2</sub>, O<sub>2</sub>, H<sub>2</sub>) in PDMS is well understood,

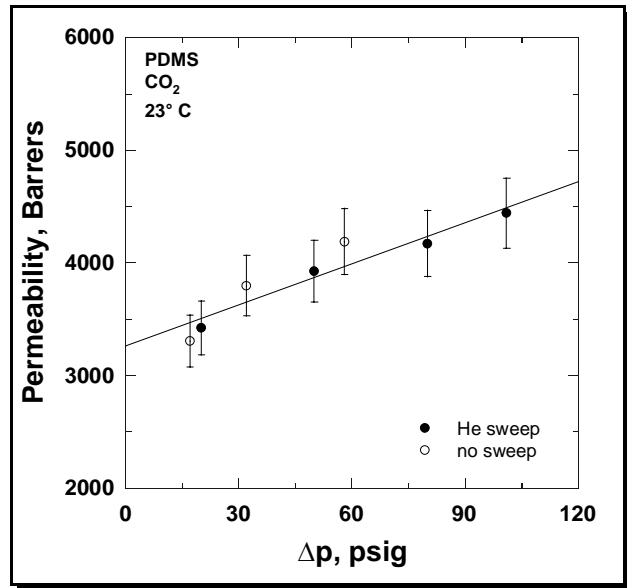


Figure 2-13. Pure gas CO<sub>2</sub> permeability coefficients in PDMS as measured by direct flux (no sweep) and via gas chromatograph analysis of permeate composition (He sweep).

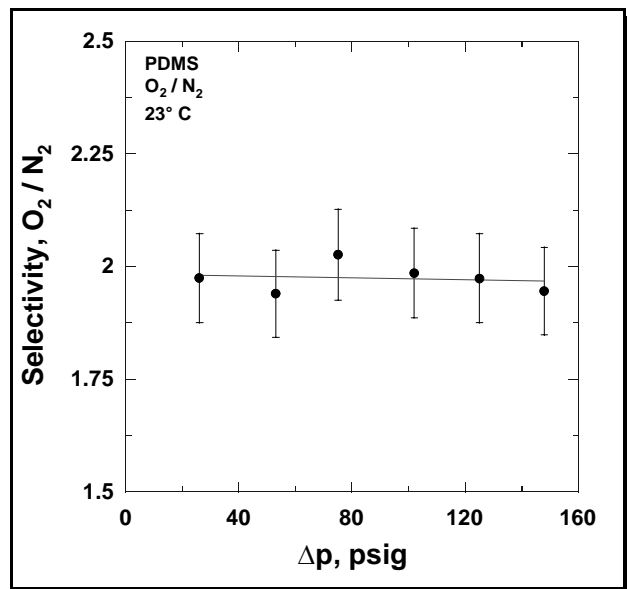
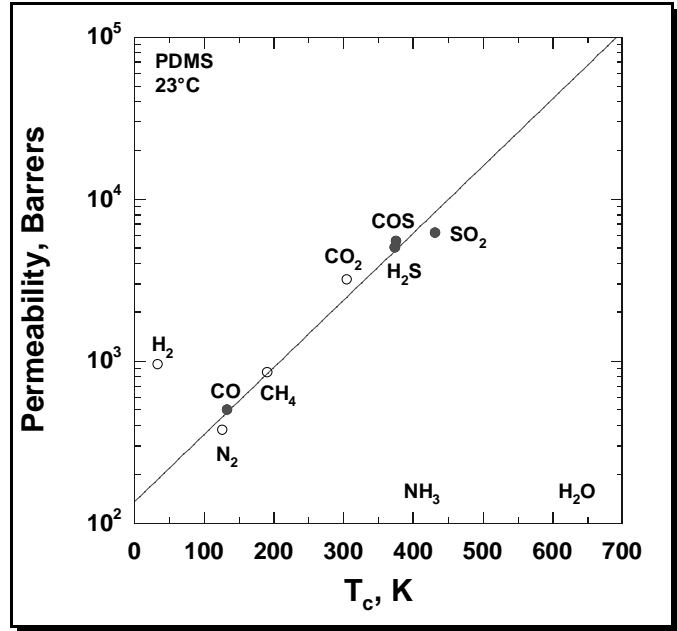


Figure 2-14. Mixed-gas O<sub>2</sub>/N<sub>2</sub> selectivity of PDMS as a function of transmembrane pressure difference.

this polymer will serve as a valuable baseline material to compare with novel candidate polymers to be tested later. Figure 2-15 presents the permeability coefficients of syngas components at room temperature in PDMS as a function of the gas critical temperature,  $T_c$  (Merkel et al., 2001). Frequently, in a solubility-selective polymer such as PDMS, there is a strong correlation between the logarithm of gas permeability and  $T_c$  (Freeman and Pinnau, 1997; Van Amerongen, 1964). Generally, as critical temperature increases, a penetrant becomes more soluble in the polymer and therefore more permeable, since permeability is equal to the product of solubility and diffusivity.



**Figure 2-15. Syngas permeability coefficients in PDMS as a function of gas-critical temperature. Experimental conditions: upstream pressure = 20 psig, room temperature.**

The results in Figure 2-16 follow this trend with the exception of hydrogen. This is often the case, as the extremely small molecular size of hydrogen results in a high diffusion coefficient and, consequently, a higher permeability coefficient than expected based on its  $T_c$ . Most important for this project, note that the permeability coefficients of CO, COS, SO<sub>2</sub>, and H<sub>2</sub>S gases, for which almost no transport data exist, follow the general trendline through the other penetrants. This confirms the assumption that the permeation properties of these compounds are consistent with their molecular properties. Consequently, H<sub>2</sub>S as well as COS and SO<sub>2</sub> are more permeable than H<sub>2</sub> (Stern and Bhide, 1989) in PDMS and will preferentially permeate through the membrane. Additionally, the high critical temperatures of H<sub>2</sub>O and NH<sub>3</sub> indicate that these compounds will also be much more permeable than H<sub>2</sub> (this assertion is supported by literature permeation data). Meanwhile, CO is less permeable than H<sub>2</sub> and will be retained predominantly in the main syngas stream as is desired. These permeation results are critical for the proposed process to be economically viable.

In addition to room temperature data (Figure 2-15), data on how polymer permeation properties change with temperature were gathered. Figure 2-16 presents permeability coefficients of H<sub>2</sub>, N<sub>2</sub>, CO, CO<sub>2</sub>, and H<sub>2</sub>S in PDMS as a function of system temperature. The data in this figure for temperatures above approximately 90°C (194°F) are novel for all penetrants, even common gases such as nitrogen. For each of the penetrants examined, permeability coefficients increase with temperature. This behavior is typical of gases in many polymers and can be described by an Arrhenius relation (Ghosal and Freeman, 1994):

$$P = P_0 \exp\left(\frac{-E_p}{RT}\right) \quad (7)$$

where  $P$  = permeability coefficient  
 $P_o$  = front factor  
 $E_p$  = activation energy of permeability  
 $R$  = universal gas constant  
 $T$  = absolute temperature.

Based on this definition, permeability increases with temperature for positive values of  $E_p$ , and the greater the magnitude of  $E_p$ , the stronger is the temperature dependence.

From the data presented in Figure 2-15, activation energies of permeation in PDMS were calculated via Equation 7 and are listed in Table 2-7 along with available literature values (Bixler and Sweeting, 1971). There is excellent agreement between previous results and the  $E_p$  values for  $H_2$  and  $N_2$ . Based on the data in Table 2-7 and Figure 2-16, the temperature dependence of permeability is much weaker for  $H_2S$  and  $CO_2$  as compared to the light gases. This result may be explained as follows: light gases, such as  $H_2$ , have very low solubility in PDMS. As temperature increases,  $H_2$  solubility in PDMS decreases, but only slightly since solubility is low to begin with. This solubility effect is more than offset by the large increase in hydrogen's diffusion coefficient as temperature increases. Consequently,  $H_2$  permeability in PDMS increases rather substantially with temperature. In contrast, more condensable vapors, such as  $CO_2$ , are much more soluble in PDMS than  $H_2$ . As temperature increases,  $CO_2$  solubility decreases at a rate nearly equal to the increase in diffusion coefficient of  $CO_2$ . As a result, the composite property, permeability, increases only slightly with temperature.

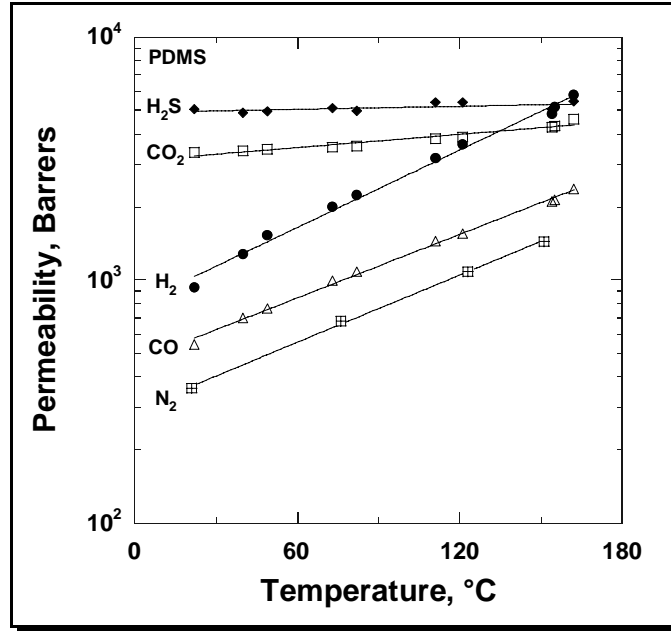


Figure 2-16. Permeability coefficients in PDMS as a function of system temperature.

The effect of solubility on the temperature dependence of permeability in PDMS is illustrated in Figure 2-17. This figure presents activation energies of permeability in PDMS as a function of gas critical temperature. As mentioned previously,  $T_c$  is a scaling factor for gas solubility in a polymer. Based on the data in this figure, as gas critical temperature (or solubility) increases, activation energies of permeation decrease monotonically. Thus, the increase in

Table 2-7. Activation Energies of Permeation in PDMS

Penetrant	Activation Energy of Permeation ( $E_p$ ), kJ/mol	
	This Study	Literature Values (Bixler & Sweeting, 1971)
$H_2$	13.4	13.7
$N_2$	10.9	10.8
CO	11	--
$CO_2$	2.2	--
$H_2S$	0.5	--

permeability with temperature becomes smaller in magnitude as penetrant solubility increases, and, in fact, for species more soluble than H<sub>2</sub>S, permeability may decrease with temperature. Note that values for H<sub>2</sub>S and CO fall on the trendline through the other penetrants, indicating once again that the transport properties of these rarely studied penetrants are consistent with their critical temperatures.

Figure 2-18 presents the selectivity of PDMS for CO<sub>2</sub> and H<sub>2</sub>S over H<sub>2</sub> as a function of temperature. At room temperature, PDMS is approximately 5.5 and 3.6 times more permeable to H<sub>2</sub>S and CO<sub>2</sub>, respectively, than to H<sub>2</sub>. However, because of the effects discussed above, both selectivities decrease markedly as temperature increases. For example, at 150°C (302°F), PDMS is more permeable to H<sub>2</sub> than to either H<sub>2</sub>S or CO<sub>2</sub>. This result, which could be predicted from low-temperature data, is the first experimental documentation of a CO<sub>2</sub> (or H<sub>2</sub>S)/H<sub>2</sub> selectivity reversal in PDMS. The loss of acid gas/hydrogen selectivity in PDMS, demonstrates the need to develop novel solubility selective polymers to perform high-temperature separations.

### 2.5.3 Characterization of MEDAL Polymer Samples

Numerous polymeric samples, with potential for selective permeation of CO<sub>2</sub> over H<sub>2</sub> at high temperatures, were synthesized by MEDAL. Polymers with sufficient molecular weight and solubility properties were cast as a dense film of approximate dimensions 10 cm x 10 cm and ~50 μm thickness. Pure gas CO<sub>2</sub>

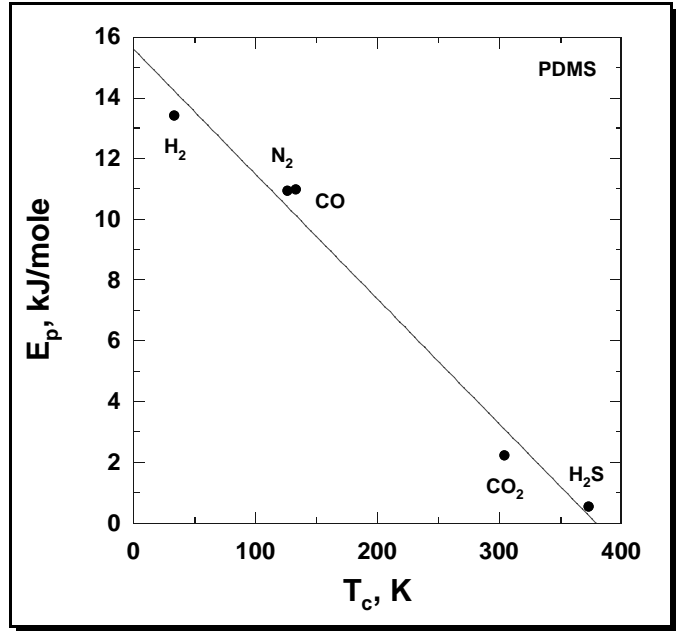


Figure 2-17. Activation energies of permeation in PDMS as a function of gas-critical temperature.

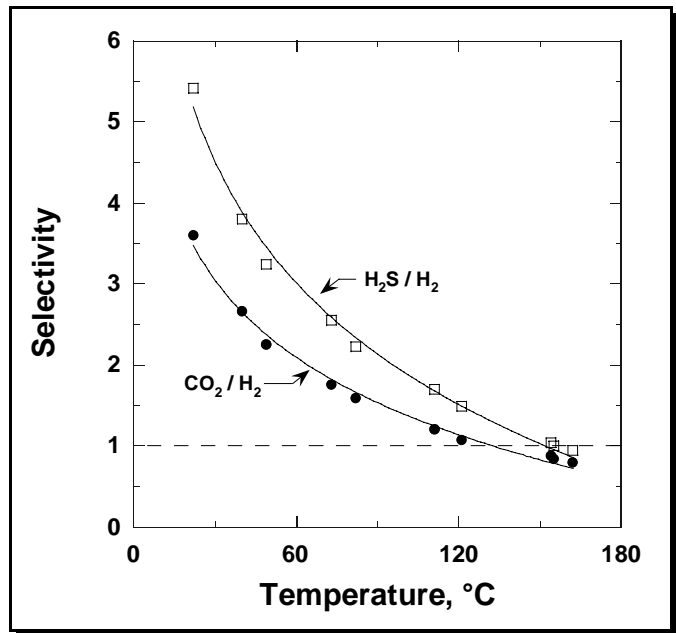


Figure 2-18. Mixed-gas H<sub>2</sub>S/H<sub>2</sub> and CO<sub>2</sub>/H<sub>2</sub> selectivity of PDMS as a function of system temperature.

and H<sub>2</sub> permeation tests were performed on the dense film samples at approximately 8 atm (abs) and 30°C (86°F) at MEDAL. After this initial screening, samples exhibiting preferential CO<sub>2</sub> selectivity were supplied to RTI for additional mixed gas and high-temperature testing. Table 2-8 summarizes permeation and selectivity data for these polymers at room temperature. Pure gas CO<sub>2</sub> permeability coefficients measured by MEDAL are somewhat higher than mixed gas values obtained at RTI. This result is consistent with the fact that CO<sub>2</sub> transmembrane pressure difference was substantially higher in the MEDAL pure gas experiments (116 psia) compared to the mixed gas experiments at RTI (10-20 psia) (CO<sub>2</sub> permeability increases with transmembrane partial pressure difference). Most important for this project, note that the H<sub>2</sub>S/H<sub>2</sub> selectivity of MEDAL polymers generally increases with sample number. For example, while the early samples (i.e., MEDAL 001-005) have selectivities comparable to that of PDMS, more recent batches have selectivities greater than 20, with MEDAL 018 having a selectivity of 36 for H<sub>2</sub>S/H<sub>2</sub> at ambient temperatures, which is close to the project target of 40. However, this selectivity value drops rapidly as the temperature is increased, which is not completely unexpected. At 93°C (>200°F), the best selectivity value obtained was about 10 for H<sub>2</sub>S/H<sub>2</sub>. The effect of temperature on H<sub>2</sub>S/H<sub>2</sub> selectivity for all of the polymers listed in Table 2-8 is presented in Figure 2-19. In each case, selectivity drops systematically as temperature increases. This behavior is typical for solubility selective membranes where transport occurs by a solution-diffusion mechanism and underscores the inherent difficulty in performing high-temperature separations of this nature. Nevertheless, note that the MEDAL polymers maintain substantially higher selectivities as compared to PDMS at elevated temperatures. Similar temperature effects are observed for the gas pair CO<sub>2</sub>/H<sub>2</sub>.

**Table 2-8. Summary of MEDAL Polymers Permeation Properties**

Polymer	CO <sub>2</sub> Permeability (Barrers)		Mixed Gas Selectivity	
	MEDAL Pure Gas	RTI Mixed Gas	CO <sub>2</sub> /H <sub>2</sub>	H <sub>2</sub> S/H <sub>2</sub>
PDMS <sup>a</sup>	--	3400	3.6	5.4
MEDAL 001 <sup>b</sup>	59	19	3.3	8.3
MEDAL 002 <sup>b</sup>	14	7.5	3.5	12
MEDAL 003 <sup>b</sup>	530	300	3.6	4.9
MEDAL 004 <sup>b</sup>	300	200	3.5	4.9
MEDAL 005 <sup>b</sup>	340	120	3	4.5
MEDAL 006 <sup>b</sup>	450	74	4.2	16
MEDAL 007 <sup>b</sup>	330	47	4.3	17
MEDAL 016 <sup>c</sup>	240	115	4.6	33
MEDAL 017 <sup>c</sup>	--	92	4.7	26
MEDAL 018 <sup>c</sup>	--	115	6.4	36
MEDAL 019 <sup>b</sup>	--	38	3	--
MEDAL 020 <sup>b</sup>	--	42	4.5	22
MEDAL 021 <sup>b</sup>	--	95	6.5	27
MEDAL 022 <sup>b</sup>	--	34	6.2	22

All data are room temperature. Pure gas experiments conducted at 116 psia upstream pressure.

<sup>a</sup>20 psig upstream pressure.

<sup>b</sup>100 psig upstream pressure.

<sup>c</sup>200 psig upstream pressure.

### 2.5.4 Characterization of NCSU Polymer Samples

Table 2-9 summarizes the permeation properties of NCSU polymer samples tested at RTI. Pebax 4011 is a block copolymer that possesses the highest reported CO<sub>2</sub>/H<sub>2</sub> selectivity at room temperature (Bondar et al., 1997). Results confirm this relatively high separation factor and show that its H<sub>2</sub>S/H<sub>2</sub> selectivity is near the values obtained for some of the better-performing MEDAL samples. Similarly, poly(ethylene oxide) [PEO], which is a component of Pebax 4011, exhibits good room temperature selectivities and was examined for its capacity to serve as a host matrix for acid gas affinity salts. The bulk of the remaining

NCSU polymers tested at RTI were fluorinated materials (i.e., AF1600, AF2400, DuPont 9918, 6F-6F PI) and were examined because of their known chemical and thermal stability. All of these fluoropolymers were unexpectedly found to be quite H<sub>2</sub> selective over H<sub>2</sub>S. This result is related to previously unknown permeation behavior, which is discussed in the following paragraph.

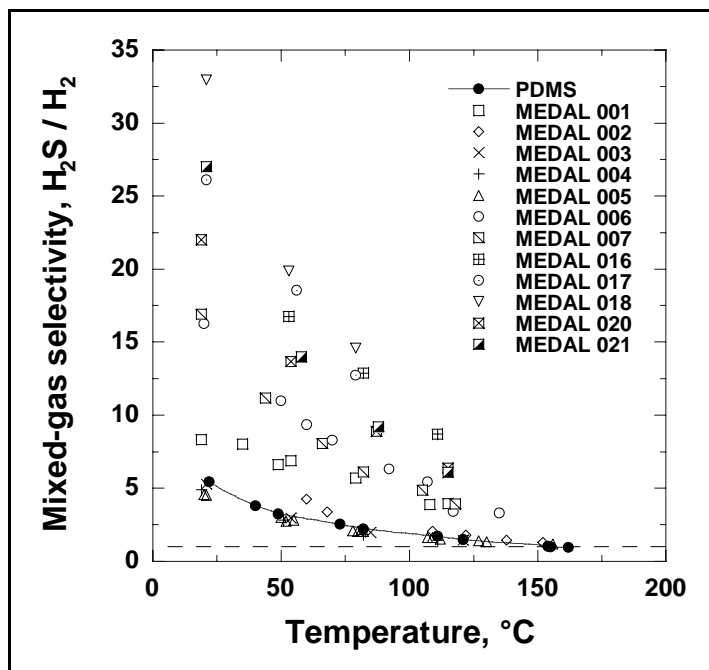


Figure 2-19. Mixed-gas H<sub>2</sub>S/H<sub>2</sub> selectivity as a function of system temperature.

Table 2-9. Summary of Permeability and Selectivity Data for NCSU Samples

Polymer	CO <sub>2</sub> Permeability (Barrers)		Mixed Gas Selectivity	
	NCSU Pure Gas	RTI Mixed Gas	CO <sub>2</sub> /H <sub>2</sub>	H <sub>2</sub> S/H <sub>2</sub>
PDMS	3300	3400	3.6	5.4
Pebax 4011	--	58	6.4	31
PEO	--	13	6.4	31
PTMSP <sup>a</sup>	25000	18000	1.5	1.8
AF1600 <sup>b</sup>	490	720	1	0.15
AF2400 <sup>a</sup>	2100	2300	1.3	0.22
DuPont 9918	0	28	0.6	0.1
6F-6F PI	--	61	1.2	0.2

Figure 2-20 presents permeability coefficients in rubbery PDMS and a glassy copolymer of tetrafluoroethylene and 2,2-bis(trifluoromethyl)-4,5-difluoro-1,3-dioxole [AF1600] as a function of gas critical temperature. For both polymers, permeability generally increased with gas condensability; however, note that the permeability coefficient of H<sub>2</sub>S in AF1600 was much lower than predicted by the trendline through the other penetrants. Consequently, in contrast PDMS where H<sub>2</sub>S is more permeable than CO<sub>2</sub>, the permeability coefficient of H<sub>2</sub>S is substantially lower than that of CO<sub>2</sub> in AF1600.

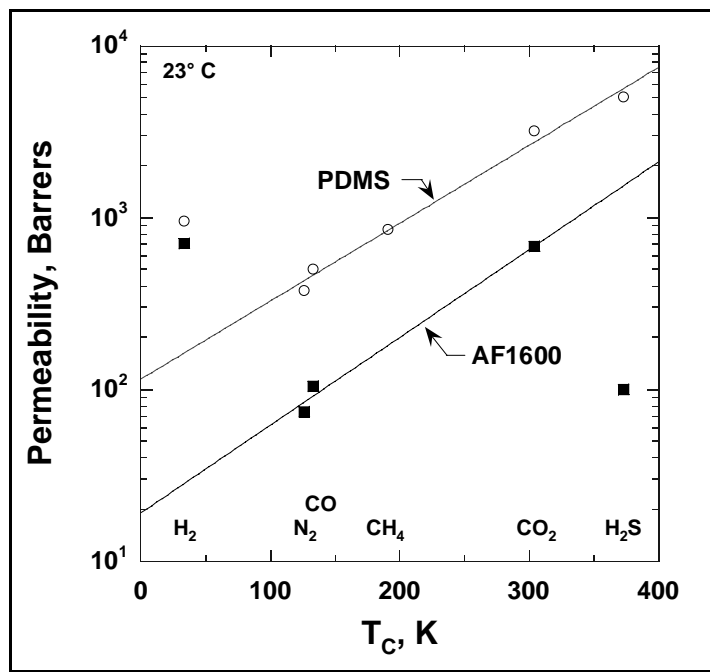


Figure 2-20. Permeability coefficients in PDMS and AF1600 as a function of gas-critical temperature.

This unexpectedly low H<sub>2</sub>S permeability is probably related to very low H<sub>2</sub>S solubility in the fluorinated matrix of AF1600. Similar results were exhibited by the other fluorinated polymers examined, suggesting an important material selection guideline: fluorinated polymers, while attractive because of their stability, will likely not possess the high H<sub>2</sub>S permeability required to selectively remove H<sub>2</sub>S from syngas. At the same time, this unusual permeation behavior results in atypical CO<sub>2</sub>/H<sub>2</sub>S selectivities that could possibly be useful in other applications.

Table 2-10 illustrates this point by comparing CO<sub>2</sub>/H<sub>2</sub>S selectivities in fluorinated and nonfluorinated polymers. Typical hydrocarbon-based polymers, such as PDMS, tend to be selective for H<sub>2</sub>S over CO<sub>2</sub> because of hydrogen sulfide's greater condensability.

In contrast, the fluoropolymers are selective for CO<sub>2</sub> because of their low permeability to H<sub>2</sub>S, and this selectivity increases as polymer permeability decreases. This result is likely due to the fact that less permeable polymers tend to have less free volume and thus closer contact between penetrant and polymer. This close contact may enhance the

Table 2-10. CO<sub>2</sub>/H<sub>2</sub>S Selectivity of Fluorinated and Nonfluorinated Polymers

Polymer	CO <sub>2</sub> Permeability, Barrers	Selectivity CO <sub>2</sub> /H <sub>2</sub> S
PDMS <sup>a</sup>	3200	0.63
Pebax 1657 <sup>b</sup>	69	0.27
Pebax 1074 <sup>b</sup>	122	0.22
DuPont 9918	28	8
AF1600	680	6.8
AF2400	2300	6

<sup>a</sup>Merkel et al., 2001.

<sup>b</sup>Chatterjee et al., 1997.

unfavorable fluorocarbon-H<sub>2</sub>S interaction, further suppressing hydrogen sulfide permeability and increasing CO<sub>2</sub>/H<sub>2</sub>S selectivity.

## 2.6 MEMBRANE MODULE SIMULATIONS

Using a membrane simulator developed at NCSU (Coker et al., 1998), preliminary calculations were made to estimate the loss of H<sub>2</sub> and CO as a function of the extent of H<sub>2</sub>S (or CO<sub>2</sub>) removed from syngas. These simulations were based on the standard syngas composition, feed conditions, and the separation properties of MEDAL 018 at room temperature. Figure 2-21 presents the percent of inlet hydrogen that permeates the membrane as a function of the percent of inlet CO<sub>2</sub> that is removed in the permeate. Of course, ideally, all of the CO<sub>2</sub> would be removed in the permeate without any H<sub>2</sub> loss through the membrane (corresponding to the bottom right corner of the plot). Because the RTI membrane has a finite selectivity, there is a tradeoff, with the amount of hydrogen lost increasing as the amount of carbon dioxide removed increases. The data in Figure 2-21 give valuable information about the operating envelope for the polymer materials studied to date.

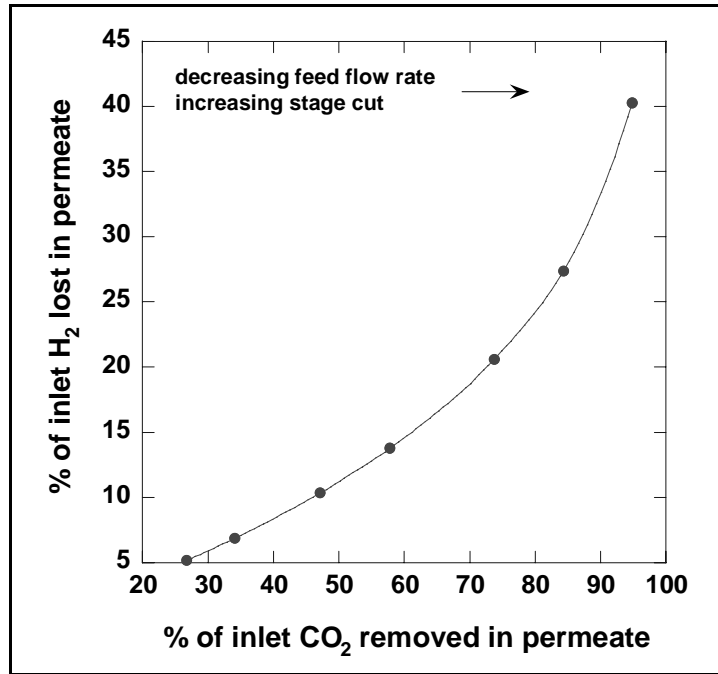


**Figure 2-21.** NCSU simulator's calculated H<sub>2</sub> loss as a function of CO<sub>2</sub> removal. Based on the transport data of MEDAL 018 at room temperature with a standard syngas feed at 600 psia.

Figure 2-22 presents additional useful information from the membrane simulation. These data are presented in the same manner as the CO<sub>2</sub> results (Figure 2-21) with the addition of a second y-axis, which provides information about the amount of H<sub>2</sub>S remaining in the CO/H<sub>2</sub>-enriched residue stream. As an example, removing 80% of the inlet H<sub>2</sub>S from syngas leaves approximately 1,500 ppm of H<sub>2</sub>S in the H<sub>2</sub>-enriched syngas, about 13% of the inlet H<sub>2</sub> will permeate the membrane, and 50% of CO<sub>2</sub> will be removed from syngas. Based on this membrane performance, 80% to 90% removal of H<sub>2</sub>S from syngas is feasible without appreciable loss of H<sub>2</sub> and CO (Btu value). Additionally, this loss of H<sub>2</sub> and CO in the permeate stream is not really a loss in terms of overall thermal efficiency for an IGCC configuration since this stream can be used as a reductant for the direct sulfur recovery process (DSRP) and/or to heat the regeneration inlet gas for the monolith system. Various process design configurations

are being considered to optimize heat integration, including use of a size-selective membrane to strip H<sub>2</sub> from the permeate stream of the solubility-selective membrane.

## 2.7 SUMMARY AND FUTURE WORK

Significant progress was made in synthesizing polymer membranes which exhibit high H<sub>2</sub>S/H<sub>2</sub> selectivities. During the research, it was established that transport behavior in these polymers was consistent with the penetrant's molecular properties. An increase in system temperature resulted in a systematic decrease in H<sub>2</sub>S/H<sub>2</sub> selectivity. Process simulations indicated that 80-90% H<sub>2</sub>S removal was possible without appreciable H<sub>2</sub> loss.

Future work under the Option Program will involve fabrication, production and testing of membrane modules in RTI's HTHP facility.

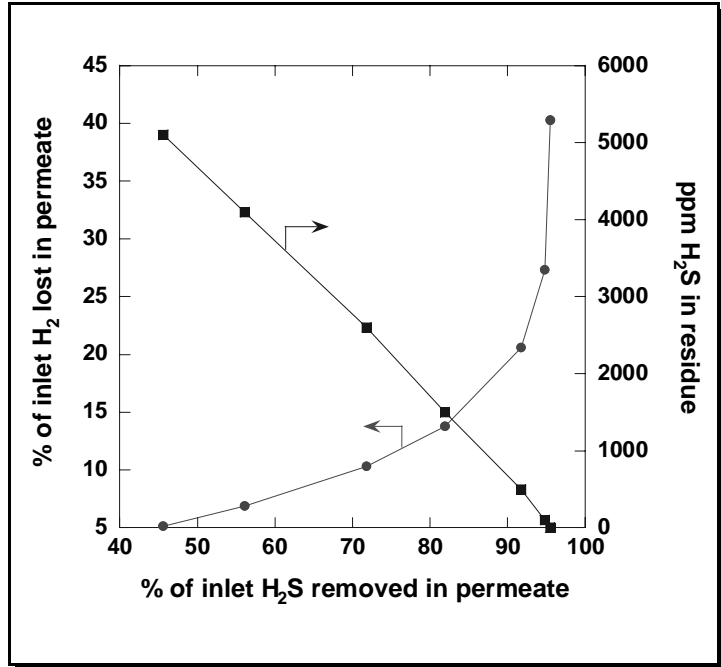


Figure 2-22. NCSU simulator's calculated H<sub>2</sub> loss and H<sub>2</sub>S remaining in the residue as a function of CO<sub>2</sub> removal. Based on the transport data of MEDAL 018 at room temperature with a standard syngas feed at 600 psia.

## CHAPTER 3

### SULFUR POLISHING THROUGH MONOLITH TECHNOLOGY

The use of polymer membranes to reduce syngas  $H_2S$  concentrations to sub-ppm levels would be impractical because excessive amounts of hydrogen and carbon monoxide would be removed from the syngas with the acid gases. Regardless of the selectivity of a polymer membrane for acid gas components and  $H_2$  or  $CO$ , there is always a finite non-zero permeability for hydrogen and carbon monoxide that allows some of these gases to be removed with the acid gases. The fact that acid gases are present at trace concentrations also means the driving force for permeation of the acid gas components is much smaller than for primary syngas components like  $H_2$  and  $CO$ . This factor becomes more pronounced as the contaminant concentration in the syngas drops—a natural consequence of contaminant removal. Thus, preliminary membrane simulation studies and initial system integration schemes, as discussed in Chapter 2, suggest that at 60 to 90% removal of the  $H_2S$ , loss of the syngas Btu value (due to  $H_2$  and  $CO$  loss) would be acceptable. Any additional  $H_2S$  removal required for fuel cell or chemical production applications of the syngas would require a polishing sulfur removal step.

The two commercially available materials currently used for polishing sulfur removal to the sub-ppm levels are (1) activated carbons and molecular sieve adsorbents and (2) disposable  $ZnO$  pellets. The activated carbon and molecular sieve adsorbents are widely used in the chemical industry for sulfur removal from natural gas at ambient temperature. The major problem with application of these adsorbents in the polishing sulfur removal process is that their use is limited to ambient temperature. Additional disadvantages include a low sulfur capacity (typically <1 wt%) inability to remove low-boiling sulfur compounds, such as  $COS$ , and generation of malodorous tailgas during steam regeneration, which presents its own technical challenges in complying with environmental regulations. Attempts to increase sulfur capacity in the activated carbon adsorbents, including impregnation with transition metals such as copper, have had limited success. These adsorbents are also expensive, costing from \$1 to \$2/lb. The combination of low sulfur capacity and high cost makes the use of these adsorbents in the polishing sulfur removal process commercially unattractive.

The disposable  $ZnO$  materials are very effective. While the actual equilibrium amount of  $H_2S$  in the effluent depends on the steam content of the syngas, Figure 3-1 shows that sub-ppm  $H_2S$  concentrations are possible with  $ZnO$ . The disposable nature of these  $ZnO$  materials is their only problem. In spite of being used only for a polishing sulfur removal process, the expense of continuously replacing this material unfavorably drives up the cost of sulfur treatment for syngas making disposable  $ZnO$  materials less attractive than other competing technologies.

Emerging desulfurization technologies based on regenerable sorbents have been developed for bulk desulfurization at higher temperatures. Their potential to reduce sulfur to sub-ppm levels, particularly at temperatures below 260°C (500°F), is limited because reactivity and capacity are seriously diminished by slow diffusion rates.

In the reaction between H<sub>2</sub>S and ZnO, H<sub>2</sub>S molecules must first diffuse to the surface of the ZnO. There, H<sub>2</sub>S reacts with ZnO to form ZnS, and the H<sub>2</sub>O formed must diffuse away. Finally, the sulfide ion must diffuse into the lattice and the oxide ions diffuse to the surface. Under normal conditions, the equilibrium is strongly in favor of sulfide formation; but at lower temperatures, overall rate of reaction is controlled by pore and lattice diffusion. As a result, only part of the ZnO is converted to ZnS. The disposable ZnO materials overcome this limitation by preparing the ZnO with a surface area of 30 to 50 m<sup>2</sup>/g.

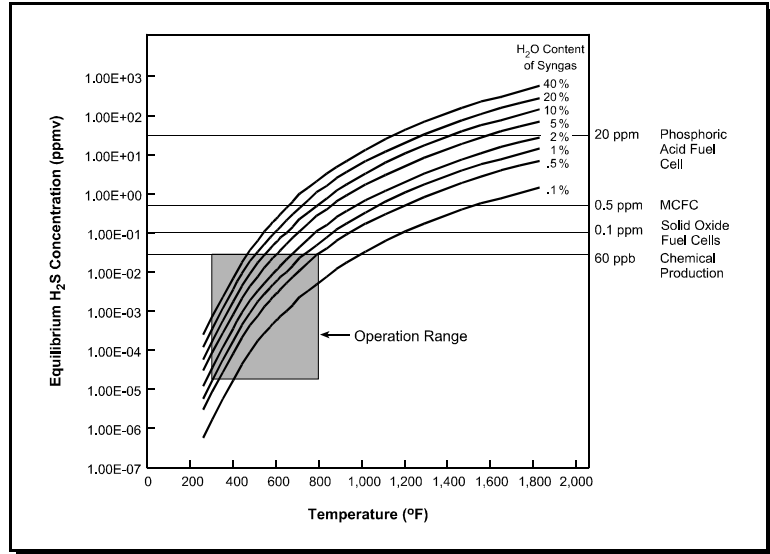


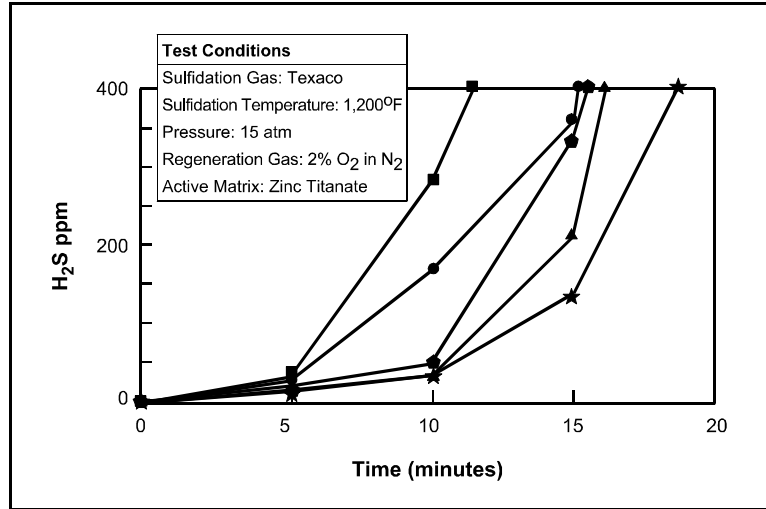
**Figure 3-1. Equilibrium H<sub>2</sub>S concentration in syngas as a function of temperature and H<sub>2</sub>O content.**

### 3.1 USE OF MONOLITHS IN HYBRID SULFUR REMOVAL PROCESS (POLISHING)

A solution that can overcome the low reactivity and limited capacity due to slow diffusion at temperatures below 260°C (500°F) and allow multiple regenerations is to use a monolith with a thin coating of high-surface-area ZnO. Monolith materials coated with palladium, platinum, and/or rhodium are used extensively in catalytic converters in automobiles to reduce emissions of unburned hydrocarbons, CO, and NO<sub>x</sub> (Kolb et al., 1992). The typical coating thickness of the active materials is about 100 μm. Because the diffusion pathlength in this type of monolith material is relatively small compared to a pellet, and hence diffusion resistances are minimized, the overall kinetics of the desulfurization reaction would be significantly faster.

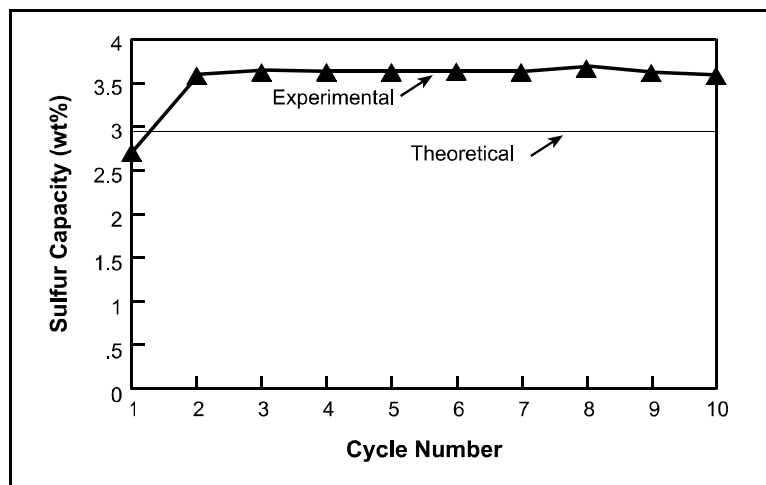
Desulfurization with monoliths is a concept that has been tested at RTI. Unfortunately, the target operating conditions for this application were bulk desulfurization at temperatures in excess of 699°C (1200°F). To mitigate zinc vaporization losses at these high operating temperatures, the active component was zinc titanate and not zinc oxide. However, examination of the results from bench-scale testing with these monoliths provides evidence that monoliths may be suitable for polishing desulfurization at lower temperatures.

Figure 3-2 shows the breakthrough behavior of the monolith for a 10 sulfidation-regeneration cycle test. Sulfidation test conditions involved a simulated Texaco gas with 7,500 ppmv of H<sub>2</sub>S at 699°C (1200°F) and 15 atm. Regeneration was performed at 15 atm with 2 vol% O<sub>2</sub> in N<sub>2</sub>. Both sulfidation and regeneration were intentionally conducted at space velocities of 86,000 h<sup>-1</sup> to determine kinetic limitations of the process. Despite both the high space velocity and high H<sub>2</sub>S feed concentrations, the monoliths did achieve extremely low effluent H<sub>2</sub>S concentrations for the first 5 minutes. Reactivity also improved with cycling. Figure 3-3 shows the sulfur capacity values calculated from the breakthrough data along with the theoretical capacity of the monolith material used. The experimentally measured capacity is about 0.5 wt% higher than the theoretical capacity, most likely a result of adsorption of H<sub>2</sub>S by the porous substrate. These sulfur capacity results, however, prove that, unlike sorbent pellets, complete capacity utilization is possible with monolith materials.



**Figure 3-2. Breakthrough profiles for selected cycles of a Zn-Ti coated cordierite monolith.**

For the lower operating temperatures in this application, use of zinc oxide used as the active component is preferred rather than zinc titanate. If 45 wt% ZnO can be loaded (the zinc titanate loading of the monoliths tested was 45 wt%, based on zinc titanate loading), the sulfur capacity of the resulting monolith will be 17.7 wt%, which will be comparable or better than most of the ZnO-based pelletized sorbent materials. Furthermore, an order-of-magnitude higher space velocity can be used because of the fast kinetics discussed previously, thereby reducing the reactor size by an order of magnitude. However, a major technical challenge is to maintain a high surface area of the active matrix in repeated sulfidation-regeneration cycles, particularly



**Figure 3-3. Sulfur capacity of Zn-Ti coated monolith at breakthrough.**

when a regeneration temperature in the range of 427 to 538°C (800 to 1000°F) is used. Therefore, the principal objective of this monolith development effort was to optimize the manufacture of these ZnO-coated materials to maximize the long-term performance with respect to chemical reactivity and thermal stability. The target desulfurization temperature range was from 149 to 427°C (300 to 800°F).

Although a monolith provides a very high surface area to mass ratio, the cordierite substrate is a dense material with very low surface area. Therefore, monolith substrates are often covered with a washcoat that consists of a high surface area material providing additional surface for deposition of active materials. Potential washcoat materials include titania, zirconia and alumina. Thermogravimetric screening tests, discussed in the next section, were used to evaluate the potential advantages of each of these washcoat materials. These screening tests also included a blank monolith substrate and monolith with an active coating, but no washcoat.

The application or deposition of either washcoat or active material is generally conducted by filling the monolith channels with the slurry. During this process, part of the water contained in the slurry is absorbed by the porous monolith walls, resulting in a coating in the form of a filter cake. The effectiveness of the coating process depends primarily on the rheological behavior of the slurry, i.e., solids content, pH, zeta potential, shear rate and viscosity. The thickness of the coating depends on the substrate porosity and dimensions, slurry properties, and rate at which the channels are filled. After filling, the channels are cleared of excess slurry by forced air. The slurry filling and removal steps can be repeated a number of times to reach the required loading of active material. Following deposition, the monolith is calcined.

## **3.2 SAMPLE PREPARATION**

RTI worked with Süd-Chemie Prototech, Inc., a subsidiary of Süd-Chemie, Inc., to develop a monolith desulfurizer for polishing applications. There were two primary issues in making suitable monolith materials: selection of the substrate and selection of washcoat and active material. Several options were available as candidate materials for a suitable substrate. After careful evaluation of the available substrates, it appeared that cordierite was the best candidate for the current desulfurization application. The relatively easy coating preparation processes, extensive use in catalytic converters, and large selection available made cordierite the most promising candidate for monolith substrate.

## **3.3 THERMOGRAVIMETRIC TESTING**

### **3.3.1 Washcoat Screening Tests**

Prototech prepared monolith samples for these screening tests with assistance from RTI. All samples testing for this project used 400 cells (channels) per square inch (cpsi) cordierite substrate. The reasons for selecting a cordierite substrate were discussed in the previous section. The first set of monoliths produced by Prototech had a target loading of 17 wt% ZnO,

but different washcoats. The materials used for the washcoat in these samples included titania, alumina, and zirconia. Additional monolith samples prepared included a blank monolith substrate and monolith with a ZnO coating, but no washcoat. The complete matrix of monolith samples prepared for thermogravimetric screening is shown in Table 3-1.

**Table 3-1. BET Surface Areas for Various Monolith Samples**

Support	Washcoat	Target ZnO Amount	BET Surface Area (m <sup>2</sup> /g)	
		(wt%)	Before 1.5-cycle Test	After 1.5-cycle Test
Cordierite*	None	None	0.38	1.61
Cordierite*	None	17	0.98	0.86
Cordierite*	Titania	17	7.6	5.17
Cordierite*	Zirconia	17	3.54	1.02
Cordierite*	Alumina	17	22.92	19.11

\*400 cpsi.

Each of the samples in Table 3-1 was subjected to a standard 1.5-cycle test in a thermogravimetric analyzer (TGA) at RTI. The steps, gas compositions, and other important features of a 1.5-cycle test are summarized in Table 3-2. Figure 3-4 shows the weight profiles during the 1.5 cycle TGA tests. As expected, the blank monolith sample did not show any activity.

Breaking the weight profiles in Figure 3-4 down to the individual segments reveals a number of important features. During the first segment, the monolith sample is heated in helium. Any weight changes observed during this segment are the result of chemical changes in the monolith sample. The weight loss during this heating segment for most of the samples in Figure 3-4 is probably the result of water desorption. The fact that monolith samples with washcoats, which have larger available surface areas to absorb water, have larger weight losses supports this theory. The much larger weight loss of the monolith sample with alumina washcoat is also most probably related to water desorption, but potential interactions of the cordierite, alumina and ZnO cannot be overlooked.

The next segment of the 1.5-cycle test is a reduction. As the support materials and ZnO are stable under reducing conditions at these temperatures, very little weight loss is expected during this segment. All samples in Figure 3-4 experience very small weight losses that could be the result of buoyancy effects of the sample or reduction of metal oxide impurities or excess oxygen in the sample.

During the first sulfidation segment of the 1.5-cycle test, the sample is expected to gain weight resulting from reaction of the active ZnO in the sample with the H<sub>2</sub>S. The rate of weight gain is

**Table 3-2. Summary of Temperatures, Gas Compositions, and Events in a 1.5-Cycle Test**

Elapsed Time (min)	Temperature (°C)	Gas	Event
0	20	Inert A	New temperature setpoint 550°C (1022°F); start helium
10	550	Inert B	Start steam
15	550	Reducing	Start reduction
25	550	Sulfidation	Stop reduction; start sulfidation
55	550	Inert B	Stop sulfidation; new temperature setpoint 650°C (1202°F)
60	650	Inert B	Inert purge
65	650	Regeneration	Stop inert purge; begin regeneration
95	650	Inert B	Stop regeneration; new temperature setpoint 550°C (1022°F)
100	550	Inert B	Inert purge
105	550	Reducing	Start reduction
115	550	Sulfidation	Stop reduction; begin sulfidation
>400	550	Inert A	Stop extended sulfidation

The composition of the gas mixtures is as follows:

Inert A	Pure helium
Inert B	Helium and 11 vol% steam
Reducing	42 vol% CO, 13 vol% CO <sub>2</sub> , 11 vol% H <sub>2</sub> O and 34 vol% H <sub>2</sub>
Sulfidation	1.3 vol% H <sub>2</sub> S, 12 vol% CO <sub>2</sub> , 11 vol% H <sub>2</sub> O, 34 vol% H <sub>2</sub> , and 41.7 vol% CO
Regeneration	2 vol% O <sub>2</sub> and 11 vol% H <sub>2</sub> O in N <sub>2</sub>

indicative of the rate of reaction between the ZnO and H<sub>2</sub>S. The amount of weight gain is representative of the sulfur capacity of the sample. Figure 3-4 shows that all the monolith samples have some desulfurization activity. All the monolith samples, except the monolith with an alumina washcoat, have very similar desulfurization activities and sulfur capacities. The monolith sample with an alumina washcoat has approximately the same desulfurization activity as the other samples, but significantly more sulfur capacity.

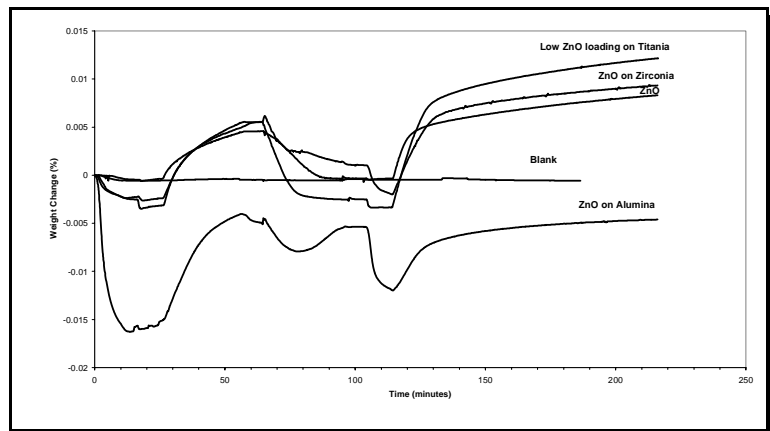


**Figure 3-4. 1.5-cycle TGA tests of monolith samples for washcoat screening tests.**

During the regeneration segment, the samples are expected to experience a rapid and steady decrease in weight as the sulfur on the sample is removed and the ZnO regenerated. Figure 3-4 shows significant differences in the weight profiles for the different samples resulting from the influences of the washcoat on the regeneration chemistry. The most significant change from the expected pattern is the monolith with an alumina washcoat, which initially loses

weight, but eventually gains weight as the regeneration proceeds. Thus, net weight change for the monolith sample with an alumina washcoat is almost zero. This pattern is often associated with interaction of the support and active component and results in chemical deactivation of the sorbent. The monolith sample with a zirconia washcoat also shows some deviation with the expected pattern, as the weight loss during regeneration is less than the weight gain observed during sulfidation. The remaining samples demonstrate the expected regeneration pattern and the monolith sample with a TiO<sub>2</sub> washcoat has the fastest regeneration rate.

The next segment in the 1.5-cycle test is the second reduction. Except for the monolith samples with the alumina and zirconia washcoat, the weight changes are similar to the small weight changes observed in the first reduction segment. For monolith samples with the alumina and zirconia washcoat, there is a significant increase in the weight loss during the second reduction segment. The potential implication of this is that thermodynamically favored compounds formed during regeneration are not the active compounds for desulfurization, but can be reduced. Although it is possible that the reduction is necessary to completely regenerate the active sulfur compounds, these conditions are more frequently associated with chemical deactivation.

The extended sulfidation segment of the 1.5-cycle test demonstrates that the sample can be regenerated and is evidence of the desulfurization activity and sulfur capacity after regeneration. Figure 3-4 shows the desulfurization activity of all samples was equal to or better than in the first cycle. Furthermore the sulfur capacity of all except the monolith sample with an alumina washcoat experienced an increase in sulfur capacity during the extended sulfidation.

A closer examination of the extended sulfidation results in Figure 3-4 shows that the weight gain for the samples was roughly 1 wt%, which is equivalent to 2 wt% sulfur capacity. In order to measure the theoretical sulfur capacity, the amount of ZnO on the fresh monolith with TiO<sub>2</sub> washcoat was measured both by Prototech and RTI. The results from this testing are shown in Table 3-3. Based on the ZnO loading provided in Table 3-3, the theoretical sulfur capacity for the monolith with a TiO<sub>2</sub> washcoat was 3.9 wt%. Thus, the observed sulfur capacity was roughly half of the theoretical capacity.

**Table 3-3. Measurements of Zn Content for Cordierite Monolith Samples with Titania Washcoat and Zinc Oxide**

Sample			Prototech		RTI (ICP)	
			Weight <sup>a</sup>	ICP	Zn	Ti
Monolith	Washcoat	ZnO	(wt%)	(wt%)	(wt%)	(wt%)
Cordierite	Titania	Low	14.85	12.84	10.5	4.48
Cordierite	Titania	High	NM	NM	22.4	4.65

NM = Not measured.

<sup>a</sup>Calculated using initial and final firing weights.

The BET surface area for each monolith sample was measured before and after the 1.5 cycle test. These values are provided in Table 3-1. The two monolith samples with no washcoat had very low surface areas. The monolith samples with a washcoat had much larger surface areas. The ranking of the monolith samples with washcoats in order of decreasing surface area is alumina > titania > zirconia. As expected, the surface area in each monolith sample decreased after the 1.5-cycle testing. The ranking of monolith samples on the loss of surface area during 1.5-cycle testing in order of decreasing loss is zirconia > titania > alumina.

The conclusion drawn from the results of these 1.5-cycle screening tests was the TiO<sub>2</sub> washcoat provided least reactive and most stable support for the ZnO loading. The monolith sample with the TiO<sub>2</sub> washcoat had the best desulfurization and regeneration activities and showed minimal evidence of deactivation. Two problems observed with this monolith sample were a loss of surface area during cyclic operation and low sulfur capacity. However, these results were not only observed for the monolith sample with titania washcoat, but all the monolith samples.

One possible solution to the low sulfur capacity was to increase the ZnO loading. Previous results with monoliths indicated the ZnO loading could be substantially increased. Prototech prepared a new set of monolith samples with TiO<sub>2</sub> washcoat for thermogravimetric testing with about twice the ZnO loading.

The weight profiles and surface area results for these new monolith samples with higher ZnO loading and the previous results for the low ZnO loading are shown in Figure 3-5 and Table 3-4. The weight profiles in Figure 3-5 show the two samples have very similar profiles for the 1.5 cycle test. Some noteworthy differences include the sulfur capacity of the higher loading ZnO sample, which is about 30 wt% greater than for the low ZnO loaded sample. In addition the regeneration rate for the higher ZnO loaded sample is slightly slower than the low ZnO loaded sample.

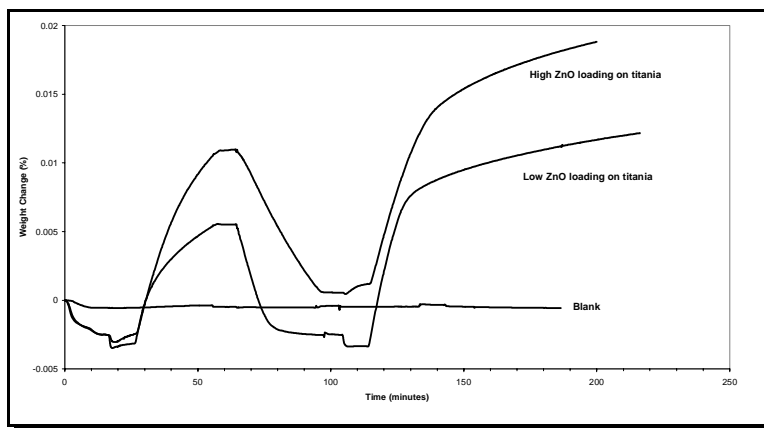


**Figure 3-5. Comparison of weight profiles for 1.5 cycle TGA test for monoliths with TiO<sub>2</sub> washcoat and high and low ZnO loading.**

The monolith sample with high-ZnO loading had a slightly smaller surface area than the monolith with the low ZnO loading. This was not unexpected as the monolith with the high loading was made by loading additional ZnO onto the low ZnO loading monolith. The change in

the surface area during the 1.5-cycle test was about 60% for the sample with the high ZnO loading vs. 40% for the sample with the low ZnO loading.

### 3.3.2 Temperature Screening Tests

Because target operating temperatures for the monolith polishing desulfurizer are below 550°C (1022°F), temperature studies were conducted to study sulfidation performance as the sulfidation temperature was reduced. The testing sequence

was essentially the same used for the 1.5-cycle test, except during each subsequent cycle, the sulfidation temperature was dropped by 50°C (90°F) and the extended sulfidation was not performed. This testing was performed on a monolith sample with cordierite core, TiO<sub>2</sub> washcoat and a target ZnO loading of 17 wt%. The lowest temperature tested was 200°C (392°F). Figure 3-6 shows the temperature effect on sulfidation activity of the monolith where the percent weight change is plotted vs. sulfidation time for each cycle.

Figure 3-6 shows that at temperatures above 500°C (932°F), the desulfurization reactivity and sulfur capacity of the monolith are essentially constant. Below 450°C (842°F), both the desulfurization reactivity and sulfur capacity decrease. From a maximum weight change of 1% at 500°C (932°F), the total weight change at 200°C (392°F) was 0.2%. Although the desulfurization activity decreases with

temperature, the overall pattern of higher reactivity at the start of sulfidation, followed by lower reactivity as the sulfur capacity is consumed, remained at 200°C (392°F). However, at 200°C (392°F), the high reactivity portion of the sulfidation could not be easily distinguished from the low reactivity section at the scale shown in Figure 3-6.

The effect of low-temperature sulfidation on the monoliths with ZnO and titania washcoats was examined in a 4.5-cycle test. During sulfidation the temperature was held at 200°C (392°F); during regeneration it was held at 650°C (1202°F). The weight profile for this test is shown in

**Table 3-4. BET Surface Areas for Various Monolith Samples with High and Low ZnO Loadings**

Support	Washcoat	Target ZnO Amount	BET Surface Area (m <sup>2</sup> /g)	
		(wt%)	Before	After
Cordierite*	Titania	17	7.60	5.17
Cordierite*	Titania	34	5.41	2.28
Cordierite*				

\*400 cpsi.

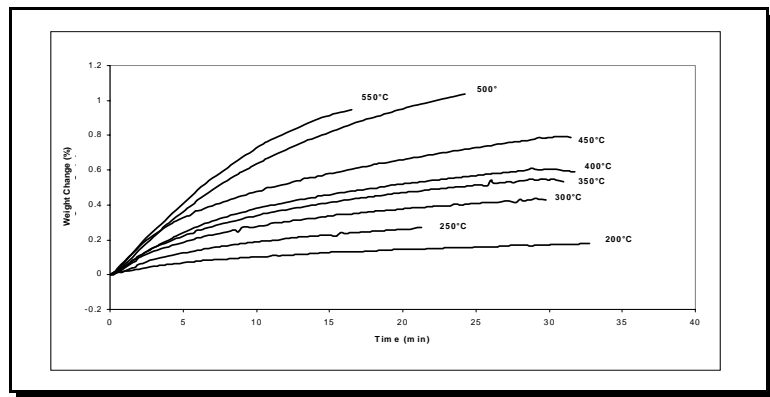


**Figure 3-6. TGA tests with ZnO-TiO<sub>2</sub>-washcoated monolith as a function of temperature.**

Figure 3-7. After the initial cycle, the amount of sulfur removed and subsequently released during regeneration was almost identical from cycle to cycle. The amount of sulfur removed during Cycle 4 appears to be less, but the sulfidation was cut 10 minutes short by the temperature program prematurely starting the temperature increase for regeneration. Another promising observation was that the rate of reaction during both sulfidation and regeneration did not seem to be decreasing.

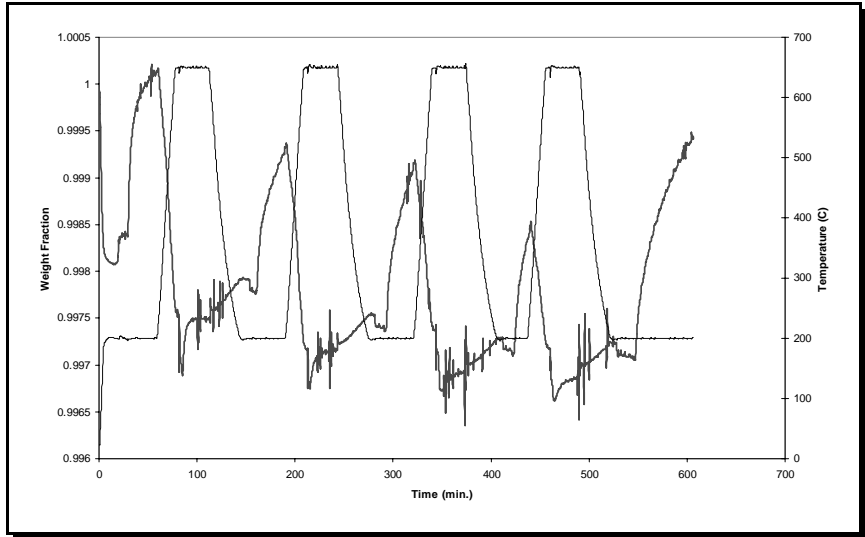


**Figure 3-7. 4.5-Cycle TGA test of zinc on titania-washcoated 400-cpsi cordierite monolith with sulfidation temperature of 200°C (392°F), regeneration temperature of 650°C (1202°F).**

The BET surface area of the monoliths after both this test and the preceding temperature test are shown in Table 3-5. Although the BET surface area after the tests was roughly only 50% of the initial surface area, the main decrease in surface area appears to occur during the first couple of cycles based on the results from the 1.5-cycle and multiple cycle tests.

With TiO<sub>2</sub>-coated cordierite monolith samples with both the low and high ZnO loading, a series of 5-cycle tests both with and without steam were conducted. These tests were performed with a sulfidation temperature of 200°C (392°F) and regeneration temperature of 650°C (1202°F). The results are very similar. After the first cycle, the results for each of the subsequent cycles are almost identical. The reaction rates at the beginning of sulfidation and regeneration are both very rapid. However, the amount of weight gain seems to be limited to about 0.12 wt% for the monolith samples with the low ZnO loading and 0.2 wt% with the high ZnO loading.

**Table 3-5. Posttest BET Surface Area for ZnO and Titania Washcoated Cordierite Monolith**

<b>Test</b>	<b>BET Surface Area (Posttest) (m<sup>2</sup>/g)</b>
Temperature reduction	4.30
4.5 cycle (200°C [392°F] sulfidation)	3.64

### **3.3.3 Summary of Thermogravimetric Testing**

Overall results from the thermogravimetric testing of monolith samples have demonstrated that monolith-based polishing desulfurization units do have some technical potential. A titania washcoat provided superior desulfurization and regeneration reactivity than either alumina or zirconia washcoats. Desulfurization reactivity and sulfur capacity were observed to decrease as the desulfurization temperature decreased, but a high initial reactivity was observed even at 200°C (392°F) and after multiple cycles. The actual observed sulfur capacity was less than theoretical, but was increased by increasing the ZnO loading. As expected, the surface area was found to decrease after cyclic operation; however, a majority of the surface area loss occurred during the first cycle.

## **3.4 BENCH-SCALE TESTING**

The thermogravimetric testing discussed in the previous section provided evidence that monoliths could potentially be used in polishing desulfurization units, but also emphasized the need for more research on sulfidation and regeneration performance. Because this additional evaluation of sulfidation and regeneration performance required the ability to vary sample temperature, feed gas flow and composition and operating pressure, bench-scale testing of the monolith samples was initiated. Bench-scale testing also provided the opportunity to measure reactor effluent compositions not possible during thermogravimetric testing.

The objective of this bench-scale testing was to continue the evaluation of regenerable monolith materials for polishing desulfurization. The first multicycle tests were aimed at measuring the effluent sulfur concentrations during both sulfidation and regeneration. The information would confirm the results observed during thermogravimetric testing and more accurately measure sulfidation performance. During subsequent multicycle tests, parametric tests of temperature, gas composition, and flow rate were conducted. This testing and its results are discussed in the following sections.

### **3.4.1 Monolith Preparation**

Because RTI's HTHP reaction system has been designed predominantly for testing sorbent samples in pellet and powder form, monolith testing required a few minor system changes, special monolith preparation, and special reactor loading. As the standard multiple thermocouple assembly could not be inserted into the monolith sample without damaging the monolith, a special thermocouple was installed to replace the multiple thermocouple assembly and to measure the temperature of the outlet gas 1 inch above the monolith.

Prototech also prepared special monolith samples that were 4 inches long and 2 inches in diameter. These dimensions would allow the monolith sample to be readily inserted into the quartz reactor in RTI's HTHP reactor system. The monolith formulation for these monolith

samples included a 400 cpsi cordierite monolith and TiO<sub>2</sub> washcoat loaded with ZnO. One batch of these monolith samples was loaded with 28 wt% ZnO and labeled RTI1-11-1. The other set was loaded with 13 wt% ZnO and labeled RTI1-12-1.

Although the monolith samples were prepared to readily fit into the 2-inch quartz reactor, a small annulus between the reactor wall and the monolith would still exist. In order to minimize the flow bypassing the monolith through this annulus, Fiberfax insulation was wedged into this annulus after the monolith was installed in the reactor. The Fiberfax insulation increased the flow resistance through the annulus, significantly reducing any bypass flow.

### **3.4.2 Multicycle Performance Tests**

Two multicycle tests were conducted to measure effluent sulfur concentrations and sulfur capacity. The first test was a 5-cycle test. During this test the H<sub>2</sub>S feed concentration was varied between 2,000 and 10,000 ppmv. Based on the target sulfur removal levels for the bulk membrane desulfurization system, the H<sub>2</sub>S concentration at the inlet of the polishing desulfurization unit would be between 2,000 and 6,000 ppmv. The high inlet H<sub>2</sub>S concentrations were used to increase the sulfur-loading rate compressing the cycle time sufficiently to complete a cycle in an 8- to 10-h period. During this test, the monolith sample was regenerated with both neat air and dilute oxygen mixture in nitrogen.

In the second test, the same sulfidation and regeneration conditions were used for each cycle. With identical conditions, no influence of different sulfidation and regeneration conditions would be present to mask performance changes associated with cyclic operation. This second test was a 4-cycle test.

**3.4.2.1 Multicycle Performance Test 1.** An RTI1-11-1 monolith sample weighing 106 g was loaded in the quartz reactor in RTI's HTHP reactor system. Sulfidation conditions for this test were 563°C (1050°F), 280 psig and a space velocity of 2,000 h<sup>-1</sup>. The H<sub>2</sub>S concentration of the feed gas was increased from 2,000 ppmv to 4,000 ppmv to 10,000 ppmv over the course of the sulfidation in Cycles 1 through 3. In Cycles 4 and 5, the H<sub>2</sub>S feed concentration started at 4,000 ppmv and was increased to 10,000 ppmv after a period of at least 60 minutes. The sulfidation was terminated when the total sulfur concentration in the reactor effluent was ≥100 ppmv. During sulfidation, a Hewlett-Packard gas chromatograph (GC) equipped with a Sievers chemiluminescence detector analyzed a dry reactor effluent for H<sub>2</sub>S, COS, and SO<sub>2</sub>. Rapidly cooling the reactor effluent in a cold-water heat exchanger condensed the steam generating the dry reactor effluent gas for GC sampling.

After sulfidation, the monolith was heated to 677°C (1250°F) in nitrogen. When the monolith temperature reached the set point and the syngas mixture had been purged from the reactor, the regeneration was started. Regeneration conditions were 677°C (1250°F), 280 psig and a space velocity of 2,000 h<sup>-1</sup>. The composition of the regeneration gas was neat air for Cycle 1

and a 2 vol% O<sub>2</sub> in N<sub>2</sub> for the remaining cycles. The SO<sub>2</sub> in the reactor effluent was monitored with a Bovar Series 900 photometric analyzer. The effluent O<sub>2</sub> concentration was measured with a Model 326 Teledyne O<sub>2</sub> analyzer. Regeneration was terminated when a significant change in the rate of decrease in the effluent SO<sub>2</sub> concentrations occurred. A detailed summary of the test conditions for both sulfidation and regeneration is presented in Table 3-6.

**Table 3-6. Summary of Operational Conditions During 5-Cycle Performance Test**

	Sulfidation					Regeneration	
	1	2	3	4	5	1	2 to 5
Pressure (psig)	280					280	
Space velocity (h <sup>-1</sup> )	2000					2000	
Temperature (°F)	1050					1250	
Cycle	1	2	3	4	5	1	2 to 5
Gas composition (vol%)							
CO							
CO <sub>2</sub>							
H <sub>2</sub>	99.8	99.6	99	99.6	99		
H <sub>2</sub> S	0.2	0.4	1	0.4	1		
N <sub>2</sub>						79	98
O <sub>2</sub>						21	2

Figure 3-8 contains the H<sub>2</sub>S effluent concentrations for this 5-cycle test. The effluent concentrations in Figure 3-8 were plotted as a function of sulfur loading to allow comparison of the results in spite of the differences in H<sub>2</sub>S feed concentration from cycle to cycle. The effluent concentrations for SO<sub>2</sub> and COS were not plotted because their concentrations were significantly less than the H<sub>2</sub>S concentration, except for Cycle 1. In Cycle 1, there was initially a large spike of SO<sub>2</sub> in the effluent concentration that dropped rapidly, but remained present for a large portion of the sulfidation. Because this result was only observed in Cycle 1, it was considered to be a consequence of SO<sub>2</sub> contamination in the lines from previous testing or a release resulting from monolith.

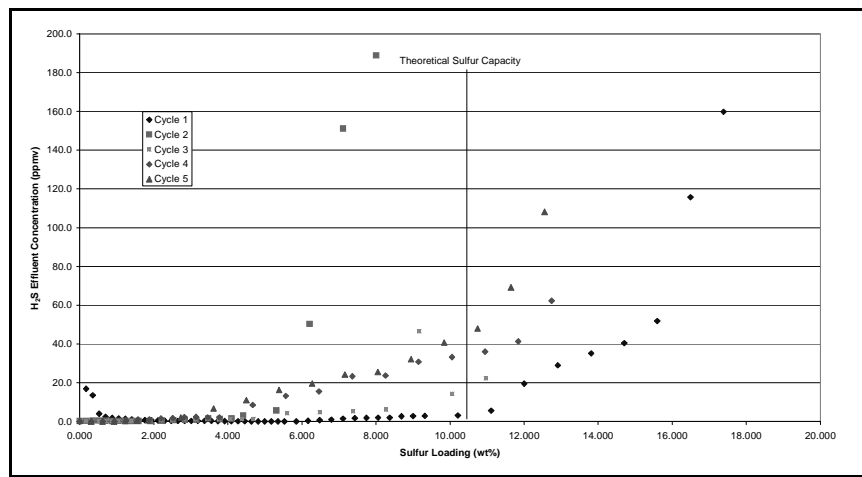


**Figure 3-8. Effluent H<sub>2</sub>S concentrations for 5-cycle test as a function of sulfur loading.**

significantly less than the H<sub>2</sub>S concentration, except for Cycle 1. In Cycle 1, there was initially a large spike of SO<sub>2</sub> in the effluent concentration that dropped rapidly, but remained present for a large portion of the sulfidation. Because this result was only observed in Cycle 1, it was considered to be a consequence of SO<sub>2</sub> contamination in the lines from previous testing or a release resulting from monolith.

A number of important observations can be made from the results in Figure 3-8. The first is that the sulfur loading in Cycle 2 is significantly lower than the other cycles. The one significant difference between this sulfidation and the others was composition of the regeneration gas in the previous cycle. For Cycle 2, neat air was used rather than a 2 vol% O<sub>2</sub> in N<sub>2</sub> mixture. This would suggest that a significant reduction in sulfur capacity is associated with neat air regeneration.

Except for Cycle 2, the actual sulfur capacity of the monolith also appears to be significantly higher than the theoretical capacity. This is completely different from the results obtained in the TGA. Since the flow in the TGA is not forced through the monolith as in the bench-scale reactor, gas-solid contacting in the bench-scale reaction may be much better than in the TGA. In previous testing, the excess sulfur capacity observed with monoliths was attributed to a small sulfur capacity of the monolith and washcoat. Currently, the explanation of this excess sulfur capacity is not known.

The final observations on the profiles in Figure 3-8 concern the effluent concentrations. The monolith is capable of reducing the effluent sulfur concentration to  $\leq 2$  ppmv. For Cycle 1, this ability to reduce the effluent sulfur concentration was observed for up to the theoretical sulfur capacity. However, with repeated cycles, this ability to reduce the effluent sulfur concentration was observed for approximately 50% of the theoretical sulfur capacity. From this testing, whether the regeneration conditions can be altered to improve sulfidation performance or this phenomenon is an irreversible deactivation is not known.

The typical effluent concentration profiles for SO<sub>2</sub> and O<sub>2</sub> during regeneration with a 2 vol % O<sub>2</sub> in N<sub>2</sub> mixture are presented in Figure 3-9. No oxygen slip is observed until the regeneration of the monolith is essentially complete. The presence of high levels of SO<sub>2</sub> and O<sub>2</sub>, as observed at the very end of regeneration, could be responsible for the formation of zinc sulfate.

Although the amount of this zinc sulfate would be small, it could possibly cause the reduction in the ability of the monolith to reduce effluent sulfur concentrations to  $\leq 2$  ppmv in the later cycles of this test.

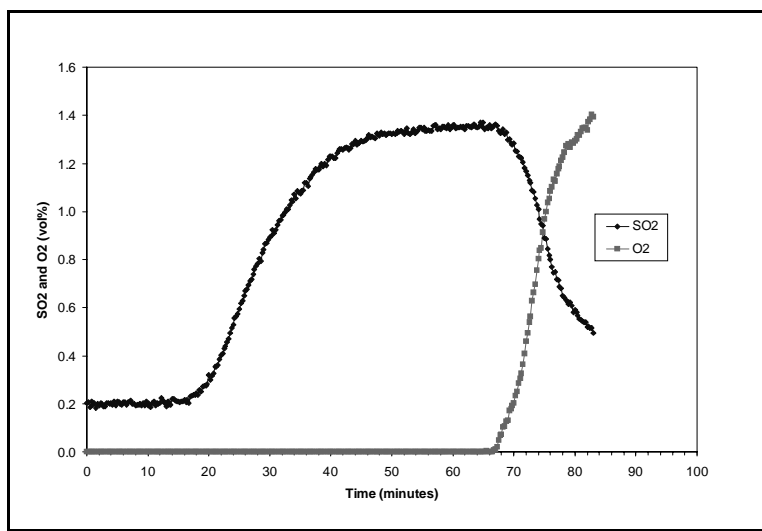


**Figure 3-9. Typical regeneration effluent concentration profile of monolith RTI1-11-1.**

**3.4.2.2 Multicycle Performance Test 2.** A fresh RTI1-11-1 monolith sample weighing 107 g was loaded in RTI's HTHP reactor system for a 4-cycle test. Conditions for sulfidation were 565°C (1050°F), 280 psig and a space velocity of 2,000 h<sup>-1</sup>. The initial H<sub>2</sub>S concentration of the feed was 4,000 ppmv, but was increased during the run to 10,000 ppmv to rapidly load the monolith with sulfur allowing the cycle to be completed within an 8-hour period. Sulfidation was terminated when the effluent sulfur concentration exceeded 200 ppmv.

After sulfidation, the reactor system was purged with nitrogen while being heated to 760°C (1400°F). When the syngas mixture had been purged from the system and the monolith temperature had increased to the set point, regeneration was started. The conditions for regeneration were 760°C (1400°F), 280 psig and a space velocity of 2,000 ppmv with a 2 vol% O<sub>2</sub> in N<sub>2</sub> mixture. The regeneration was terminated when the rate of decline in the effluent SO<sub>2</sub> concentration began to decrease significantly. The summary of the testing conditions for both sulfidation and regeneration is presented in Table 3-7.

**Table 3-7. Summary of Operational Conditions During 4-Cycle Performance Test**

	Sulfidation		Regeneration
Pressure (psig)	280		280
Space velocity (h <sup>-1</sup> )	2,000		2,000
Temperature (°F)	1050		
Gas composition (vol%)			
CO			
CO <sub>2</sub>			
H <sub>2</sub>	99.6	99	
H <sub>2</sub> S	0.4	0.1	
N <sub>2</sub>			98
O <sub>2</sub>			2

Figure 3-10 shows the H<sub>2</sub>S effluent concentration profiles for this 4-cycle test. Many of the features observed in the previous 5-cycle test can also be seen in this test. As with the previous test, the actual sulfur loadings exceed the theoretical sulfur capacity calculated based on the ZnO loading. A distinct increase in the sulfur capacity was observed between Cycle 1 and Cycle 2. This improvement in sulfidation performance was also observed during the thermogravimetric testing. Many sorbents exhibit this behavior known as activation.

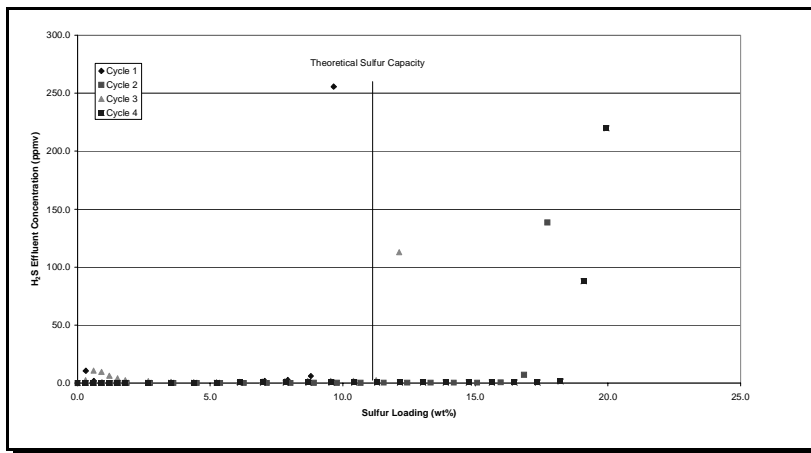


**Figure 3-10. Effluent H<sub>2</sub>S concentrations for 4-cycle test as function of sulfur loading.**

Two features for Cycle 3 cause its sulfidation performance to stand out. The first is a significant decrease in the sulfur capacity. The second is a period near the start of sulfidation when there is a minor increase in the H<sub>2</sub>S effluent concentration. A systematic analysis showed that in Cycle 2 regeneration was allowed to continue for 10 minutes with larger amounts of SO<sub>2</sub> and O<sub>2</sub> present than in any of the other regenerations. As speculated previously, this leads to the formation of zinc sulfate that deactivates the monolith. The minor H<sub>2</sub>S peak in the reactor effluent was probably the decomposition of this sulfate under reducing conditions.

Except for Cycle 3, the monolith readily reduces the effluent H<sub>2</sub>S concentrations to  $\leq 2$  ppmv up to a sulfur loading of 15 wt%. This performance is considerably better than observed in the previous 5-cycle test. One change in the operating conditions that may have caused this improvement in performance is an increase in regeneration temperature from 677 to 760°C (1250 to 1400°F).

**3.4.2.3 Summary of Multicycle Monolith Testing.** The overall conclusions learned from these two multicycle tests indicate that monolith with a TiO<sub>2</sub> washcoat and ZnO loading have an actual sulfur capacity greater than the theoretical capacity based on the ZnO loading. These monoliths also have the potential to reduce the effluent sulfur concentration to  $\leq 2$  ppmv. Regeneration conditions are extremely important to maintain optimal sulfidation performance. Regeneration temperatures above 760°C (1400°F) demonstrated the best sulfidation performance. At a regeneration temperature of 677°C (1250°F) a mixture of 2 vol% O<sub>2</sub> in N<sub>2</sub> resulted in better sulfidation performance obtained with neat air. Monoliths seem to require activation similar to some sorbents.

### 3.4.3 Parametric Testing

In this series of tests, bench-scale testing continued to study activation, sulfidation temperature, feed composition and space velocity. The first multicycle test was divided into three distinct portions. The first four cycles were used to study monolith activation. During the next portion of the test, the sulfidation temperature was consistently decreased each cycle from 538 to 93°C (1000 to 200°F). In the last portion of this multicycle test, the syngas feed composition was tested at temperatures between 260 and 371°C (500 and 700°F). In a separate 5-cycle test, the performance of a monolith at a space velocity near 30,000 h<sup>-1</sup> was tested.

**3.4.3.1 Monolith Activation.** A fresh RT11-11-1 monolith weighing 120 g was loaded in RTI's HTHP reactor system. For four cycles, the monolith was sulfided at 538°C (1000°F), 280 psig at a space velocity of 2,000 h<sup>-1</sup>. For each test the H<sub>2</sub>S feed concentration was kept constant for the entire sulfidation; however, the H<sub>2</sub>S feed concentration was varied between 2,500 and 10,000 ppmv in different cycles. The end of sulfidation was determined by an effluent sulfur concentration of  $\leq 200$  ppmv.

In preparation for regeneration, the sample was heated to 677°C (1250°F) in nitrogen at a space velocity of 2,000 h<sup>-1</sup>. In addition to increasing the temperature, the system pressure was reduced to 50 psig. When the system had achieved the new operation conditions and ample time had passed to purge any remaining syngas from the system, regeneration was started with a 2 vol% O<sub>2</sub> in N<sub>2</sub> mixture. Regeneration was terminated after a significant drop in the SO<sub>2</sub> effluent concentration, reducing the period when high concentrations of both SO<sub>2</sub> and O<sub>2</sub>, favoring zinc sulfate formation, occurred in the reactor. A summary of the operating conditions for these four cycles is presented in Table 3-8.

Figure 3-11 presents the H<sub>2</sub>S effluent concentrations as a function of the sulfur loading. In each cycle, the sulfur capacity, the H<sub>2</sub>S peak observed at the beginning of sulfidation, and the average prebreakthrough effluent H<sub>2</sub>S concentration decrease with each consecutive cycle. By the fourth cycle, all these performance characteristics have reached stable values. This confirms that sulfidation performance of monoliths will improve over the first few cycles of operation as the monolith is activated. The sulfidation for Cycles 2 and 3 was stopped prior to sulfur breakthrough to permit completion of the regeneration within a normal 8-hour day. This fractional loading of the monolith did not stop activation, but may have increased the total number of activation cycles necessary. Therefore, the activation conditions used in this test represent the worst possible conditions and indicate four cycles as the maximum number of activation cycles necessary.

### 3.4.3.2 Parametric Temperature Testing.

After completing the test sequence described in the previous section, parametric temperature testing was started. During this testing, the sulfidation temperature was decreased 55°C (100°F) in

**Table 3-8. Summary of Operational Conditions for Monolith Activation During Parametric Testing**

	Sulfidation				Regeneration
Pressure (psig)	280				50
Space velocity (h <sup>-1</sup> )	2,000				2,000
Temperature (°F)	1050				
Cycle	1	2	3	4	1 to 4
Gas composition (vol%)					
CO					
CO <sub>2</sub>					
H <sub>2</sub>	99	99.5	99.75	99.5	
H <sub>2</sub> S	1	0.5	0.25	0.5	
N <sub>2</sub>					98
O <sub>2</sub>					2

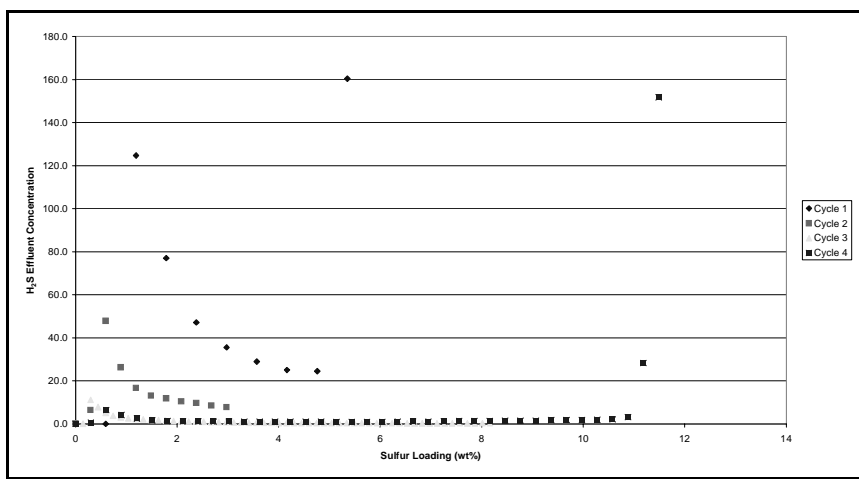


**Figure 3-11. Effluent H<sub>2</sub>S concentrations for monolith activation during parametric testing.**

each subsequent cycle. The initial sulfidation temperature was 538°C (1000°F); the final temperature was 93°C (200°F). The other operating conditions for sulfidation include 280 psig, a space velocity of 2,000 h<sup>-1</sup> and H<sub>2</sub>S feed concentration of 5,000 ppmv. The same conditions used in the monolith activation cycles were used to determine the end point of sulfidation and for conducting the regeneration. These conditions are summarized in Table 3-9.

The average prebreakthrough H<sub>2</sub>S effluent concentration and the sulfur loading for each cycle during this parametric temperature testing are presented in Figure 3-12. Figure 3-12 shows that the monolith readily maintains the effluent sulfur concentrations below 10 ppmv at operating temperatures ranging from 93 to 538°C (200 to 1000°F). Actual sulfur capacity is observed to decrease rapidly for temperatures between 209 and 371°C (400 and 700°F). The sulfur capacity at temperatures above 371°C (700°F) was ≤10 wt%, whereas below 204°C (400°F) the sulfur loading was about 2 wt%. The ability of the monolith to maintain the low effluent sulfur concentrations reflects the fact that the thermodynamics of the sulfidation reaction become more favorable at the lower temperatures. The low sulfur capacity indicates the kinetics of the sulfidation reaction are sufficiently slow to limit reaction to a small fraction of the ZnO extremely close to the surface. Similar decreases in sulfur capacity were observed during thermogravimetric testing of the monolith samples.

**Table 3-9. Summary of Operational Conditions for Parametric Temperature Testing**

	Sulfidation	Regeneration
Pressure (psig)	280	50
Space velocity (h <sup>-1</sup> )	2,000	2,000
Temperature (°F)	1000-2000 <sup>a</sup>	1250
Gas composition (vol%)		
CO		
CO <sub>2</sub>		
H <sub>2</sub>	99.5	
H <sub>2</sub> S	0.5	
N <sub>2</sub>		98
O <sub>2</sub>		2

<sup>a</sup> Test began at 538°C (1000°F) and temperature was decreased 55°C (100°F) each cycle until 93°C (200°F).

**3.4.3.3 Parametric Temperature Testing with Syngas.** Testing with the monolith sample used in the testing described in the previous section continued. In the last three cycles of testing, the composition of the sulfidation gas was altered to include 45 vol% CO, 4.5 vol% CO<sub>2</sub>, 35 vol% H<sub>2</sub>, 15 vol% N<sub>2</sub> and 5,000 ppmv of H<sub>2</sub>S. The sulfidation temperatures were also increased by 55°C (100°F) during each cycle with a starting temperature of 260°C (500°F) and a final temperature of 371°C

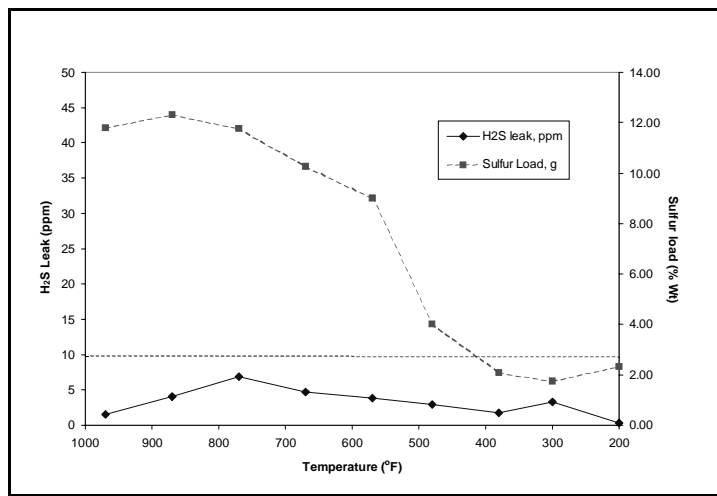


**Figure 3-12. Temperature effect on H<sub>2</sub>S leak and sulfur load.**

(700°F). The remainder of the sulfidation operating conditions and the regeneration conditions are identical to those used in the previous section and summarized in Table 3-10.

The results of parametric temperature testing with syngas are presented in Figure 3-13. In contrast to previous testing where H<sub>2</sub>S was by far the largest sulfur species in the effluent, Figure 3-13 shows that the effluent concentration of COS was significantly higher than H<sub>2</sub>S at all three temperatures tested. Since COS was not a component of the syngas feed, the COS was being formed by a reaction between H<sub>2</sub>S and CO. The observed increase in COS effluent concentrations indicate conditions for this reaction become more favorable at lower temperatures. This also indicates that the ability of ZnO to remove COS decreases more rapidly than for H<sub>2</sub>S as the sulfidation temperature is decreased.

**Table 3-10. Summary of Operational Conditions During Parametric Temperature Testing with Syngas**

	Sulfidation	Regeneration
Pressure (psig)	280	50
Space velocity (h <sup>-1</sup> )	2,000	2,000
Temperature (°F)	500-700 <sup>a</sup>	1250
Gas composition (vol%)		
CO	45	
CO <sub>2</sub>	4.5	
H <sub>2</sub>	35	
H <sub>2</sub> S	0.5	
N <sub>2</sub>	15	98
O <sub>2</sub>		2

<sup>a</sup> Test began at 260°C (500°F) and was increased 55°C (100°F) each cycle until 371°C (700°F).

The steady increase in sulfur loading during these three cycles confirms the results seen in the previous parametric temperature testing that sulfur capacity decreases significantly between 204 and 371°C (400 and 700°F).

#### 3.4.3.4 High Space Velocity Testing.

A 114 g RTI1-111-1 monolith was loaded in RTI's HTHP reactor system for a 5-cycle test. Sulfidations were performed at a space velocity of about 29,000 h<sup>-1</sup> with a H<sub>2</sub>S feed concentration of 1,000 ppmv and at 438°C (820°F) and 280 psig. An effluent sulfur concentration ≥200 ppmv signaled the end of sulfidation. In preparation for regeneration, the temperature was increased to 649°C (1200°F) and the pressure reduced to 50 psig in a N<sub>2</sub> purge. When the system had stabilized at these new operating conditions and the syngas had been purged out of the reactor system, regeneration was started. The composition of the regeneration gas was 2 vol% O<sub>2</sub> in N<sub>2</sub>. The

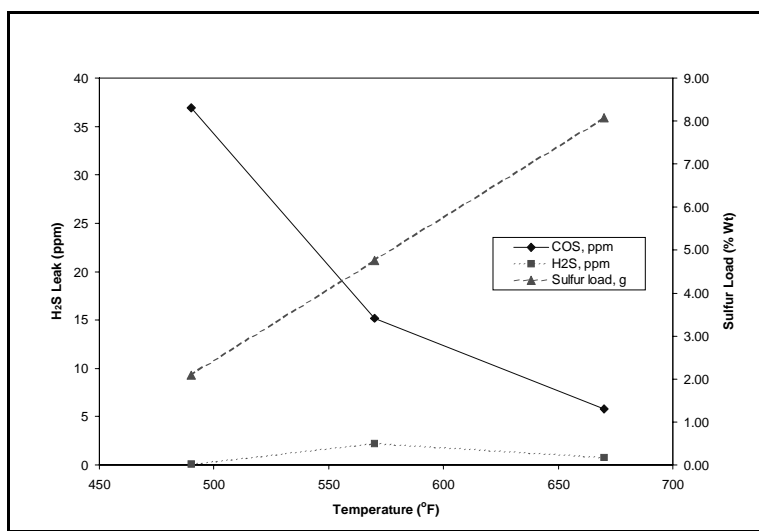


**Figure 3-13. Sulfur load H<sub>2</sub>S and COS effluent versus temperature using syngas.**

regeneration was stopped when the rate of decrease in the effluent SO<sub>2</sub> concentrations dropped significantly. The objective was to minimize exposure of the monolith to a gas mixture with both SO<sub>2</sub> and O<sub>2</sub>. A summary of the operating conditions for this 5-cycle test is provided in Table 3-11.

**Table 3-11. Summary of Operational Conditions During High Space Velocity Testing**

	Sulfidation	Regeneration
Pressure (psig)	280	50
Space velocity (h <sup>-1</sup> )	29,000	2,000
Temperature (°F)	820	1200
Gas composition (vol%)		
H <sub>2</sub>	99.9	
H <sub>2</sub> S	0.1	
N <sub>2</sub>		98
O <sub>2</sub>		2

The effluent H<sub>2</sub>S concentrations for this 5-cycle test are shown as a function of sulfur loading in Figure 3-14. As

observed with previous monolith testing, the ability to reduce effluent sulfur concentrations and sulfur capacity increased with each cycle. The effluent concentrations for Cycle 4 are higher than expected. Examination of the regeneration results for Cycle 3 revealed significant concentrations of SO<sub>2</sub> and O<sub>2</sub> in the reactor and reactor temperatures below the target value of 649°C (1200°F). In previous tests these conditions had also been associated with poor sulfidation performance in subsequent cycles.

The other important piece of information that can be seen in Figure 3-14 is the sulfur loading at this space velocity is about 4 wt%, which is about 25% of the sulfur capacity seen at low space velocity. At the high space velocity, the residence time of the gas in the monolith is very short. The short residence time limits the reaction to a small fraction of the available ZnO near the surface.

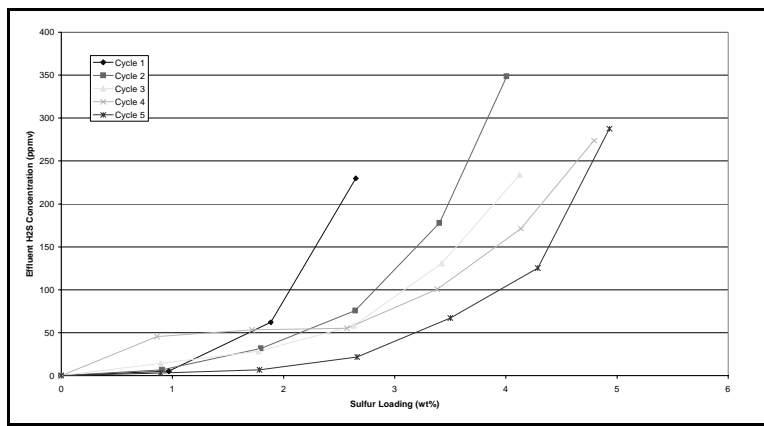


**Figure 3-14. Effluent H<sub>2</sub>S concentrations during monolith testing at a space velocity of 29,000 h<sup>-1</sup>.**

**3.4.3.5 Summary of Parametric Testing.** Parametric testing confirmed observations made both previously in the thermogravimetric testing and multicycle testing that monolith sulfidation performance improves over the first few cycles during an activation period. The number of cycles necessary to fully activate a monolith is shortest when the monolith is fully loaded with sulfur and optimal regeneration conditions are employed.

Decreasing temperature and increasing space velocity were both found to reduce the sulfur capacity of the monolith. This is believed to be the result a reduction in either the reaction rate

or contact time. Above 371°C (700°F), the sulfur capacity is in excess of 10 wt%. Below 260°C (500°F), the sulfur capacity of the monolith is about 2 wt%. The monolith was found to have a sulfur capacity of about 4 wt% at a space velocity of 29,000 hr<sup>-1</sup>.

Temperature did not appear to have a significant effect on the effluent H<sub>2</sub>S concentration. The effluent H<sub>2</sub>S concentration from 93 to 538°C (200 to 1000°F) was observed to be consistently below 10 ppmv and more typically below 2 ppmv. Temperature did have a significant effect on the effluent concentration of COS. Below 371°C (700°F), the effluent COS concentration was observed to be significantly larger than the H<sub>2</sub>S in the presence of syngas containing CO and CO<sub>2</sub>. An increase in the reaction between CO and H<sub>2</sub>S and a decreased ability of ZnO to remove COS are believed to cause this effect.

The short sulfidation time during the parametric testing at the high space velocity does not allow conclusive evidence about the effluent concentration prior to breakthrough. Based on the earlier results from the sulfidations in the 5-cycle test, the indication would be that the monolith could reduce effluent sulfur concentrations to ≤10 ppmv.

### **3.5 CONCLUSIONS**

The objective of this project was to evaluate the potential of using monolith materials for a regenerable polishing desulfurization unit. A number of observations made during both thermogravimetric testing and bench-scale testing show the promise of this objective. In both thermogravimetric testing and bench-scale testing, monolith materials could be operated for multiple cycles at temperatures as low as 93°C (200°F) with no apparent decrease in sulfidation performance. The monolith materials demonstrated adequate desulfurization performance at a space velocity of 29,000 h<sup>-1</sup>. These features indicate that the increased surface area does provide a means to increase the reactivity sufficient to allow operation at very short contact times and slow reaction kinetics at low temperatures.

The full theoretical sulfur capacity of the monolith materials was utilized over multiple cycles at appropriate conditions. However, at conditions where the desulfurization reaction is limited, such as short contact time at high space velocities or slow kinetics at lower temperatures, only a fraction of the theoretical sulfur capacity could be utilized. Although lower sulfur capacities will necessitate more frequent regenerations, this will only increase the operating cost of a regenerable polishing desulfurization unit based on monoliths and not its technical feasibility.

A number of issues need to be addressed for regenerable monolith materials to be used for polishing desulfurization. The reactivity needs to be increased to allow closer approximation with the equilibrium limiting effluent concentration. Currently, the effluent concentrations are still too high for adequate polishing for chemical and fuel cell applications. Additional testing will also be necessary to address the control of COS with these regenerable monolith materials, particularly at lower temperatures in syngas. During the bench-scale testing, regeneration

conditions were found to have a very important effect on sulfidation performance and reproducibility. Parametric testing focused on optimizing regeneration conditions will also be necessary.

## CHAPTER 4

### CHLORINE AND NITROGEN COMPOUND REMOVAL

#### 4.1 INTRODUCTION

One of the primary objectives of the novel technologies project has been to develop technically feasible and cost-effective processes for reducing to ultra-low levels of chlorine- and nitrogen-containing compounds in the gas streams produced by gasification of coal. Integrated coal gasification combined cycle has been shown to be not only efficient for electric power generation, but also conducive to reduction of emissions of undesirable components that are normally associated with coal power plants. The gas streams from a coal gasifier can also be used to synthesize liquid fuels and chemicals. This research program investigates viable process concepts to reduce the contaminant levels to ultra-low values that will enable coal gasification to couple with processes for production of chemicals and power generation by fuel cells.

##### 4.1.1 Chlorine and Nitrogen Compounds in Syngas Streams

Of the several impurities found in coal, sulfur species have attracted the greatest attention because they are usually the major undesirable impurity. In some coals, such as those from Illinois, chlorine species are the second most common contaminant (Chou, 1991). The chlorine content of Illinois and other Midwest bituminous coals can be as high as 0.6 wt%, well above the estimated 0.1 wt% average chlorine content of all U.S. coals (Ruch et al., 1974 a, b). The coals with highest chlorine were found in the south-central portion of Illinois, their chlorine content increasing with the depth of the coal seams (Gluskoter and Rees, 1964). During gasification, the chlorine in the coal is volatilized as HCl or metal chlorides. Typical concentrations of HCl in syngas have not been determined precisely, but they are estimated to be in the range 1 to 500 ppm (TRW, 1981). The actual concentration of HCl vapor in the syngas stream will depend on the chlorine content of the coal, the gasification temperature, and the type of gasifier.

U.S. coals contain from 0.5 to 2 wt% nitrogen on a dry basis (Chen et al., 1982), chemically combined with the carbon in polycyclic aromatic rings (Axworthy, 1975). Fuel-bound nitrogen compounds such as ammonia and hydrogen cyanide are formed during gasification of coal. The concentration of fuel-bound nitrogen compounds in syngas depends on factors such as temperature, pressure, residence time, and coal rank. Chen et al. (1982) found that low-rank coals favored the formation of ammonia. Kilpatrick (1986) reported that gas samples taken from working gasifiers producing low- and medium-Btu gas revealed levels of  $\text{NH}_3$  in the range of 180 to 3,100 ppm, depending on the type of gasification process. Haldipur et al. (1989) reported the concentration of  $\text{NH}_3$  found in the KRW air-blown fluidized-bed pilot plant gasifier

to be from 20 to 240 ppm. Kurkela and Ståhlberg (1992) found  $\text{NH}_3$  and HCN concentrations of 500 to 9,000 ppm in fluidized-bed gasifiers operating with peat, brown coal, and wood sawdust.

#### 4.1.2 Need for Removal of HCl and $\text{NH}_3$

Halogen compounds are deleterious to the molten carbonate fuel cell (MCFC) because they can lead to severe corrosion of cathode hardware (Kinoshita et al., 1988). HCl also can react with the molten carbonate electrolyte to form corresponding halides. These halides increase the loss of electrolyte because of the high vapor pressures of LiCl and KCl. The allowable HCl concentration in the feed gas to such a fuel cell is estimated to be less than 0.5 ppm (Hirschenhofer et al., 1994). In the production of chemicals, it is often necessary to convert CO in the syngas to  $\text{H}_2$  by water gas shift reaction. Catalysts such as Cu and Zn used for shift reaction are poisoned by HCl vapor in the feedstock. The copper and zinc chlorides are relatively mobile, leading to structural changes in the catalysts (Twiggs, 1996).

$\text{NH}_3$  and HCN are readily converted to oxides of nitrogen ( $\text{NO}_x$ ) during combustion of syngas. Processes such as selective catalytic reduction (SCR) must be used to remove the  $\text{NO}_x$  before the combustion gases can be vented to the atmosphere. Such processes are expensive and add significantly to the cost of electricity. In molten carbonate fuel cell applications, when the anode exhaust gas is burned with air to supply  $\text{CO}_2$  for the regeneration of the carbonate electrolyte, the fuel- $\text{NO}_x$  formed can react with the electrolyte to form relatively volatile nitrates that lead to loss of electrolyte by evaporation (Hirschenhofer et al., 1994). Thus, removal of  $\text{NH}_3$  from syngas is essential before it is used in these applications.

#### 4.1.3 Previous Studies

**4.1.3.1 HCl Removal Studies.** Krishnan et al. (1986) evaluated a commercial sorbent and several alkali minerals for removal of HCl (at 300 ppmv) from hot syngas at atmospheric pressure in the temperature range 550 to 650°C (1022 to 1202°F). The commercial sorbent was Katalco Chloride Guard 59-3; the three carbonate minerals were nahcolite, shortite, and dawsonite. All of the sorbents reacted rapidly with the HCl and reduced its concentration to about 1 ppmv. The performance of nahcolite was superior with respect to absorption capacity; the spent sorbent contained up to 54 wt% chloride. In a subsequent study conducted by a team of SRI International, RTI, and General Electric Corporate Research and Development, the HCl removal in syngas streams was conducted in bench- and pilot-scale reactors (Krishnan and Gupta, 1999). The results of bench-scale experiments in fixed- and fluidized-bed reactors demonstrated that nahcolite pellets and granules are capable of reducing HCl levels to less than 1 ppmv in syngas streams in the temperature range 400 to 650°C (752 to 1202°F). The sorbents, prepared by pelletizing or spray-drying the natural mineral, have a high capacity for HCl vapor. Tests conducted with the product gas of a pilot-scale fixed-bed gasifier confirmed that nahcolite effectively reduced HCl vapor to less than 15 ppm with a high degree of sorbent utilization (>70%) when operated in a circulating fluidized-bed reactor.

**4.1.3.2 NH<sub>3</sub> Removal Studies.** Although NH<sub>3</sub> is not a highly stable molecule ( $G_f^\circ = 0$  at ~175°C (350°F)), its dissociation requires very high temperature because of high activation of energy (92 kcal•mol<sup>-1</sup>) (Yamura and Asabe, 1981). Several investigators have studied the use of catalysts for the decomposition of NH<sub>3</sub> in hot gas streams. Krishnan et al. (1988) studied the removal of fuel-bound nitrogen compounds in a laboratory-scale reactor using simulated syngas compositions representative of several types of gasifiers. HTSR-1, a catalyst proprietary to Haldor-Topsøe A/S, Copenhagen, Denmark, exhibited excellent activity, even in the presence of 2,000 ppm of H<sub>2</sub>S and high temperature stability. G-65\*, an SRI catalyst, demonstrated superior activity in the temperature range 550 to 650°C (1022 to 1202°F) at H<sub>2</sub>S levels below 10 ppm. The presence of impurities such as HCl and HCN did not affect the catalyst performance in the temperature range studied. Tar contaminants can lead to carbon deposits that are easily removed at 800°C (1472°F). Jothimurugesan and Gangwal (1996) have reported that a zinc-based sorbent containing nickel exhibited a moderate activity for NH<sub>3</sub> decomposition while removing H<sub>2</sub>S. Leppälähti et al. (1996) reported that NH<sub>3</sub> can be removed by reacting with NO and O<sub>2</sub> at 450°C (842°F) (selective catalytic oxidation). In these tests, conducted at 20 atm pressure and on alumina catalysts, NH<sub>3</sub> removal decreased with temperature but increased with O<sub>2</sub>/NH<sub>3</sub> and NO/NH<sub>3</sub> ratios. Formations of N<sub>2</sub>O and NO<sub>2</sub> were also observed.

#### 4.1.4 Project

This chapter describes the results of an evaluation of the technical and economic feasibility of reducing HCl vapor levels to approximately 10 ppb and NH<sub>3</sub> levels to 10 ppm. Bench-scale experiments were conducted at SRI International to determine the technical feasibility, and preliminary cost calculations were made to determine the economic feasibility. Based on the results of this evaluation, recommendations are made for further studies.

## 4.2 REMOVAL OF HYDROGEN CHLORIDE VAPOR

### 4.2.1 Theoretical Considerations

Thermodynamic equilibrium calculations of the reaction of HCl vapor with various alkaline and alkaline earth carbonates indicated that sodium and potassium compounds are superior to alkaline earth carbonates in removing HCl vapors to trace levels. Sodium-based sorbents are preferred because they are more economical than potassium-based sorbents. At these temperatures, the vapor pressure of NaCl is approximately more than 1 order of magnitude lower than HCl vapor levels. The contribution of NaCl vapor to the residual chloride levels will be negligibly small. To achieve the desired goal of 10 ppb of chloride vapor, the gas stream needs to be cooled to less than 350°C (622°F) (Figure 4-1).

#### 4.2.2 Sorbent Requirements

Synthetic sorbents (chloride guards) are often used in the chemical industry to reduce HCl vapor levels to extremely low levels. These sorbents are usually a sodium compound (typically sodium carbonate) impregnated in a high surface area support such as alumina (~200 m<sup>2</sup>/g). However, they are expensive (typically \$1 to \$2/kg) and their capacity to absorb HCl vapor is limited (<5 wt%). These two characteristics tend to limit the use of commercial chloride guards in syngas applications.

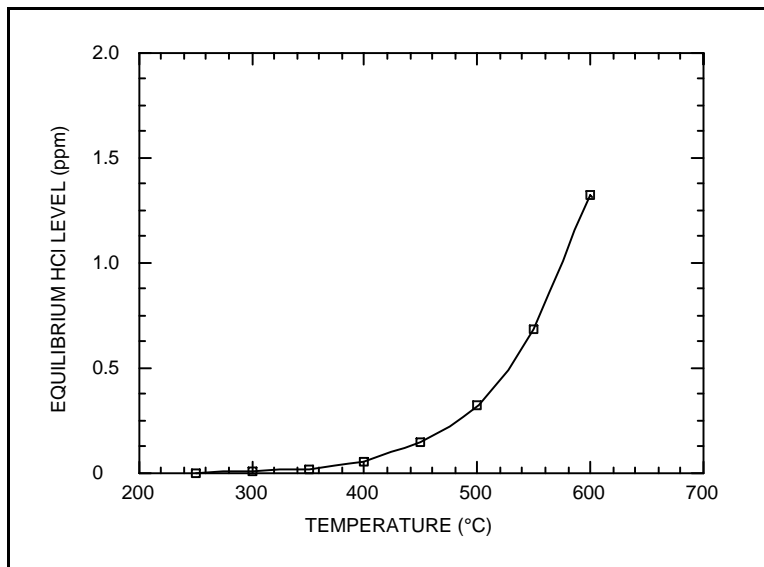


**Figure 4-1. The equilibrium partial pressure of HCl is a function of temperature at 20 atm in a Texaco col gasifier gas stream.**

Although earlier studies have shown that the natural mineral, nahcolite, has sufficient reactivity and capacity for use in high-temperature syngas applications, its reactivity and capacity are limited at temperatures below 400°C (752°F). The reason for this decrease in capacity is because of the low surface area of these sorbents. In contrast to synthetic sorbents, the nahcolite mineral pellets or granules do not have high surface areas; hence, the thickness of the sodium carbonate grains is large. Slow diffusion through the product NaCl layer limits the rate of reaction at the interior of the carbonate grains.

As alternatives to the high cost of catalyst supports, several low-cost and moderate surface area materials were considered as support media for the active ingredient, sodium carbonate. Such materials include pyrolyzed rice hulls, diatomaceous earth, and sepiolite mineral.

The rice hulls are the waste products of the agriculture industry and do not have many uses. After pyrolysis of the organic portion, the rice hulls become mainly porous silica. When the rice hulls are extruded with a binder and agglomerated, moderate surface area pellets are formed. Diatomaceous earth is a naturally occurring mineral consisting mainly of silica with small amounts of alumina, iron oxides annually, and alkali. In the United States, more than 600,000 tons of diatomaceous earth is mined, mainly in California, Nevada, Oregon, and Washington states. This natural mineral has a moderate surface area (10 to 20 m<sup>2</sup>/g) and is used as fillers, filter media, and catalyst supports. Because of its low cost, it should be considered as a support for disposable sorbents. Sepiolite is a fibrous clay mineral that occurs in the United States and Europe. The mineral is used as a support for catalysts in petrochemical applications (dual functional cracking catalyst) and environmental applications

(selective catalytic reduction of nitrogen oxides). Sepiolite is a hydrous magnesium silicate and has a relatively high surface area ( $\sim 140 \text{ m}^2/\text{g}$ ) and large pore volume ( $0.65 \text{ cm}^3/\text{g}$ ).

Sorbents based on rice hulls or diatomaceous earth are silica-based and their reactivity toward sodium carbonate must be considered. The reaction between silica and  $\text{Na}_2\text{CO}_3$  leads to the formation of sodium silicate. Experiments conducted at SRI as part of a separate program showed that the reaction between silica and  $\text{Na}_2\text{CO}_3$  is rapid only at temperatures above  $700^\circ\text{C}$  ( $1292^\circ\text{F}$ ). At temperatures below  $400^\circ\text{C}$  ( $752^\circ\text{F}$ ), the rate of interaction between  $\text{Na}_2\text{CO}_3$  and silica would be very slow. Even if sodium silicate is formed, it will react with HCl to form NaCl, as shown in previous programs of HCl removal under DOE sponsorship (Krishnan and Gupta, 1999). Since sepiolite is a silicate-based compound, its reaction with  $\text{Na}_2\text{CO}_3$  may not be significant.

#### **4.2.3 Detection of Trace Levels of HCl Vapor**

To demonstrate the effectiveness of the sorbents in meeting the objective of the program, an analytical method to determine HCl vapor at ppb levels must be devised. In previous programs, SRI demonstrated the usefulness of contacting the HCl vapor in the hot reactor effluent gas stream with a solution of  $\text{NaHCO}_3$  and analyzing the dissolved chloride by the ion chromatographic (IC) analysis. This method was automated to measure the chloride concentration in the solution intermittently. The partial pressure of residual HCl vapor was calculated by differentiating the accumulated chloride levels. Care was taken to avoid condensation of steam on the walls of the reactor or tubing before the gas was analyzed for HCl vapor. Ion chromatography is an established technique for analyzing cations such as chloride in the presence of other constituents such as sulfide or ammonia. Using the procedure outlined above, HCl vapor levels of less than 1 ppm were detected routinely.

This procedure could be modified to extend the sensitivity to ppb levels. Dionex Corporation, a manufacturer of IC equipment, has published a procedure to determine trace levels of anions in high-purity water using a large sample volume ( $\sim 1 \text{ mL}$ ) and mixtures of boric acid and sodium hydroxide as eluents. This procedure is more complex than the previous one, but  $1\text{-}\mu\text{g/L}$  (ppb) levels of chloride could be detected in about 5 min, as shown in Figure 4-2. In fact, Dionex claims that the detection limit for chloride under this procedure is 0.044 ppb.

This procedure is suitable for analyzing effluents from simulated syngas streams because the anions such as fluoride, acetate, and formate, which elute ahead of chloride, would not be present. However, carbonate ions would be present in a significant quantity from the dissolution of  $\text{CO}_2$  in the aqueous solution. The carbonate ions elute after chloride ions and, hence, the presence of the carbonate ions would not interfere with chloride analysis.

#### 4.2.4 Experimental Determination of Sorbent Reactivities for HCl Vapor

A bench-scale fixed-bed system was used to determine the achievable residual HCl vapor level, the rate of chloride uptake as a function of time, and the maximum achievable chloride capacity of the sorbents. The atmospheric pressure systems used in this study are described in Krishnan and Gupta (1999). The ion chromatograph was modified to perform the trace level HCl vapor analysis.

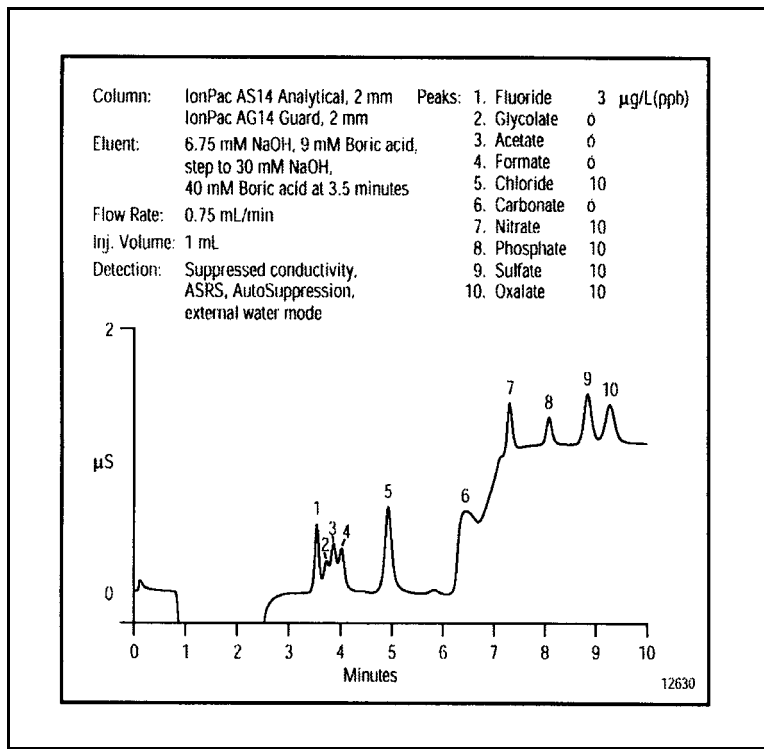


Figure 4-2. Detection of trace levels of anions, including chloride in an aqueous solution.

Moderate surface area pellets of diatomaceous earth and sepiolite powder were extruded in a bench-scale extruder with bentonite as a binder. The pellets were impregnated with a sodium carbonate solution and calcined at 450°C (842°F) in air. Pyrolyzed rice hulls that were available at SRI were too fragile, and severe gas channeling occurred.

The sorbent granules were tested in the bench-scale reactor at about 350°C (662°F) and a space velocity of 2,000 h<sup>-1</sup> (at STP) using a simulated gas containing 50 ppm HCl vapor, 10% steam, 5% CO<sub>2</sub>, and the balance N<sub>2</sub>. Although this gas stream did not contain H<sub>2</sub> or CO, they do not affect the uptake of HCl vapor by these sorbents. The observed results with sepiolite-based (S-01) and diatomaceous earth-based (D-01) sorbents are shown in Figure 4-3 and summarized in Table 4-1.

These results are encouraging in that they demonstrate that HCl vapor could be reduced to trace levels. The observed steady-state HCl levels are higher than equilibrium values and they could be due to channeling of the gas through the bed. The sorbent utilization (the ratio of Na<sub>2</sub>CO<sub>3</sub> converted to the initial amount of Na<sub>2</sub>CO<sub>3</sub>) could be improved by changing the impregnation and calcination procedures to provide an optimum pore size distribution. Although micropores contribute to the surface area, access to the interior of the micropores could limit the reactivity. Presence of both macropores and micropores are essential in optimizing the sorbent utilization. These changes could increase the capacity of the sorbent for HCl uptake significantly.

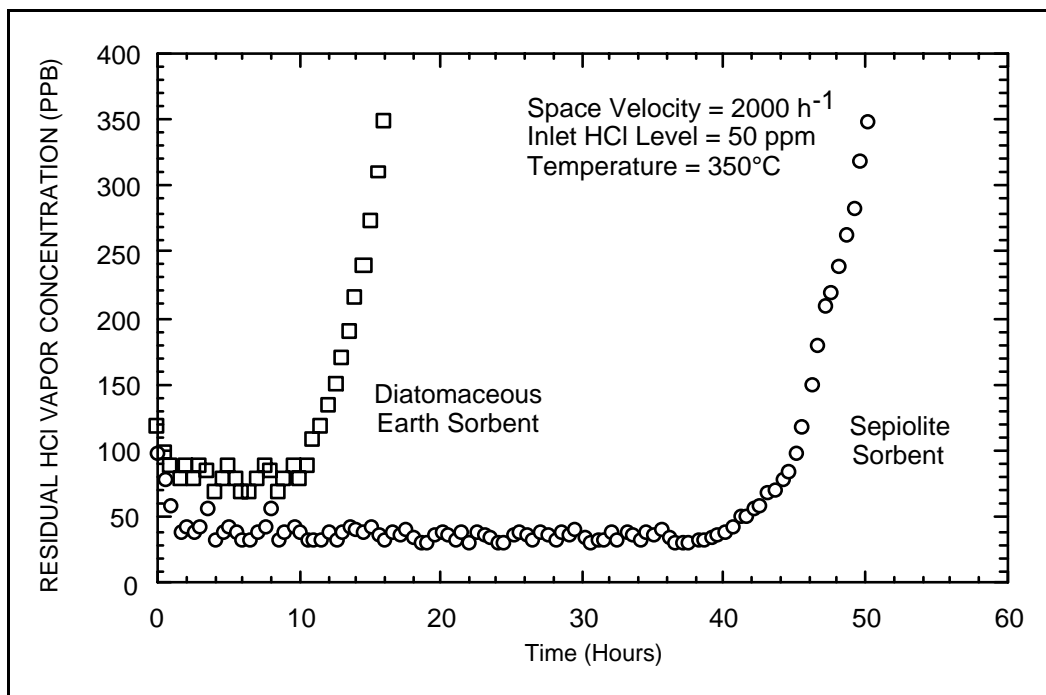


Figure 4-3. HCl breakthrough curves for sepiolite- and earth-based sorbents.

#### 4.2.5 Preliminary Economic Analysis

Figure 4-4 illustrates the process scheme envisioned for the removal of HCl vapor from syngas streams to trace levels. In this scheme, the bulk of HCl vapor removal will be

accomplished using nahcolite sorbent (developed in the previous DOE program downstream of the particulate removal step. The optimum temperature for this step is about 450 to 550°C (842 to 1022°F), and the HCl vapor level could be reduced to about 1 ppm in bench-scale fixed-bed reactors. Tests conducted at the GE Corporate Research and Development pilot-scale facility demonstrated that HCl vapor levels could be reduced to less than 15 ppm when sodium bicarbonate-based sorbents were used in a circulating fluidized-bed reactor. The actual value of residual could have been lower than 15 ppm because that was the detection limit. Hence, it is reasonable to assume that the bulk removal step could reduce the HCl level to about 5 ppmv.

A fixed-bed reactor system is preferred for the removal of HCl vapor to sub-ppm levels using high surface area sorbents. Such reactors containing chloride guards are used in the chemical industry for dechlorination of feedstocks for ammonia and methanol synthesis.

Table 4-1. Results of HCl Vapor Removal Experiments

Property	S-01	D-01
Surface area (m <sup>2</sup> /g)	98.3	10.8
Weight % Na <sub>2</sub> CO <sub>3</sub>	5.1	1.8
Steady-state HCl level (ppb)	35	80
Time for 0.1-ppm breakthrough (h)	40	10
Percent sorbent utilization	18.8	13

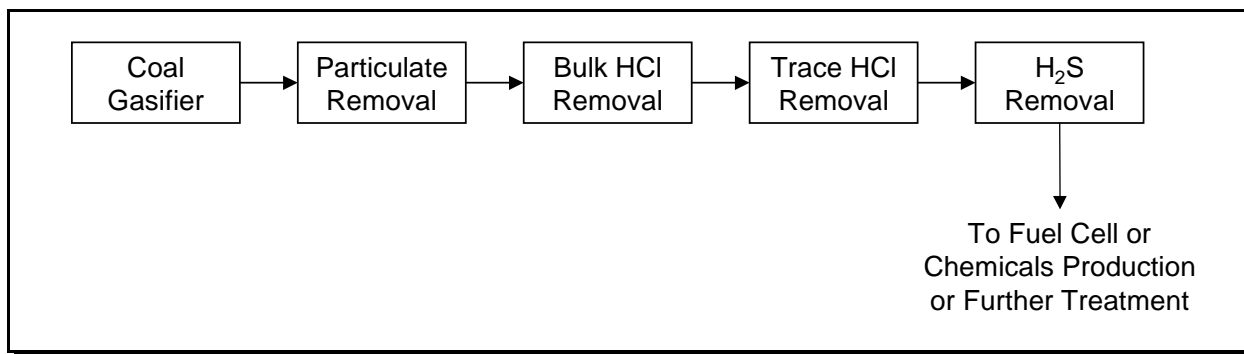


Figure 4-4. Process block diagram for removal of HCl vapor from hot syngas streams.

#### 4.2.6 Bulk HCl Removal Cost

Krishnan and Gupta (1999) estimated the cost of bulk HCl removal in an earlier study. In this study, both fixed- and circulating fluidized-bed systems were considered. Economic calculations (Table 4-2) indicated that the cost of removal of HCl vapor from hot syngas streams is only about \$0.001/kWh (0.9 to 1.4 mill/kWh). Fixed-bed reactors were estimated to be the least expensive option (0.9 mill/kWh) because of their simple configuration and ability to achieve high chloride capture capacities. Major cost components are the cost of feed sorbent and the disposal of the spent sorbent. The cost of using circulating fluidized-bed (CFB) reactor systems was higher (1.4 mill/kWh) because of smaller chloride capacity and the cost of granulating the sorbent by a spray drying process. The use of commercially available baking soda powder in CFB reactors would result in higher cost (1.8 mill/kWh) because of decreased reactivity and chloride capacity.

Table 4-2. Annual Cost of Bulk HCl Removal Unit (Texaco Entrained-Bed, Oxygen-Blown Gasifier, 400 MWe)

Materials	Rate	Annual Cost (\$)
Sorbent	\$225/st	774,800
Maintenance materials	3% of TIC	50,800
Sorbent disposal	\$250/st	827,500
Labor		
Operating	\$45/h	394,200
Maintenance	2% TIC	33,900
Fixed costs		
General and administrative	1.5% TIC	25,400
Taxes and insurance	2.5% TIC	42,300
Cost of capital	25% TCC	667,400
Total annual operating costs		2,786,200
Annual operating cost (\$/kWh)		0.00094
Annual operating cost (mills/kWh)		0.94

Inlet gas composition (% v/v): HCl = 300 ppmv; H<sub>2</sub> = 30.7; CO = 41.6; CO<sub>2</sub> = 10.2; H<sub>2</sub>O = 15.2; N<sub>2</sub> = 0.8; H<sub>2</sub>S = 0.7.

Type of reactor: Fixed-bed, 3-reactor unit.  
 Total installed cost (TIC) = \$1,693,200.  
 Total capital cost (TCC) = \$2,699,500.

#### 4.2.7 Trace HCl Removal Cost

Table 4-3 lists the parameters for the unit process for the trace HCl removal system. As in the case of the bulk HCl removal unit, it consists of three fixed-bed reactors, two of which will be in service at any time while the third is being readied (Figure 4-5). The vessels were assumed to be of carbon steel with a refractory lining. Each vessel is about 113 m<sup>3</sup> and holds about 125 tons (metric ton) of sorbent pellets. The sorbent was assumed to consist of 3-mm-diameter pellets made of sepiolite mineral and impregnated with 6 wt% Na<sub>2</sub>CO<sub>3</sub>. The sorbent utilization was assumed to be 20% at 50-ppb breakthrough level. The beds were sized for a cycle time of 30 days before the spent sorbent would be emptied and fresh sorbent loaded. Before the reactor is unloaded, it is depressurized and nitrogen gas is circulated to cool the bed.

**Table 4-3. Process Design Basis for Trace HCl Removal Unit (Texaco Entrained-Bed, Oxygen-Blown Gasifier, 400 MWe)**

Parameter	Value
Operating temperature °C	350
Mass flow rate of gas (kg/h)	262,080
Inlet HCl level (ppm)	5
Outlet HCl level (ppm)	0.05
Na <sub>2</sub> CO <sub>3</sub> loading (wt%)	6
Sorbent utilization (% Na <sub>2</sub> CO <sub>3</sub> converted)	20
Sorbent chloride capacity at 50-ppb breakthrough (kg Cl per ton of sorbent)	8
Reactor cycling time (days)	30

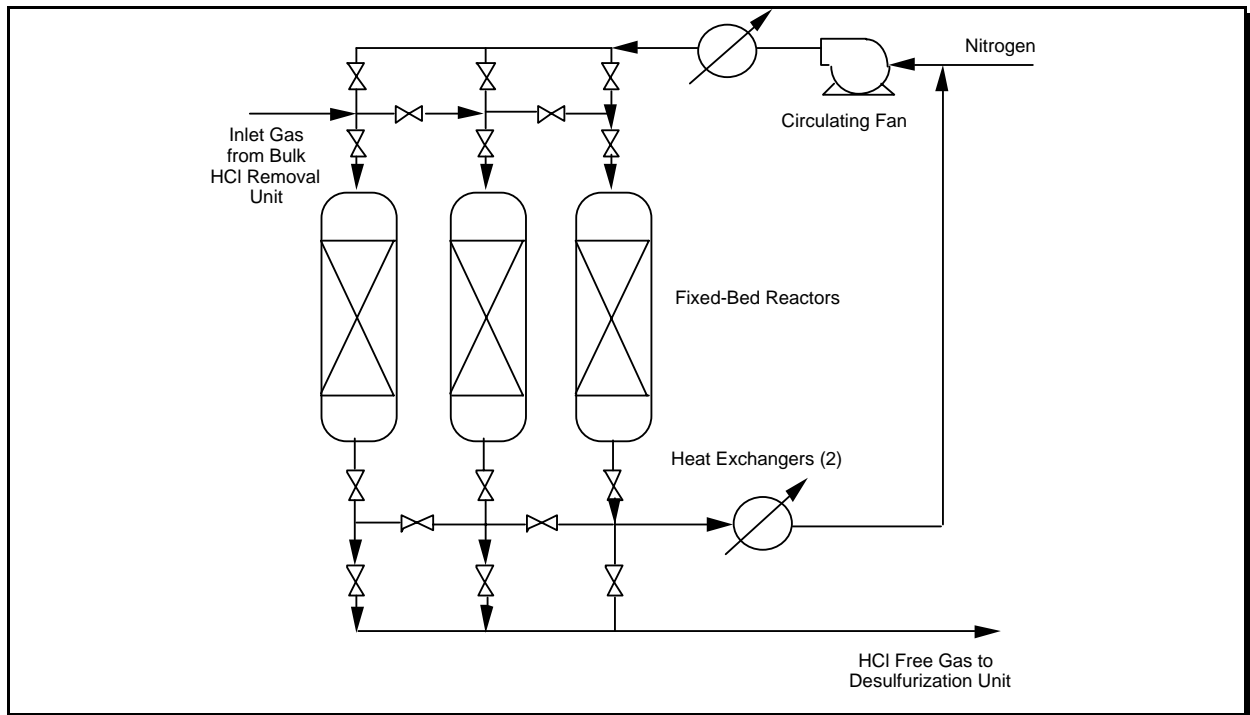


**Figure 4-5. Schematic diagram of trace HCl removal process using fixed-bed reactors.**

Capital cost estimates for the trace HCl removal systems are shown in Table 4-4. The cost estimates were based on the design of the reactors for the bulk removal system modified for 30-day sorbent capacity. The costs were also adjusted for year 2000 construction using the *Chemical Engineering Plant Index*. These include total installed equipment costs (TIC), indirect costs (at 30% of TIC), contingency (at 20% of TIC), initial sorbent charge, and startup costs (at 5% of TIC). The capital costs for the trace removal system are only 20% higher than that for the bulk removal unit, mainly because of the larger size of the reactor. However, the cycle time is twice as long as that for bulk HCl removal.

**Table 4-4. Capital Cost of Trace HCl Removal System (Texaco Entrained-Bed, Oxygen-Blown Gasifier, 400 MWe)**

Equipment	Quantity	Cost (\$)
Sorbent vessels	3	1,135,000
Sorbent cooler blower	1	26,000
Heat exchangers	2	54,000
Total FOB equipment cost		1,215,000
Total installed cost (TIC): (170% Total FOB Cost)		2,065,000
Indirect costs (30% of TIC)		619,600
Contingency (20% TIC)		413,100
Initial sorbent charge (250 tons at \$300/ton)		75,000
Startup costs (5% of TIC)		103,300
Total capital cost (TCC)		3,276,000

Other reactor configurations, such as moving- or fluidized-bed reactors, may not be as attractive as the fixed-bed reactor, especially given the long cycle time of the fixed-bed reactor. Moving- and fluidized-bed reactors will require lock hoppers that are expensive for high-pressure operation. They will also need either elliptically shaped pellets or granulated sorbents, which would increase the cost of sorbent. These reactors will also require more labor attention and maintenance than fixed-bed reactors. Based on the long cycle time and their long-time use as chloride-guard reactors in the chemical industry, this analysis was limited to fixed-bed reactors only for this preliminary cost estimate.

**Table 4-5. Annual Cost of Trace HCl Removal Unit (Texaco Entrained-Bed, Oxygen-Blown Gasifier, 400 MWe)**

Materials	Rate	Annual Cost (\$)
Sorbent	\$300/ton	741,200
Maintenance materials	3% of TIC	62,000
Sorbent disposal	\$10/ton	24,700
Labor		
Operating	\$45/h	394,200
Maintenance	2% TIC	41,300
Fixed costs		
General and administrative	1.5% TIC	31,000
Taxes and insurance	2.5% TIC	51,600
Cost of capital	25% TCC	819,000
Total annual operating costs		2,165,000
Operating cost (\$/kWh)		0.00064
Operating cost (mill/kWh)		0.64

The annual operating cost estimates for the sepiolite-based chloride removal systems for both types of reactor configurations are detailed in Table 4-5 along with the assumed values for cost parameters.

The principal factors in the operating costs for the trace HCl removal system are sorbent-

related items (the cost of feed sorbent), operating labor, and capital-related items, which account for 34%, 18%, and 38%, respectively. The dominance of sorbent-related costs are due to a single-time use of the sorbent and low utilization of the sorbent. The spent sorbent disposable was assumed to be nonhazardous because trace metals are likely to be captured by the nahcolite-based, bulk HCl removal sorbent was assume. Hence, only \$10/ton for disposal of the sepiolite-based sorbent. The operating labor costs could be reduced if a single operator per shift could be shared with other unit operations in the power plant. The simple trace HCl removal unit may not require the full attention of a single operator.

A set of economic sensitivity calculations was performed to test the effects of varying design and economic assumptions on the annual operating costs of the trace HCl removal system. The results of these estimates are presented in Table 4-6.

Assumed changes in capital-related costs (capital cost and capital recovery factor) change the operating cost by about 10%. If the operating labor can be reduced by half by sharing with other unit operations such as bulk HCl removal, then the cost of trace HCl removal is reduced by 0.05 mill/kWh. Changes in the sorbent feed cost by about 30% change the operating cost by less than 10%.

**Table 4-6. Economic Sensitivity Analysis of Trace HCl Vapor Removal System**

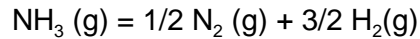
<b>Parameter</b>	<b>Value</b>	<b>Operating Cost (mill/kWh)</b>
Capital investment	75%	0.58
	100%	0.64
	125%	0.71
Capital recovery	15%	0.55
	25%	0.64
Labor (operator/shift)	0.5	0.59
	1.0	0.64
Feed sorbent cost	\$200/t	0.57
	\$300/t	0.64
	\$400/t	0.72
Feed gas HCl level (ppm)	105	0.87
		0.64
Sorbent chloride capture capacity (% active sorbent)	20	0.64
	30	0.57
	50	0.42

The sorbent utilization capacity has a significant effect on the operating cost. The base case assumes that 20% of the active ingredient in the sorbent is used up before HCl breakthrough occurs. Changes in the pore structure of the sorbent could increase the sorbent utilization. Increasing the utilization from 20% to 30% decreases the cost by about 10%. But if 50% of the sorbent capacity could be used, then 35% reduction in the operating cost could be realized. At these high capacity levels, only two reactors may be needed, resulting in decreased capital and operating costs. If the operating labor is shared and the sorbent utilization is increased to 30%, then the cost of trace HCl removal could be as low as 0.5 mill/kWh.

## 4.3 REMOVAL OF AMMONIA VAPOR

### 4.3.1 Theoretical Considerations

Although  $\text{NH}_3$  is not a highly stable molecule thermodynamically ( $\Delta G^\circ_f(298) = -3.9 \text{ kcal/mol}$ ), the activation energy for dissociation is high ( $92 \text{ kcal} \cdot \text{mol}^{-1}$ ). Furthermore, the high concentration of  $\text{H}_2$  in syngas streams such as those representative of slugging gasifiers limits the level to which  $\text{NH}_3$  can be dissociated under equilibrium conditions.



The calculated thermodynamic equilibrium levels of  $\text{NH}_3$  in a Texaco coal gasifier stream (assumed to be 5,000 ppm in the feed gas) at 20 atm as a function of temperature is shown in Figure 4-6. Two cases were considered in these calculations: (1) complete thermodynamic equilibrium is achieved, and (2) equilibrium is achieved except for the formation of  $\text{CH}_4$  in the gas. The results show that 90% or greater dissociation can be achieved at temperatures above  $700^\circ\text{C}$  ( $1292^\circ\text{F}$ ). The extent of dissociation decreases with decreasing temperature in the absence of  $\text{CH}_4$  formation. If  $\text{CH}_4$  is allowed to form at equilibrium levels,  $\text{NH}_3$  levels of about 20 ppm can be reached at  $300^\circ\text{C}$  ( $572^\circ\text{F}$ ), again under equilibrium conditions. These results are due to the conversion of  $\text{H}_2$  to  $\text{CH}_4$ , which reduces the  $\text{H}_2$  levels in the gas. Because the  $\text{NH}_3$  equilibrium level is a strong function of the  $\text{H}_2$  partial pressure, any reduction in  $\text{H}_2$  level will facilitate  $\text{NH}_3$  dissociation.

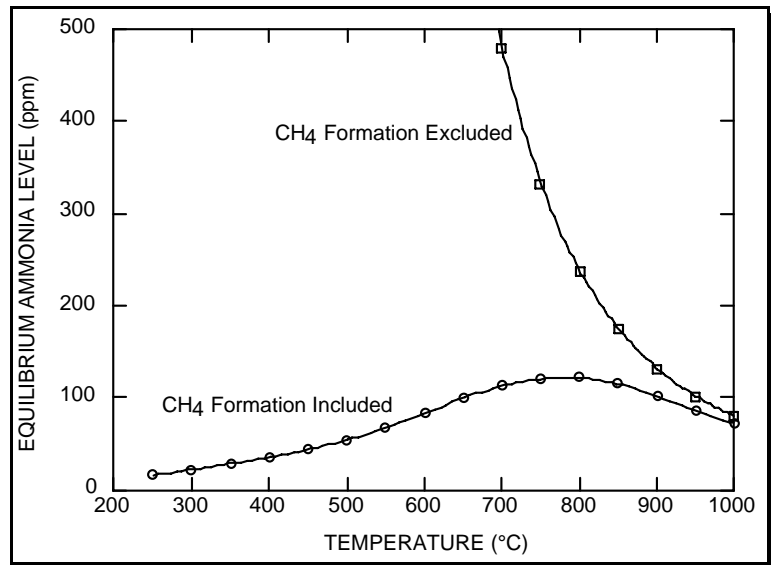


Figure 4-6. The equilibrium partial pressures of  $\text{NH}_3$  as a function of temperature at 20 atm in a Texaco coal gasifier gas stream.

In the absence of equilibrium methane formation, reducing the levels of  $\text{NH}_3$  below 10 ppm requires temperatures above  $1200^\circ\text{C}$  ( $2192^\circ\text{F}$ ). Even at that temperature, catalysts may be needed to attain equilibrium levels. Heating the gas to such a temperature is not cost-effective. Hence, thermal decomposition is not an effective technique to remove  $\text{NH}_3$  from syngas streams.

These calculations show that a residual  $\text{NH}_3$  level lower than 10 ppm could be achieved at a temperature of  $250^\circ\text{C}$  ( $482^\circ\text{F}$ ) or below if significant amounts of  $\text{H}_2$  are converted to  $\text{CH}_4$ . Such low temperature operation may require development of efficient catalysts that can function in the presence of significant levels of  $\text{H}_2\text{S}$  and steam. Sulfur-tolerant methanation catalysts based on  $\text{MoS}_2$  are available, but they are not as reactive as conventional nickel-based methanation catalysts. Nickel-based catalysts are extremely susceptible to sulfur poisoning.

The formation of  $\text{CH}_4$  has no adverse effect and may be beneficial if the syngas is to be used for combustion in a gas turbine. The reaction is exothermic, and, under adiabatic conditions, the exit gas will be at a higher temperature than the feed gas. Moreover, the volume of feed gas is reduced. However, the formation of  $\text{CH}_4$  is not desired if syngas is to be used for MCFC applications because  $\text{CH}_4$  is not easily oxidized at the MFCF cathode. MCFC systems often incorporate methane reformers to convert  $\text{CH}_4$  into  $\text{H}_2$ . Methane, again, is not a desirable feedstock for chemical production of alcohols or other hydrocarbon liquid fuels. In fact, in many chemical applications, such as hydrocarbon or methanol syntheses reactions, hydrogen is synthesized by reforming methane. Hence, reducing  $\text{NH}_3$  levels using reactions that involve methane formation may not be the best use of syngas for fuel cells and chemical synthesis applications.

An alternative process is to absorb  $\text{NH}_3$  on high-surface-area adsorbents. In contrast to the catalytic decomposition process, the adsorption of  $\text{NH}_3$  is facilitated at high pressure, but the quantity that could be adsorbed decreases at high temperatures. Molecular sieve sorbents, especially those high acid types, have significantly high capacity for basic molecules such as  $\text{NH}_3$ . In these sorbents, the acid strength is often measured by its ability to adsorb a base such as  $\text{NH}_3$ . The acidity of molecular sieves depends on various factors, such as the composition, method of preparation, temperature of dehydration, and possible treatment with steam.

#### **4.3.2 Sorbents for Ammonia Removal**

The quantity of  $\text{NH}_3$  adsorbed on various molecular sieves as a function of temperature has been reported by Hidalgo (1984). A temperature-programmed desorption (TPD) technique was used to obtain these results. In these experiments,  $\text{NH}_3$  was adsorbed on the catalyst at  $100^\circ\text{C}$  ( $212^\circ\text{F}$ ), the catalyst was heated to  $600^\circ\text{C}$  ( $1112^\circ\text{F}$ ) at a linear rate of  $10^\circ\text{C}$  ( $18^\circ\text{F}$ )/min, and the quantity of  $\text{NH}_3$  desorbed was measured. The TPD spectra of mordenites and ZSM-5 molecular sieve showed two desorption peaks, a low-temperature peak centered around  $125^\circ\text{C}$  ( $257^\circ\text{F}$ ) and a high-temperature peak centered around  $400^\circ\text{C}$  ( $752^\circ\text{F}$ ). These results showed that these molecular sieves have strong and weak acid sites on which  $\text{NH}_3$  can be chemisorbed. The Y-type molecular sieves had a broad peak only. The amount of  $\text{NH}_3$  adsorbed can be calculated from the area under the TPD curve, and it is proportional to the acid strength of the catalyst. The acid strengths of the catalysts were of the order  $\text{HM} > \text{HZSM-5} > \text{HY}$ . Cation exchange decreased the strong acid sites preferentially, whereas dealuminization reduced the strong and weak acid sites.

Table 4-7 summarizes the reported quantity of NH<sub>3</sub> desorbed at temperatures above 227°C (440°F).

**Table 4-7. Amount of NH<sub>3</sub> Adsorbed and Maximum Desorption Temperatures**

Catalyst	NH <sub>3</sub> Desorbed <sup>a</sup> (10 <sup>-3</sup> mol/g Catalyst)	
	Temperature (°C)	Amount
HM (decaionized H-mordenite)	408	0.75
Ca-HM (calcium-exchanged H-mordenite)	408	0.87
K-HM (potassium-exchanged H-mordenite)	362	0.21
HZSM-5 (hydrogen-exchanged ZSM-5)	339	0.71
DM (dealuminated H-mordenite)	404	0.43
K-DM (potassium-exchanged DM zeolite)	357	0.24
HY (Na Y zeolite exchanged with NH <sub>4</sub> Cl)	Broad peak	0.26
K-HY (potassium-exchanged Y zeolite)	Broad peak	0.81
Rb-HY (rubidium-exchanged Y zeolite)	Broad peak	0.66

<sup>a</sup> Amount of NH<sub>3</sub> desorbed above 227°C (531°F).

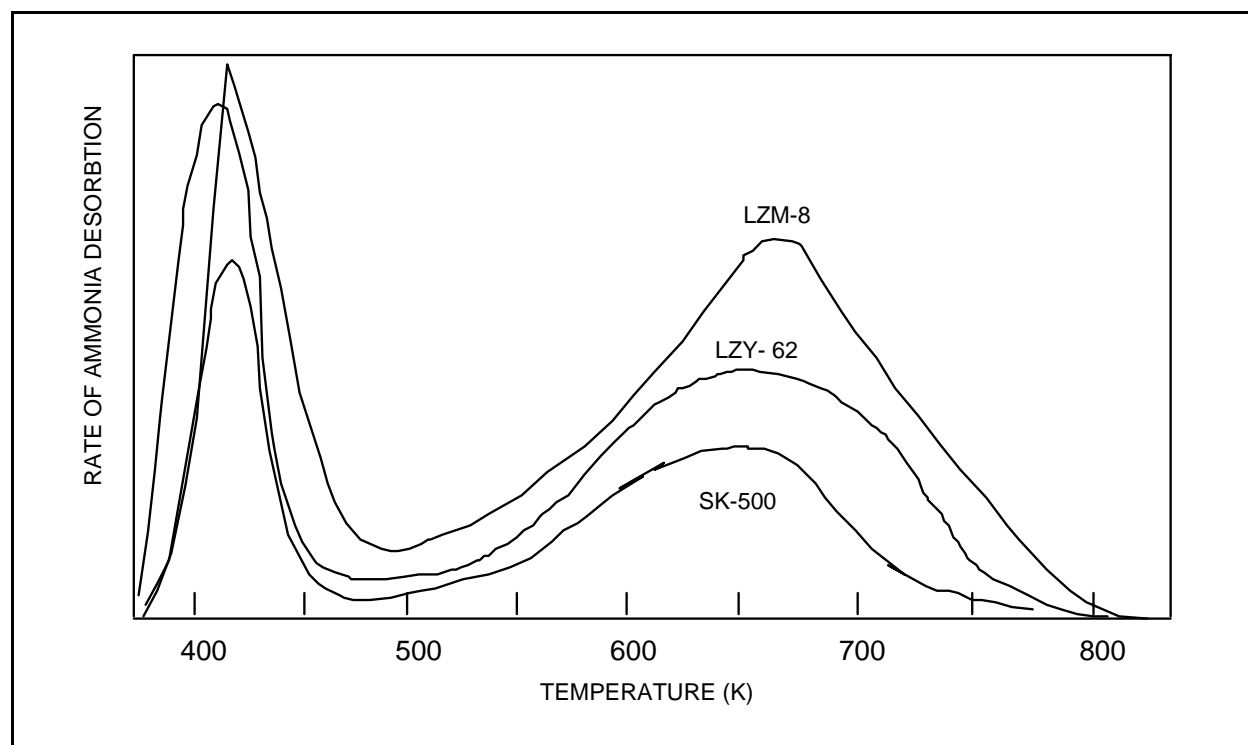
A temperature-programmed reactor was used to determine the adsorption and desorption behavior of NH<sub>3</sub> on selected sorbents. NH<sub>3</sub> was adsorbed at a low temperature 225°C (437°F) by using pulses of a gas stream containing 0.5% NH<sub>3</sub>. The adsorption capacity was calculated from the differences in the feed and exit gas NH<sub>3</sub> concentrations. Subsequently, the catalyst containing adsorbed NH<sub>3</sub> was heated to desorb the NH<sub>3</sub>.

Three molecular sieves were selected for experimental determination of NH<sub>3</sub> adsorption and desorption studies: H-mordenite (LZ M-8), Y-type zeolite (LZY-62), and rare-earth exchanged Y zeolite (SK-500). The LZY-62 catalyst was treated with NH<sub>4</sub>Cl to exchange the Na present in the catalyst with H<sup>+</sup> ions. It was washed until no chloride was detected in the washwater. The catalyst was dried and calcined at 400°C (752°F) to remove any adsorbed NH<sub>3</sub>.

A temperature-programmed desorption reactor was used to determine the performance of catalysts for NH<sub>3</sub> adsorption and desorption under atmospheric pressure conditions. A small amount of catalyst was placed inside the reactor and was heated in N<sub>2</sub> to a temperature of 225°C (437°F). After the temperature stabilization, pulses of 0.5% NH<sub>3</sub> in N<sub>2</sub> were introduced and the residual NH<sub>3</sub> levels were recorded. The capacity of the catalyst for NH<sub>3</sub> adsorption was calculated from the differences in the feed and residual levels. When the residual levels of NH<sub>3</sub> reached a value close to the feed gas value, the catalyst was heated at about 10°C (18°F)/min to 500°C (932°F) while monitoring the desorbed NH<sub>3</sub> levels. Table 4-8 summarizes the results, and Figure 4-7 illustrates the desorption spectra of the three selected catalysts.

**Table 4-8. Properties of Molecular Sieves for NH<sub>3</sub> Adsorption**

Property	LZM-8	LZY-62	SK 500
Surface area (m <sup>2</sup> /g)	450	650	520
SiO <sub>2</sub> /Al <sub>2</sub> O <sub>3</sub> (mol)	17.1	2.4	4.9
NH <sub>3</sub> adsorption at 225°C (mol/g)	0.4 x 10 <sup>-3</sup>	0.35 x 10 <sup>-3</sup>	0.25 x 10 <sup>-3</sup>
Peak desorption temperature (°C)	395	Broad	Broad

**Figure 4-7. Temperature-programmed desorption of NH<sub>3</sub> adsorbed on various molecular sieves.**

The NH<sub>3</sub> adsorption capacities of these catalysts at 225°C (437°F) are somewhat lower than reported in the literature for H-mordenite catalyst (0.75 x 10<sup>-3</sup> mol/g). The differences might be a result of using different vendors or pretreatment procedures. A ZSM-5 type molecular sieves from Zeolyst International. These materials have very high acidity (SiO<sub>2</sub>/Al<sub>2</sub>O<sub>3</sub> = 50 to 280) and high surface areas (400 to 425 m<sup>2</sup>/g). They were heated to 400°C (752°F) to desorb moisture and subsequently exposed to pulses of 0.5% NH<sub>3</sub> at 225°C (437°F). The adsorption capacity of ZSM-type zeolites was similar to that of H-mordenite (~0.4 x 10<sup>-3</sup> mol/g), and the desorption temperature was about 350°C (662°F).

### 4.3.3 Process Considerations

Figure 4-8 illustrates the process scheme envisioned for the removal of ammonia from syngas streams. In this scheme, the syngas from the gasifier will go through particulate removal filters followed by a dechlorination step. Hydrogen sulfide and steam will be removed using the process that is under development at RTI. The gas stream will then pass through a circulating fluidized-bed reactor containing a molecular sieve adsorbent. The adsorbent will remove  $\text{NH}_3$  by adsorption at about  $200^\circ\text{C}$  ( $392^\circ\text{F}$ ). The molecular sieve adsorbent particles will be stripped of adsorbed  $\text{NH}_3$  in a regenerator through which a purge stream of  $\text{N}_2$  is passed and the temperature of the sorbent is increased to about  $500^\circ\text{C}$  ( $932^\circ\text{F}$ ). The regenerated adsorbent will be recycled to the adsorption step. Because of the fast circulation of the molecular sieve in the reactor, the capacity of the adsorbent for  $\text{NH}_3$  need not be high.

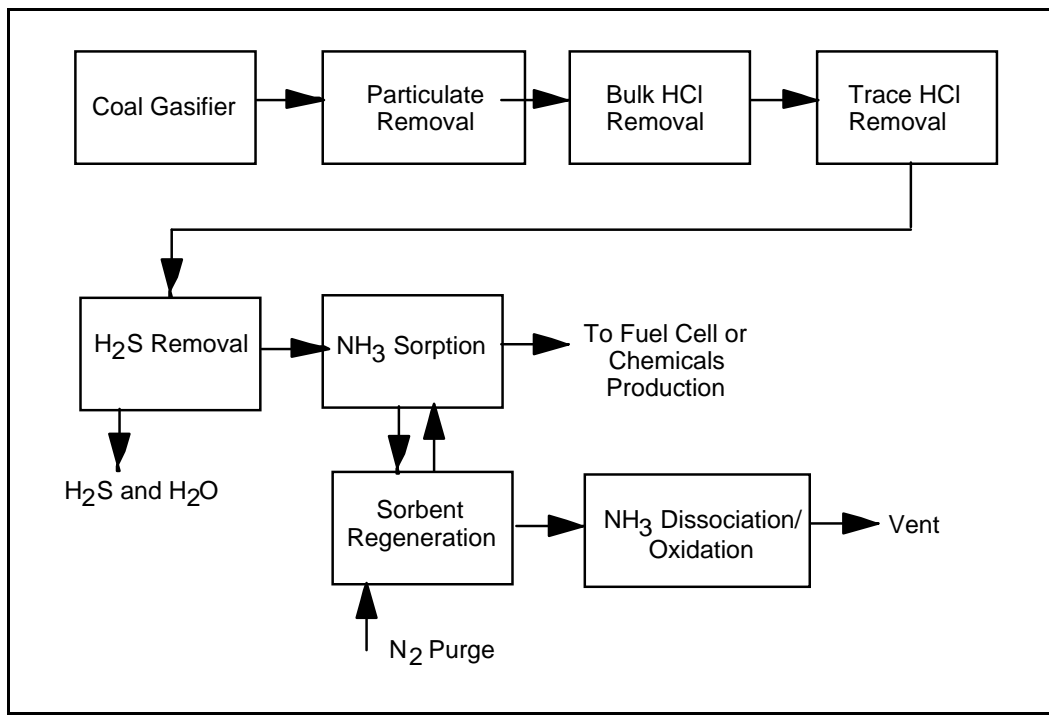


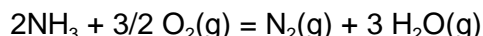
Figure 4-8. Process block diagram for removal of  $\text{NH}_3$  from hot syngas stream.

The  $\text{NH}_3$  removal reactor is placed downstream of the desulfurization step because of the potential adsorption of steam by the molecular sieves. Adsorption of steam is more likely as the temperature is lowered to enhance  $\text{NH}_3$  adsorption. Hence, removal of steam would add flexibility to the  $\text{NH}_3$  sorption step. Removal of  $\text{H}_2\text{S}$  also prevents the formation of both  $(\text{NH}_4)_2\text{S}$  and  $\text{NH}_4\text{HS}$  on the surface of molecular sieves.

During the regeneration step, the molecular sieves are heated to temperatures of about  $460^\circ\text{C}$  ( $860^\circ\text{F}$ ) to desorb  $\text{NH}_3$ . The recovered  $\text{NH}_3$  could be disposed of by several known methods. The disposal of  $\text{NH}_3$  in the regeneration sweep gas stream can be accomplished by catalytic

decomposition to its elements because of the absence of H<sub>2</sub>S and H<sub>2</sub>. In previous programs funded by the DOE, SRI developed efficient catalysts for decomposition of NH<sub>3</sub> in the hot syngas streams. In the absence of H<sub>2</sub>S, low-temperature catalysts such as G-65\* (Ni-based catalysts) could be used at temperatures of 500 to 600°C (932 to 1112°F). The absence of H<sub>2</sub> will also facilitate the decomposition, and very low values of residual NH<sub>3</sub> could be achieved. If surface ammonium sulfides are formed during the adsorption step, they could release H<sub>2</sub>S during regeneration, which will require sulfur-tolerant catalysts. Catalysts such as HTSR-1 are sulfur tolerant, but require a temperature of about 900°C (1652°F) for efficient operation.

An alternative treatment of disposing of NH<sub>3</sub> is to oxidize it to N<sub>2</sub> and H<sub>2</sub>O:



In the absence of suitable catalysts, combustion of NH<sub>3</sub> could lead to production of nitrogen oxides. However, transition metal oxide catalysts containing chromium oxide and cobalt oxide supported on alumina can efficiently oxidize NH<sub>3</sub> to N<sub>2</sub> at a temperature above 600°C (1112°F) (Prasad et al., 1981).

#### 4.3.4 Preliminary Economic Analysis

A suitable process scheme appears to be a circulating fluidized-bed reactor consisting of an absorber operating at about 225°C (437°F) and a regenerator operating at 460°C (860°F) (Figure 4-9). The residence time of the gas in the absorber is about 10 s, a sufficient time for equilibration of the gas and solid and for chemisorption of NH<sub>3</sub> on the molecular sieve surface. The spent sorbent is regenerated in the regenerator using N<sub>2</sub> as the stripping gas. The NH<sub>3</sub>-N<sub>2</sub> stream is then sent to a decomposition unit or an oxidizer with a transition metal catalyst to convert to N<sub>2</sub>. The design characteristics of the system are shown in Table 4-9.

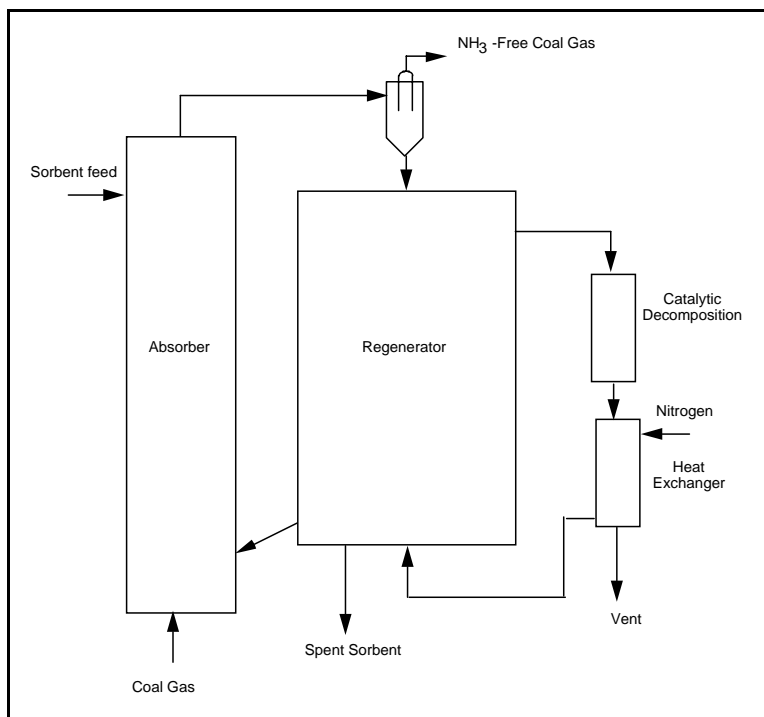


Figure 4-9. Schematic diagram of ammonia removal unit.

**Table 4-9. Process Design Basis for Ammonia Removal Unit (Texaco Entrained-Bed, Oxygen-Blown Gasifier, 400 MWe)**

Parameter	Value
Operating temperature of absorber (°C)	225
Operating temperature of absorber (°C)	460
Inlet NH <sub>3</sub> level (ppm)	1000
Outlet NH <sub>3</sub> level (ppm)	10
NH <sub>3</sub> capacity of the sorbent in the absorber (mol/g)	4 x 10 <sup>-5</sup>
Absorber size (diameter x height, m)	0.6 x 20
Regenerator size (diameter x height, m)	2 x 8
Residence time of gas in the absorber (s)	10
Residence time of solids in the regenerator (s)	50
Mass flow rate of syngas (kg/h)	262080
Mass flow rate of stripper gas (kg/h)	26200
Sorbent inventory in the absorber (tons)	0.9
Sorbent inventory in the regenerator (tons)	4.5
Replacement sorbent rate (% inventory/d)	3
Stripper gas replacement (% circulation)	10
Stripper gas inlet temperature (°C)	725

Capital cost estimates for the ammonia removal systems are shown in Table 4-10. The cost estimates were based on a circulating fluidized-bed reactor system. These cost assumptions include total installed equipment costs that are 170% of the FOB cost, indirect costs (at 30% of TIC), contingency (at 20% of TIC), the initial sorbent charge, and startup costs (at 5% of TIC). Other reactor configurations such as fixed- and moving-bed reactors may not be as attractive for ammonia removal because of the very short cycle time for NH<sub>3</sub> adsorption and regeneration.

**Table 4-10. Capital Cost of NH<sub>3</sub> Removal System (Texaco Entrained-Bed, Oxygen-Blown Gasifier, 400 MWe)**

Equipment	Quantity	Cost (\$)
Absorber	1	50000
Regenerator	1	150000
Lockhoppers, cyclones, valves		100000
Heat exchangers	1	25000
NH <sub>3</sub> converter (catalytic decomposition)	1	50000
<b>Total FOB equipment cost</b>		<b>325000</b>
Total installed cost (TIC): (170% Total FOB Cost)		<b>552500</b>
Indirect costs (30% of TIC)		165800
Contingency (20% TIC)		110500
Initial catalyst charge (25 tons at \$3,000/ton)		75000
Startup costs (5% of TIC)		27600
<b>Total capital cost (TCC)</b>		<b>931400</b>

The cycle time is short because NH<sub>3</sub> is chemisorbed on the surface rather than forming a bulk compound as in the case of HCl removal sorbent.

The annual operating costs are summarized in Table 4-11. The principal factors in the operating costs in the NH<sub>3</sub> removal system are regeneration of the spent sorbent (29%), operating labor (32%), capital-related items (19%), and cost of replacement sorbent (14%). The dominance of the regeneration step is due to heating the sorbent by about 300°C (572°F). The actual heating costs may be low, because only the surface of the sorbent needs to be heated to desorb the NH<sub>3</sub>. The spent sorbent may not contain any trace metals and thus should be considered nonhazardous. The operating cost for NH<sub>3</sub> removal is only \$0.0004 (0.4 mill)/kWh.

**Table 4-11. Annual Cost of NH<sub>3</sub> Removal Unit (Texaco Entrained-Bed, Oxygen-Blown Gasifier, 400 MWe)**

<b>Materials</b>	<b>Rate</b>	<b>Annual Cost (\$)</b>
Replacement sorbent	\$3,000/ton	170,000
Maintenance materials	3% of TIC	16,600
Sorbent disposal	\$100/ton	5,700
Replacement N <sub>2</sub>	\$0.035/m <sup>3</sup>	38,100
Labor		
Operating	\$45/h	394,200
Maintenance	2% TIC	11,100
Utilities (natural gas)	\$5/MM Btu	360,900
Fixed costs		
General and administrative	1.5% TIC	8,300
Taxes and insurance	.5% TIC	13,800
Cost of capital	25% TCC	232,800
Total annual operating costs		1,251,300
Operating cost (\$/kWh)		0.00037
Operating cost (mill/kWh)		0.37

#### 4.4 SUMMARY AND FUTURE WORK

Based on the results of the experimental work HCl vapor concentration could be reduced to <50 ppbv levels using a 2-stage process, consisting of bulk removal (to 1 ppmv) followed by trace removal (to <50 ppmv). Based on a preliminary economic analysis, cost of total HCl removal processes is about 1.5 mils/kWh.

Removal of NH<sub>3</sub> vapors from coal-derived syngas could be carried out by adsorption onto acidic type, high-surface area molecular sieves. The adsorbed ammonia could be desorbed at high temperatures in an inlet stream. Preliminary economic analysis indicated cost of NH<sub>3</sub> removal to be about 0.6 mil/kWh.

In the Option Program, a bench-scale reactor system will be setup to conduct bulk and trace HCl removal steps sequentially in two fixed-bed reactors. NH<sub>3</sub> removal tests will be conducted in a high-pressure fluidized-bed reactor in a cyclic manner.

## CHAPTER 5

### TECHNICAL AND ECONOMIC EVALUATION

Over the past 2 years, RTI and its research group have been carrying out studies directed at developing novel technologies for gaseous contaminants control. Although the research has been, in large part, focused on obtaining experimental data to verify and develop the novel control concepts, RTI and its collaborators have never lost sight of the idea that these novel concepts must offer economic advantages as well as technical advantages over state-of-the-art control techniques. Rough estimates of the cost of the integrated modular approach of bulk sulfur removal from syngas by membranes and fine sulfur control by ZnO-coated monoliths with chlorine and nitrogen compounds removal by sorbents has been addressed repeatedly by RTI, starting with its proposal to DOE and in subsequent reports and meetings with DOE.

In April of 2001, RTI sent information concerning the details of RTI's modular process to Nexant, Inc. Nexant was awarded a contract by DOE to evaluate the RTI process technically and economically and compare this process to state-of-the-art processes used to carry out contaminant removal from syngas. Based on Nexant's considerable experience and database for process design and equipment cost estimation, RTI presents Nexant's process review and economic evaluation in place of RTI's own evaluation in this chapter. While the cost figures arrived at by Nexant for the RTI process seem somewhat elevated in comparison to RTI's own rough estimates, RTI defers to Nexant's evaluation in view of their process design experience and extensive equipment cost database. The Nexant technical and economic evaluation of RTI's model process is presented in its entirety in Section 5.1 of this report.

The Nexant evaluation is based on realistic, achievable performance of the equipment involved in the RTI design. For example, the design of the bulk sulfur removal membrane was based on a low operating temperature of 52°C (125°F) rather than the goal of operating at 204°C (400°F). The process information, which RTI sent to Nexant in April 2001, and on which Nexant carried out its evaluation, was based on what was realistically achievable at that time as determined by RTI's experimental results. Because of this low membrane operating temperature, which RTI and its collaborators are in the process of increasing, ammonia and hydrogen chloride were condensed out of the syngas prior to the membrane module. Therefore, the removal of these two components by disposable and regenerable sorbents, as is being investigated by RTI and its collaborators, was not addressed in the Nexant evaluation. In the absence of Nexant's evaluation, RTI and its collaborators have performed economic evaluations of the HCl and NH<sub>3</sub> removal modules. The results of these economic evaluations are provided in Sections 4.2.6, 4.2.7, and 4.3.4 of this report.

The case that Nexant evaluated, in which the HCl and NH<sub>3</sub> removal modules being developed by RTI were not necessary for removing HCl and NH<sub>3</sub> from the syngas as a consequence of low

membrane temperature, is an example of the highly flexible nature of RTI's modular contaminant control concept.

Based on the evaluation by Nexant, RTI's contaminant control process appears to be very economically competitive with a state-of-the-art process for syngas cleanup, the Rectisol process. The Rectisol process was shown by Nexant to be 75% more capital-intensive than RTI's modular contaminant control process.

## 5.1 NEXANT'S TECHNICAL AND ECONOMIC EVALUATION OF THE RTI PROCESS

### 5.1.1 Introduction

The RTI process consists of several steps. The initial step is a flashing of the raw syngas for the removal of HCl and NH<sub>3</sub>. The three major steps of the process involve polymer membrane modules for bulk H<sub>2</sub>S separation, ZnO-coated monolith reactors for fine H<sub>2</sub>S removal, and a direct sulfur recovery process coupled with partial oxidation for the conversion of H<sub>2</sub>S to elemental sulfur. Table 5-1 lists the three major process steps, the companies involved with their development, and the sulfur removal level associated with each step.

**Table 5-1. Process Sulfur Removal Efficiency**

	<b>Polymer Membrane</b>	<b>Monolithic Reactor</b>	<b>POx/SDRP Reactor</b>
Companies involved in development	RTI, North Carolina State University & MEDAL, Inc.	Monolithic Reactor	RTI, DOE/NETL
Removal efficiency	90% H <sub>2</sub> S removal	85.5% H <sub>2</sub> S removal	<95% H <sub>2</sub> S conversion to elemental sulfur

Nexant reviewed data and information provided by RTI and conducted its own evaluation by first sizing and cost-estimating a syngas cleanup facility. The process flow sheet and mass energy balance data that RTI supplied to Nexant were taken from an ASPEN PLUS simulation based on a nominal syngas flow rate of 100 lbmol/hr. The composition and condition of the raw syngas (370°C [700°F] at 40 atm [600 psia]) were typical of a Texaco, oxygen-blown gasifier. Nexant scaled the data, as appropriate, to match the syngas flow rate that would be required to achieve 500 MWe in an IGCC plant. Table 5-2 presents the details of each stream taken from the ASPEN PLUS simulation, for the nominal 100 lbmol/hr syngas flow rate.

Two commercially available technologies: (1) chemical solvent processes, amines (specifically methyl diethanolamine or MDEA), and (2) physical solvent processes (Rectisol, utilizing methanol) were considered as potential alternatives to the RTI technologies. They are widely used processes for syngas cleaning.

**Table 5-2. Mass and Energy Balance for RTI Process (nominal basis-100 lbmol/hr syngas)**

Stream Number	1	2	3	4	5	6	7	8	9	10
Description	Raw Syngas	POX Effluent	POX Air	Regenerated off gas	Filtered Syngas	Membrane Residue	Cooled Raw Syngas	Heated Residue	Cold Raw Syngas	Raw Syngas Condensate
Temperature (°F)	700	1150	80	1100	700	80	322.9	670	80	80
Pressure (psia)	600	200	200	200	600	600	600	600	600	600
Molar Flowrates (lbmol/hr)										
H <sub>2</sub>	30	0.757			30	26.643	30	26.643	30	traces
CO	40	1.012			40	38.088	40	38.088	40	
CO <sub>2</sub>	12	9.877			12	3.023	12	3.023	12	
N <sub>2</sub>	2.2	10.623	10.533	5.072	2.2	2.11	2.2	2.11	2.2	
H <sub>2</sub> S	0.84	0.068			0.84	0.069	0.84	0.069	0.84	0.004
NH <sub>3</sub>	0.18				0.18	traces	0.18	traces	0.18	0.18
H <sub>2</sub> O	15	3.37			15	0.002	15	0.002	15	14.928
SO <sub>2</sub>		0.7		0.069						
Sulfur <sup>(e)</sup>										
O <sub>2</sub>		traces <sup>(a)</sup>		traces						
HCL	0.03		2.8		0.03	traces	0.03	traces	0.03	0.03
Total Flow (lbmol/hr)	100.3	26.4	13.3	5.1	100.3	69.9	100.3	69.9	100.3	15.1
Total Flow (lb/hr)	2073.7	870.0	384.7	146.5	2073.7	1315.1	2073.7	1315.1	2073.7	273.2
Total Flow (cuft/hr)	2107.1	2290.2	385.6	432.4	2107.1	685.5	1408.5	1438.1	829.7	4.4
Vapor Fraction	1.00	1.00	1.00	1.00	1.00	1.00	1.00	1.00	1.00	0.85
Liquid Fraction	0.00	0.00	0.00	0.00	0.00	0.00	0.00	0.00	0.15	1.00
Enthalpy (Btu/hr) <sup>(b)</sup>	-5024780.6	-1905004.0	-228.9	29521.2	-5024780.6	-2324094.8	-5327111.6	-2021764.0	-5812557.2	-1861115.5
Average MW	20.7	32.9	28.9	28.5	20.7	18.8	20.7	18.8	20.7	18.0
Mole Fraction										
H <sub>2</sub>	0.299	0.029			0.299	0.381	0.299	0.381	0.299	2 PPB
CO	0.399	0.038			0.399	0.545	0.399	0.545	0.399	
CO <sub>2</sub>	0.12	0.374			0.12	0.043	0.12	0.043	0.12	
N <sub>2</sub>	0.022	0.402	0.79	0.987	0.022	0.03	0.022	0.03	0.022	
H <sub>2</sub> S	0.008	0.003			0.008	981 PPM	0.008	981 PPM	0.008	245 PPM
NH <sub>3</sub>	0.002				0.002	11 PPB	0.002	11 PPB	0.002	0.012
H <sub>2</sub> O	0.15	0.128			0.15	24 PPM	0.15	24 PPM	0.15	0.986
SO <sub>2</sub>		0.027		0.013						
Sulfur <sup>(e)</sup>										
O <sub>2</sub>		133 PPB <sup>(d)</sup>		27 PPM						
HCL	299 PPM <sup>(c)</sup>		0.21		299 PPM	3 PPB	299 PPM	3 PPB	299 PPM	0.002

(a) traces = flowrate < 0.001 lbmol/hr

(b) These enthalpy values are calculated using 80 °F as a reference temperature

(c) PPM = Parts per million by volume

(d) PPB = Parts per billion by volume

(e) Sulfur as (S8)

(f) Q (-) in the diagram denotes heat being released from each unit

Table 5-2. (continued)

Stream Number Description	11	12	13	14	16	17	18	19	20
Dewatered Raw Syngas	80	1200	80	80	1143.3	673.5	1200	1100	1200
Pressure (psia)	600	200	20	200	200	600	200	200	200
Molar Flowrates (lbmol/hr)									
H2	30		3.357	3.357	0.757				
CO	40		1.912	1.912	1.012				
CO2	12		8.977	8.977	9.877				
N2	2.2	Variable	0.09	0.09	15.695		Variable	5.072	10% stream 18
H2S	0.836		0.768	0.768	0.068	traces			
NH3	traces					traces			
H2O	0.072		0.07	0.07	3.37				
SO2					0.769				
Sulfur <sup>(e)</sup>						traces			
O2								0.103	
HCL	traces					traces			
Total Flow (lbmol/hr)	85.1	Variable	15.2	15.2	31.5		69.9		5.2 10% stream 18
Total Flow (lb/hr)	1800.4		485.4	485.4	1016.5		1314.0		145.4
Total Flow (cuft/hr)	824.9		4380.9	426.4	2725.3		1442.5		435.3
Vapor Fraction	1.00	1.00	1.00	1.00	1.00		1.00		1.00
Liquid Fraction	0.00		0.00	0.00	0.00		0.00		0.00
Enthalpy (Btu/hr) <sup>(b)</sup>	-3951657.7		-1623559.2	-1625228.2	-1875482.7		Variable		38269.4
Average MW	21.2		32.0	32.0	32.2		18.8		28.1
Mole Fraction									
H2	0.352		0.221	0.221	0.024		0.381		
CO	0.47		0.126	0.126	0.032		0.545		
CO2	0.141		0.592	0.592	0.313		0.043		
N2	0.026	1	0.006	0.006	0.498		1		0.98
H2S	0.01		0.051	0.051	0.002		392 PPB		1
NH3	9 PPB						11 PPB		
H2O	841 PPM		0.005	0.005	0.107		0.001		
SO2					0.024				
Sulfur <sup>(e)</sup>									
O2					5 PPM				0.02
HCL	2 PPB								

(a) traces = flowrate < 0.001 lbmol/hr

(b) These enthalpy values are calculated using 80 °F as a reference temperature

(c) PPM = Parts per million by volume

(d) PPB = Parts per billion by volume

(e) Sulfur as (S8)

(f) Q (-) in the diagram denotes heat being released from each

Table 5-2. (continued)

Stream Number Description	21 Tail Gas	22 DSRP Effluent	23 Regeneration Air	24 Regeneration Gas	25 Regeneration N2	26 Sulfur Product	27 Cooled DSRP Effluent	29 Cooled Heating Gas	30 Vented Heating Gas
Temperature (°F)	100	1140	80	80	80	100	100	Variable	Variable
Pressure (psia)	200	200	200	200	200	200	200	200	200
Molar Flowrates (lbmol/hr)									
H2	0.023	0.023				traces	0.023		
CO	0.275	0.275				traces	0.275		
CO2	10.614	10.614				0.001	10.614		
N2	15.695	15.695	0.387	5.072	4.685	traces	15.695	Variable	10% stream 29
H2S	0.002	0.002				traces	0.002		
NH3									
H2O	0.091	4.17				4.079	4.17		
SO2	traces	traces				traces	traces		
Sulfur <sup>(e)</sup>	traces	0.104				0.104	0.104		
O2	traces	traces	0.103	0.103		traces	traces		
HCL									
Total Flow (lbmol/hr)	26.7	30.9	0.5	5.2	4.7	4.2	30.9	Variable	10% stream 29
Total Flow (lb/hr)	916.3	1016.5	14.1	145.4	131.2	100.2	1016.5		
Total Flow (cuft/hr)	787.8	2723.9	14.2	149.9	135.7	1.5	2723.9		
Vapor Fraction	1.00	1.00	1.00	1.00	1.00	0.0	1.00	1.00	1.00
Liquid Fraction	0.00	0.00	0.00	0.00	0.00	1.0	0.00		
Enthalpy (Btu/hr) <sup>(b)</sup>	-1961002.5	-2031754.4	-8.4	-76.3	-67.8	-476842.5	-2437845.0		
Average MW	34.3	32.2	28.9	28.1	28.0	20.4	32.2		
Mole Fraction									
H2	850 PPM	744 PPM				1 PPB	744 PPM		
CO	0.01	0.009				6 PPB	0.009		
CO2	0.398	0.343				110 PPM	0.343		
N2	0.588	0.508	0.79	0.98	1	457 PPB	0.508	1	1
H2S	76 PPM	64 PPM				454 PPB	64 PPM		
NH3									
H2O	0.003	0.135				0.97	0.135		
SO2	14 PPM	12 PPM				149 PPB	12 PPM		
Sulfur <sup>(e)</sup>	< 1 PPB	0.003				0.025	0.003		
O2	5 PPM	5 PPM	0.21	0.02		< 1 PPB	5 PPM		
HCL									

(a) traces = flowrate < 0.001 lbmol/hr

(b) These enthalpy values are calculated using 80 °F as a reference temperature

(c) PPM = Parts per million by volume

(d) PPB = Parts per billion by volume

(e) Sulfur as (S8)

(f) Q (-) in the diagram denotes

### **5.1.2 Conclusions and Recommendations**

After careful examination of the existing technologies and their overall performance, Rectisol was chosen over MDEA as the more appropriate competing technology to the RTI technologies. MDEA was considered less appropriate because it cannot remove carbonyl sulfur (COS) from the syngas stream.

The proposed RTI process does not address the removal of trace metals, such as mercury, in the syngas stream.

It appears that RTI has combined a series of viable technologies for the cleanup of syngas that are about 45% less costly than the existing technology (Rectisol). Further reductions in cost can be achieved by lowering the maximum operating temperatures for both the monolithic reactors and the partial oxidation reactor, thus allowing the metallurgy to be changed to carbon steel. Cost savings may also be achieved as the monoliths become commercially fabricated on an industrial scale, thus reducing the number of blocks required per reactor.

The total installed capital cost for the syngas cleanup plants is estimated to be \$42 million with the RTI process and \$75 million with Rectisol. The Rectisol process is over 75% more capital intensive than the RTI process.

### **5.1.3 Conventional Acid Gas Removal Options**

Many processes exist for the removal of acid gases, most of which employ absorption. These processes can be categorized into two types—chemical and physical—based on operating principles.

In a chemical absorption process, the acid gas components to be removed react either with an alkaline compound dissolved in water or directly with the solvent, forming a chemical compound. The solvent is then stripped of the acid gases and recirculated to the feed gas stream for further acid gas removal.

MDEA has high efficiency for removal of H<sub>2</sub>S, but essentially no COS is removed using MDEA. In contrast, the RTI process has high removal efficiency for all sulfur-containing compounds; thus, MDEA is not suitable for comparison with the RTI process.

The physical absorption processes all use organic solvents and accomplish acid-gas removal mainly by physical absorption, rather than chemical reaction, which is directly proportional to the acid-gas partial pressure in the sour-gas stream. These processes are most applicable to high-pressure gas streams containing appreciable quantities of sour components. The high-acid-gas loadings realized account for low solvent-circulation rates, reduction in equipment size and cost, and low utilities, which are characteristic of these processes.

The Rectisol process, which uses methanol, is very efficient at stripping all impurities out of the syngas, including COS. Rectisol is the most relevant conventional acid gas removal technology for comparison with the RTI process.

#### 5.1.4 RTI Process Objective

The objective of RTI's study was to develop technologies for cleaning and conditioning IGCC-generated syngas to meet contaminant tolerance limits for fuel cell and chemical production applications.

It is generally accepted that the limits for contamination are in the ppmv levels for power generations. For chemical production and fuel cells impurities levels in syngas are more stringent, as noted in Table 5-3 which shows a detailed analysis of the impurity restrictions of the downstream uses.

**Table 5-3. Impurity Limits for Chemical and Fuel Cell Use**

	Chemical Use (ppmv)	Fuel Cell Use <sup>a</sup>
Total Sulfur	0.06	1 ppm
NH <sub>3</sub>	10	0.5 vol% combined
NO <sub>x</sub>	0.1	
HCN	0.01	
Hydrocarbons		<2 vol%
HCl		0.1 ppm
HF		0.1 ppm

<sup>a</sup>Based on molten carbonate fuel cell specifications.

#### 5.1.5 RTI Process Description

The RTI process removes acid gases from the syngas of an IGCC system. These acid gases consist of H<sub>2</sub>S, COS, NH<sub>3</sub>, HCN, HCl, and alkali (sodium/potassium macromolecules). Table 5-4 lists the process conditions, scaled-up flow rates, and compositions for the feed and products.

As shown in Figure 5-1, the raw syngas enters the cleanup process at approximately 370°C (700°F) and 40 atm (600 psia). The syngas is cooled in the first series of heat exchangers (E-100 A-G). The sensible heat

**Table 5-4. RTI Process Conditions**

	Raw Syngas	Clean Syngas	Tail Gas	Sulfur
Temperature, °F	700	674	100	100
Pressure, psia	600	600	180	180
Flow rate, lb-mol/hr	34000	23766	9078	1428
Mole fraction <sup>a</sup>				
H <sub>2</sub>	0.299	0.381	850 ppm	1 ppb
CO	0.399	0.545	0.01	6 ppb
CO <sub>2</sub>	0.12	0.043	0.398	110 ppm
N <sub>2</sub>	0.022	0.03	0.588	457 ppb
H <sub>2</sub> S	8400 ppm	392 ppb	76 ppm	454 ppb
NH <sub>3</sub>	0.002	11 ppb		
H <sub>2</sub> O	0.05	0.001	0.003	0.97
SO <sub>2</sub>			14 ppm	149 ppb
Sulfur <sup>b</sup>			< 1 ppb	0.025
O <sub>2</sub>			5 ppm	< 1 ppb

ppm = parts per million by volume.

ppb = parts per billion by volume

<sup>a</sup>Mole fractions are based on information received from RTI.

<sup>b</sup>Sulfur as (S8).

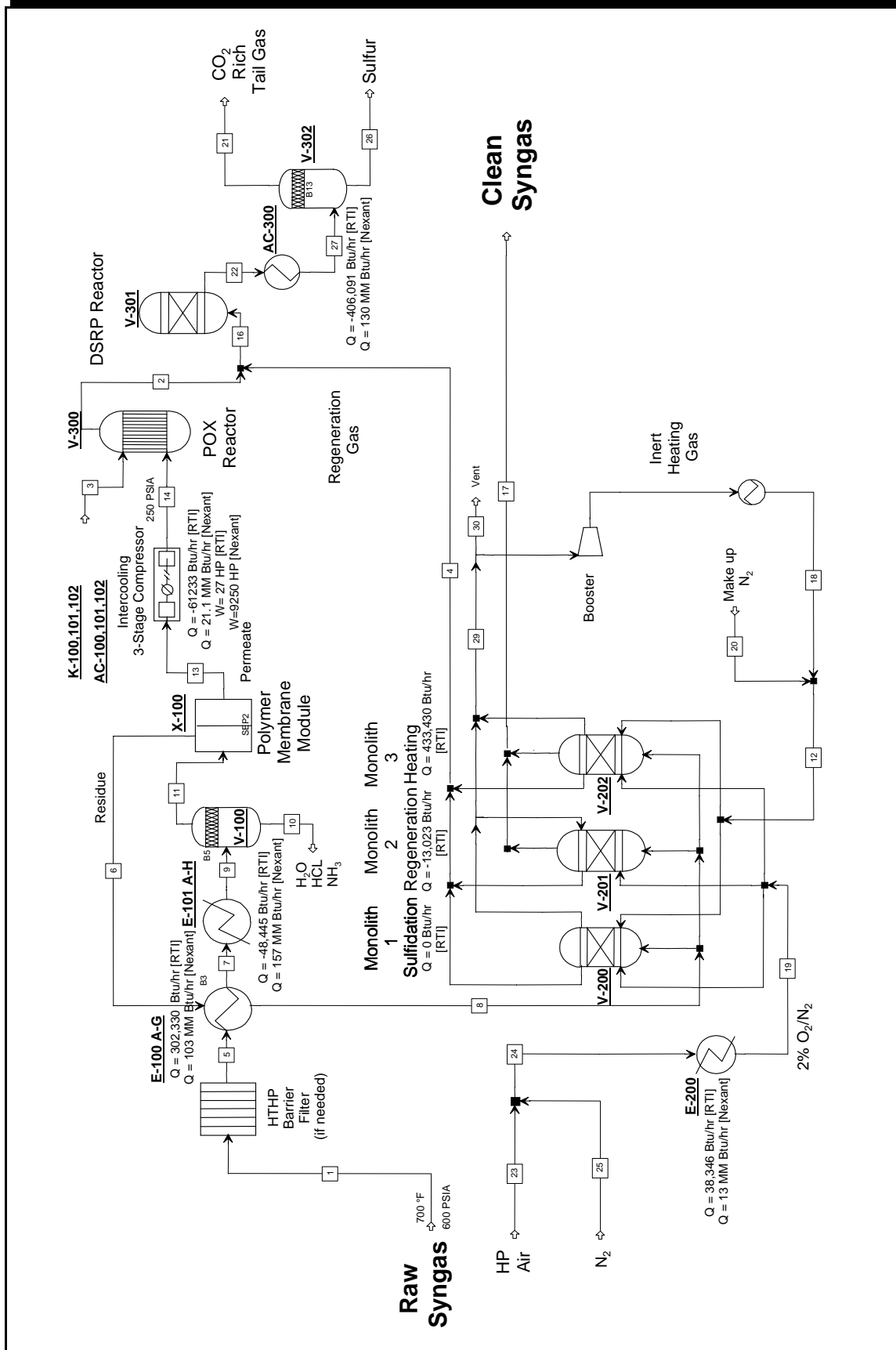


Figure 5-1. RTI process flow diagram, with Nexant equipment tag numbers and scaled-up duties.

of this raw syngas stream is used to reheat the residue from the polymeric membrane module to a temperature suitable for the operation of the monolith polishing reactors. After the first heat exchanger, the raw syngas is further cooled in a series of heat exchangers (E-101 A-H) via cooling water to 27°C (80°F). The reason for specifying 27°C (80°F) as the temperature of the raw syngas is based on the current state-of-development of the polymer membrane systems. Cooling the raw syngas to 27°C (80°F) condenses most of the water vapor present in the raw syngas.

The cooled raw syngas is then separated in the syngas flash drum (V-100, 7' ID x 24'-6" S/S). Most of the chloride and ammonia leave the system with the condensed water vapor.

The cooled, flashed raw syngas flows to the membrane module (X-100, 220,000 ft<sup>2</sup>) where the membrane design permits permeation of approximately 90% of the H<sub>2</sub>S in the raw gas to the permeate stream. This 90% number is based on the current state-of-development; with research, this percentage should increase. The residue stream from the membrane system, which contains approximately 10% of the sulfur that was in the raw syngas, is reheated using the heat of the raw syngas and is passed to one of three monolith reactors (V-200, 201, and 202, 7' ID x 28'-3" S/S each) where the ZnO-coated monolith removes, for all practical purposes, the remainder of the sulfur down to <400 ppbv in the syngas. The sulfided monolith is then regenerated using a dilute O<sub>2</sub> in N<sub>2</sub> stream.

The permeate stream from the polymer membrane module is moderately compressed to 200 psia in an air-cooled three-stage compressor (K-100, 101, and 102 and AC-100, 101 and 102, total hp 9,250). The compressed membrane permeate contains about 7.5 mol% of the CO and H<sub>2</sub> that was in the raw syngas stream.

The compressed permeate stream is partially oxidized in a catalytic PO<sub>x</sub> reactor (V-300, 3' ID x 13' S/S) so that the molar ratio of the combined H<sub>2</sub> + CO + H<sub>2</sub>S remaining in the oxidized stream to the sulfur dioxide in both the monolith regeneration offgas and the partial oxidation effluent is 2. The 2:1 molar ratio of reducing gases (H<sub>2</sub>, CO, H<sub>2</sub>S) to SO<sub>2</sub> in the combined feed to the DSRP (V301, 7' ID x 21' S/S) reactor allows production of elemental sulfur using RTI's Direct Sulfur Recovery Process (DSRP), which has been developed to pilot scale. The DSRP converts over 95% of the sulfur entering the catalytic DSRP reactor to elemental sulfur, as shown in Figure 5-1, Stream 26.

The DSRP effluent is then cooled via air coolers (AC-300) to 43°C (110°F), which is a departure from the original RTI design.<sup>1</sup> The original design used a shell and tube heat exchanger with

---

<sup>1</sup> Although Nexant suggested that air-cooled exchangers would be a good idea, it is not actually feasible for the DSRP reactor effluent. That stream must have heat removal at a high temperature-above 130°C (266°F)-to avoid solidifying the molten sulfur. For the purposes of this first pass economic assessment, the Nexant report was not revisited. In future refinements, this design issue will need to be clarified.

cooling water as the cooling medium. Changing the design to air coolers was done to reduce cooler water requirements. The cooled DSRP effluent is then separated in the sulfur flash drum (V-302, 6' -6" ID x 23' S/S), producing the final product streams of elemental sulfur and CO<sub>2</sub> rich tail gas.

### **5.1.6 Methodology for Estimating Total Installed Price for RTI Process**

The methodology for estimating the total installed cost was severalfold. Initially, each process step was individually reviewed, and existing relevant technologies were identified and examined. The design information provided by RTI was evaluated for "reasonableness" and compared with the relevant technology information acquired earlier. All the major equipment was sized based on the supplied RTI information. A cost estimator from Bechtel then priced the sized major equipment list using Questimate software. Finally, the overall facility cost was determined based on pertinent data obtained from a review of 56 completed process plants for a total installed cost. A sized equipment list and total installed cost estimate for the RTI process is provided in Table 5-5.

Each proprietary process step is discussed below, along with design information supplied by RTI, size of the equipment, and cost of each process step.

**5.1.6.1 Polymer Membrane (X-100).** The membrane module design permits permeation of approximately 90% of the H<sub>2</sub>S in the raw gas to the permeate stream. This 90% number is based on the current state-of-development; with research, this percentage should increase. Table 5-6 shows the permeability of the proprietary membrane as supplied by RTI.

Membrane pricing was based on information from the vendor of the proprietary module that 220,000 ft<sup>2</sup> of membrane is needed. This amount of surface area translates into 51 skidded units. The installed cost of the skidded membrane units is \$1.5 million.

**5.1.6.2 Monolithic Reactors (V-200, 201 & 202).** The monolithic reactors are made of a regenerable material, coated with zinc oxide, which acts as a catalyst for the reaction. This is a polishing step for removing the final amounts of H<sub>2</sub>S from the syngas stream. The monolith reactor will reduce the sulfur in the membrane residue stream to less than 400 ppbv.

The monolithic reactors were sized using RTI's guidelines. The monoliths have a theoretical sulfur capacity of 3.5 lb/ft<sup>3</sup>. A cycle time of 4 hours was assumed, yielding a single reactor size of 7' ID x 28'-3" S/S.

The monolith pricing was based on information from RTI. The price for the monolith material excluding the pressure vessel is \$800/ft<sup>3</sup>. Each monolithic reactor is approximately 1,100 ft<sup>3</sup>. The monolith material currently comes in 6" x 6" x 6" cubes. The structured packing-like material of the monoliths must be installed carefully. With the current design, each reactor

**Table 5-5. Estimated Capital for RTI Process**

Equipment List & Cost Estimate		Size	(psig)	(°F)	Mat'l	Unit Cost	Cost, \$		
Number	Description						Material	Labor	Equipment
AC-100	Cooler for 1st stage compression	8.48 MMBtu/h	100	350		45,100	9,706	54,806	
AC-101	Cooler for 2nd stage compression	8.58 MMBtu/h	190	350		46,000	9,706	55,706	
AC-102	Cooler for 3rd stage compression	4.16 MMBtu/h	250	350		38,500	9,706	48,206	
AC-300	DSRP effluent exchanger	130 MMBtu/h	250	1300	SS304	3,543,100	195,985	3,739,085	
E-100	Feed/residue exchanger	103 MMBtu/h	650	800		991,600	11,678	1,003,278	
E-101	Syngas heater	15.7 MMBtu/h	650	450		1,023,600	13,249	1,036,849	
E-200	Regeneration exchanger	13.25 MMBtu/h	250	1250	SS304	204,500	1,858	206,358	
K-100	Permeate compressor-1st stage	3802 hp	100	350		2,151,200	41,073	2,192,273	
K-101	Permeate compressor-2nd stage	3,285 hp	190	350		1,439,900	31,970	1,471,870	
K-102	Permeate compressor-3rd stage	1,555 hp	250	350		811,200	20,531	831,731	
V-100	Syngas flash drum	7' IDx24'-6" S/S	650	125		88,600	4,735	93,335	
V-200	Monolith reactor 1	7' IDx28'-3" S/S	650	1250	SS304	610,900	16,023	626,923	
V-201	Monolith reactor 2	7' IDx28'-3" S/S	650	1250	SS304	610,900	16,023	626,923	
V-202	Monolith reactor 3	7' IDx28'-3" S/S	650	1250	SS304	610,900	16,023	626,923	
V-300	Partial oxidation reactor	3' IDx13' S/S	250	1300	SS304	73,700	1,213	74,913	
V-301	DSRP reactor	7' IDx21' S/S	250	1300	SS304	569,700	11,815	581,515	
V-302	Sulfur flash drum	6'-6" IDx23' S/S	250	400		35,700	1,841	37,541	
X-100	Polymer membrane	220,000 ft <sup>2</sup>	650	125		1,170,000	309,600	1,479,600	
CT-200	ZnO monolith 1	1,086 ft <sup>3</sup>				800 ft <sup>3</sup>	868,800	14,038	882,838
CT-201	ZnO monolith 2	1,086 ft <sup>3</sup>				800 ft <sup>3</sup>	868,800	14,038	882,838
CT-202	ZnO monolith 3	1,086 ft <sup>3</sup>				800 ft <sup>3</sup>	868,800	14,038	882,838
CT-300	POx monolith	92 ft <sup>3</sup>				800 ft <sup>3</sup>	73,600	2,065	75,665
CT-301	DSRP catalyst	810 ft <sup>3</sup>				\$10/lb 80lb/ft <sup>3</sup>	648,000	10,638	658,638
	Total major equipment						17,393,000	778,000	1,8171,000
	Total major equipment (w/o catalysts)						14,065,100	722,735	14,787,835
	Total Other Direct Costs						7,454,000	3,990,000	11,444,000
	Contractor's Indirect Cost	80% of labor							3,814,000
	Total Field Cost								33,429,000
	Design Office and Management Costs	12%							4,011,000
	Overhead and Profit	10%							3,744,000
	Escalate from mid-2000 to mid-2001 price levels	3%							1,236,000
	Total								42,000,000

would need nearly 9,000 blocks. The overall monolith unit would require just over 26,000 total blocks of monolith.

Because of the high temperatures needed for regeneration, the construction material had to be upgraded to stainless steel. With the pressure of the membrane residue and the selected metal, the wall thickness for these three vessels is nearly 6 inches. As a result of the metallurgy and wall thickness, the cost of these vessels is \$1.8 million. With the addition of the catalyst, the installed cost of the monolithic reactor unit is approximately \$5 million.

**Table 5-6. Polymer Membrane Permeability**

Component	Permeability {{x 10 <sup>6</sup> , cm <sup>3</sup> STP/ [cm <sup>2</sup> s (cm Hg)]}}
H <sub>2</sub>	10
CO	4
N <sub>2</sub>	3
CO <sub>2</sub>	167
H <sub>2</sub> S	500
H <sub>2</sub> O	583

**5.1.6.3 Partial Oxidation Reactor (POx) (V-300).** The sulfur species in the membrane permeate stream are converted to elemental sulfur in the DSRP reactor. To effectively perform this conversion, H<sub>2</sub>S in the membrane permeate stream must be partially oxidized to SO<sub>2</sub>. Partial oxidation of H<sub>2</sub>S allows the presence of sufficient hydrogen and carbon monoxide in the stream after oxidation to provide the reducing gas necessary for the DSRP reaction downstream.

The main reactor sizing point for the partial oxidation reactor (POx) is the gas hourly space velocity (GHSV). The final design rate of a GHSV of 40,000 h<sup>-1</sup> was agreed upon and is the rate previously proven in the laboratory. The future target GHSV is 100,000 h<sup>-1</sup>. The lower number was used to reflect a conservative design cost estimate for this unit.

For the pricing of the monolith in the POx reactor, a value of \$800/ft<sup>3</sup> was used, which was supplied by RTI. The required volume of catalyst is 92 ft<sup>3</sup>, resulting in a cost of roughly \$73,000 for the catalyst.

As a direct result of the high temperature and the pressure, the vessel will be of stainless steel construction. The total cost for the POx reactor and catalyst is approximately \$150,000.

**5.1.6.4 Direct Sulfur Recovery Process (DSRP) (V-301).** The DSRP reactor is based on a patent by Dorchak et al. (1994). It converts over 95% of the SO<sub>2</sub> into elemental sulfur. The DSRP reactor was sized based on a space velocity of 5,000 ft<sup>3</sup>/h at STP per ft<sup>3</sup> of catalyst.

The unit price for the catalyst used was \$10/lb with a bulk density of roughly 80 lb/ft<sup>3</sup>, yielding a catalyst cost of approximately \$660,000. As a result of the high temperature of the feed gas at the operating pressure, the vessel required stainless steel metallurgy. The total cost of the DSRP unit is roughly \$1.25 million.

**5.1.6.5 Booster Monolith Regeneration Recycle.** The booster compressor and inert heating gas recycle to the monolith reactors was drawn from the original design provided by RTI. Steam was included for heat recovery purposes, but the extreme operating conditions (high temperature) of the compressor makes it infeasible.

**5.1.6.6 Areas for Cost Optimization with RTI Process.** As a result of this study, several areas of potential cost savings have been identified.

- Lowering the high temperature regeneration of the monoliths to 482°C (900°F) would change the metallurgy to carbon steel from the current thick-walled stainless steel vessels.
- Lowering the high-temperature operation of the partial oxidation reactor would change the metallurgy to carbon steel from the current design of 304 stainless steel.
- The current design of the monolithic reactor structured packing is 6" x 6" x 6" blocks. This design is not cost-effective conducive to a large industrial application because the blocks must be placed in the reactor by hand, which is very labor intensive. If the manufacturing technology could increase the size of the blocks, installation of the catalyst would be favorably impacted. It would also reduce the possible chance for channeling in the reactors.
- This study already reflects the change of converting the DSRP effluent cooler to an air cooler.<sup>2</sup>
- This study already reflects eliminating the booster compressor recycle around the monolith reactors.

**5.1.6.7 Rectisol Process.** The Rectisol process produces clean gas, CO<sub>2</sub> fraction, tail gas, and H<sub>2</sub>S fraction. The sulfur content of the clean gas is less than 0.1 ppmv.

The Rectisol process operates at low temperatures and uses methanol as the solvent. At low temperatures, methanol has rather favorable properties regarding the absorption of CO<sub>2</sub>, H<sub>2</sub>S, and COS as well as other gas impurities. The specific characteristics of methanol that make it particularly suitable as a physical solvent are listed below.

- High solubility for CO<sub>2</sub>, H<sub>2</sub>S, and COS – This keeps the solvent circulation rate low and provides for optimum economics of Rectisol plants when the impurities in the raw gas are present in high concentrations.
- High selectivity for H<sub>2</sub>S and COS versus CO<sub>2</sub> – A H<sub>2</sub>S rich offgas is obtained even with low H<sub>2</sub>S/CO<sub>2</sub> concentrations in the feed gas, which is of importance for economic sulfur recovery.

---

<sup>2</sup>See footnote on page 5-6.

- Low solubility for H<sub>2</sub>, CO, and CH<sub>4</sub> – This keeps gas losses at a very low level.
- Low vapor pressure under process conditions – Solvent losses are very low.
- High solubility for water – Rectisol plants can be used for gas dehydration at the same time.
- Low viscosity, even at low temperature – This characteristic ensures good heat and mass transfer, even at temperatures just above the freezing point of the methanol, which is very low. This also eliminates any hazard of freezing during the winter.
- Optimum chemical and thermal stability – Methanol has an extremely high thermal stability, and there is no degradation by acidic components.
- Noncorrosive – Carbon steel can, therefore, largely be used for the equipment.
- Good availability of methanol at very low cost – Methanol is produced in bulk quantities for use as solvent and as raw material for a great number of industrial applications.

**5.1.6.8 Rectisol Process Flow.** Figure 5-2 illustrates the Rectisol process flow diagram, which is described below.

#### **H<sub>2</sub>S and COS removal**

- |                 |  |
|-----------------|--|
| Equipment No. 1 | Heat exchanger—Feed gas cooling is by heat exchange with various cool product streams. Methanol is injected into the feed gas to prevent plugging by water/ice. (Separation of the methanol-water condensate and recovery of the methanol is achieved by fractionation.) |
| Equipment No. 2 | Wash column—H <sub>2</sub> S and COS are removed by scrubbing with CO <sub>2</sub> -rich methanol withdrawn from the subsequent CO <sub>2</sub> wash unit.   |
| Equipment No. 3 | Separator—The separator provides flashing of absorbed hydrogen from the rich methanol section and removal of the heat of solution in cooling stages.   |
| Equipment No. 4 | Compressor—The flashed gases are compressed and recycled to the feed gas.  |
| Equipment No. 5 | Concentration column—The sulfur compounds are concentrated by stripping CO <sub>2</sub> with stripping gas in the lower section. Sulfur-free tail gas is withdrawn from the top of the column.   |

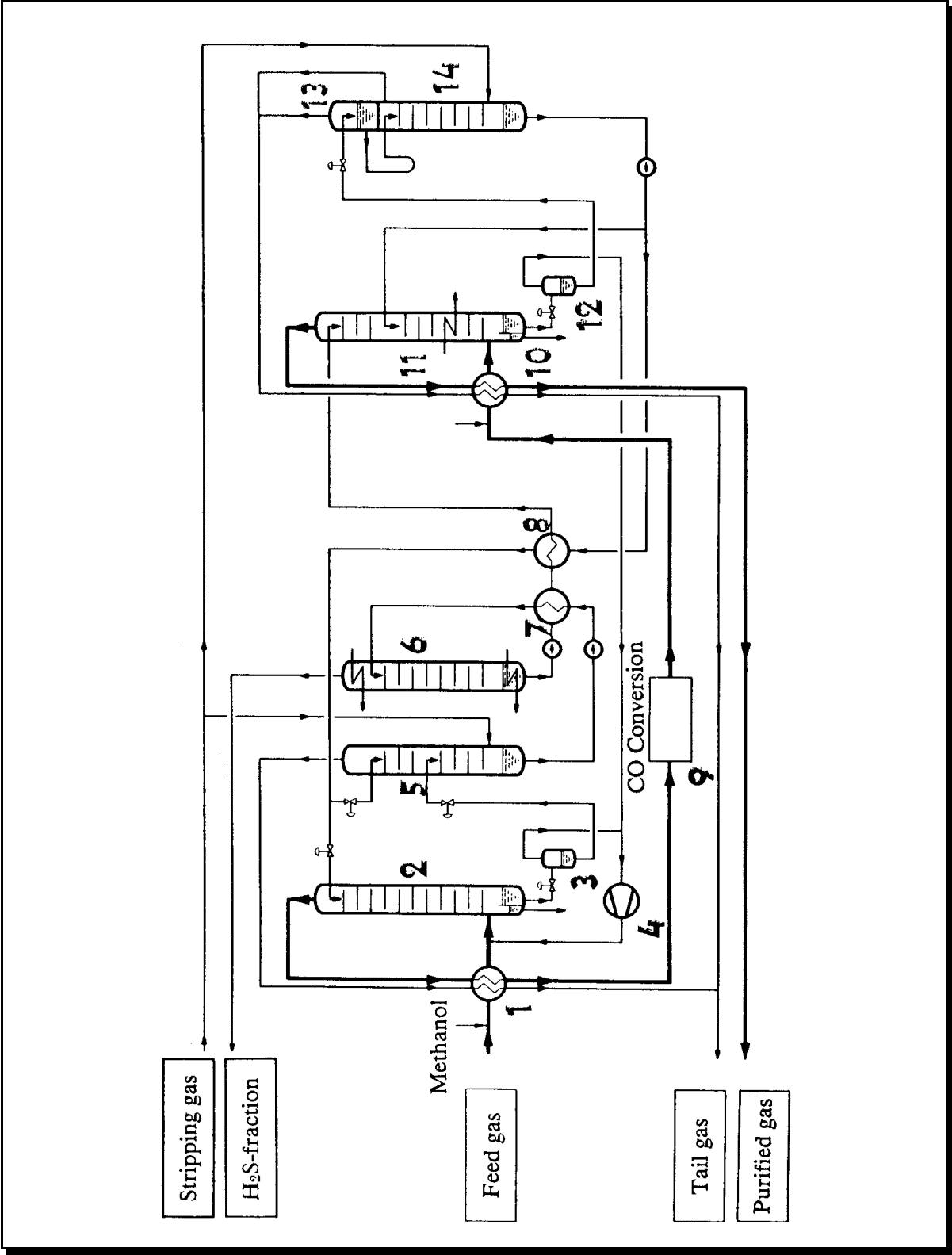


Figure 5-2. Rectisol process flow diagram.

- Equipment No. 6      Regeneration column—Concentrated sulfur compounds are separated by stripping with methanol vapor, resulting in final regeneration of the methanol. The methanol vapor is reliquefied in the condenser.
- Equipment Nos. 7,8      Heat exchangers—Cooling of the regenerated methanol is by heat exchange with cold solvent streams.

### **CO Conversion**

- Equipment No. 9      This process step does not belong to the wash system. Catalytic conversion of the CO contained in the feed gas is carried out by steam to CO<sub>2</sub> and H<sub>2</sub>.

### **CO Removal**

- Equipment No. 10      Heat exchanger—The heat exchanger cools the converted gas by exchanging heat with the cold product streams.
- Equipment No. 11      Wash column—Bulk removal of the CO<sub>2</sub> is achieved by means of stripped methanol from the stripping column (14). This occurs in the removal of the bulk of the heat of solution in cooling stages. The bulk removal is achieved by means of an evaporating refrigerant. The final removal of the CO<sub>2</sub> in the upper section is achieved by means of warm, regenerated, CO<sub>2</sub>- and H<sub>2</sub>S-free methanol after partial depressurizing.
- Equipment No. 12      Separator—Absorbed hydrogen is flashed from the rich methanol after partial depressurizing. The flashed gases are compressed and recycled to the feed gas.
- Equipment No. 13      Separator—In the separator, the rich methanol is expanded to low pressure and flashes part of the absorbed CO<sub>2</sub> (in some cases, CO<sub>2</sub> recovery).
- Equipment No. 14      Stripping column—The absorbed CO<sub>2</sub> is separated by means of a stripping gas. The methanol is returned to the methanol wash columns (11 and 2).

**5.1.6.9 Cost Comparison.** Based on the cost comparison, the RTI process was found to be much more cost effective in removing acid gases from the syngas. The Rectisol process was over 75% higher in total installed cost. All comparisons are based for the syngas from an IGCC Texaco gasifier for 500-MWe capacity.

**RTI Process.** The RTI process has an optimistic total installed cost estimate of \$42 million (U.S. \$), which includes the initial fill of all catalysts. The RTI process has a 99% + removal efficiency of H<sub>2</sub>S, with a recovery of 88% + H<sub>2</sub> and 95% + CO. This estimate is based on a sized major equipment list, with all bulks and other associated costs factored in. See Table 3-5 for the sized equipment list and total installed cost estimate for the RTI process. The factors were based on a 56-process plant study, utilizing the most optimistic factor in each case. Nearly half of the equipment costs are due to either compression or the monolithic reactors, which are skidded and hence reduce the installation factors.

**Rectisol Process.** The total installed capital cost of a Rectisol unit is \$75 million (2001 U.S. \$). The sulfur content of the clean gas is less than 0.1 ppmv. This estimate is based on a previous quote Bechtel National, Inc., received from Lotepro. The quote was from Mr. Juergen Bokaemper of Lotepro Corporation to Mr. R.S. Custer of Bechtel National, Inc., August 1, 1978. The Lotepro estimate was based on a project requiring the separation of H<sub>2</sub> and CO from the CO production from coal. This quote was adjusted to reflect the conditions of this study and converted to 2001 dollars.

**Methyl Diethanolamine.** The total installed capital cost of an MDEA system for a 500-MWe power plant is \$18 million (2001 U.S. \$). The MDEA estimate is based on the Polk County Power Plant MDEA system that Bechtel engineered, constructed, and started up in 1996 for Tampa Electric Company. That facility was a 250-MWe power plant, half the size of this study. MDEA is not a fair comparison to the RTI process because of its inability to remove COS from syngas.

At the Polk County Power Plant, more COS was produced during gasification than the plant was originally designed for. As a result, a COS hydrolysis unit was installed. The hydrolysis reactor converts COS into H<sub>2</sub>S, which can then be removed in the MDEA unit. In short, additional capital and operational costs had to be incurred to increase the total sulfur removal of MDEA to acceptable levels.

## **5.2 CONCLUSIONS**

Nexant estimated a total installed cost of \$42 million for the RTI process for a 500 MWe IGCC plant based on the current state of development. By comparison, Nexant estimated the installed cost for an equivalent-sized plant based on the Rectisol process to be \$75 million. The total installed cost for an MDEA system was estimated to be \$18 million, but the MDEA process does not achieve the required level of gas cleaning. Thus, the RTI process is economically competitive with the equivalent, commercially-available process for syngas cleanup.

## CHAPTER 6

### SUMMARY, CONCLUSIONS, AND FUTURE WORK

A major objective of DOE's Vision 21 Program Plan is to develop gas stream purification technologies for the removal of sulfur-, nitrogen-, chlorine-, and alkali-species to near zero levels from syngas generated by the gasification of carbonaceous fuels in an IGCC system. These gas cleanup technologies should be sufficient to meet contaminant tolerance limits for fuel cell and chemical product applications.

RTI's approach to the syngas cleanup consisted of a number of different modular processes that could be integrated, as needed, for the different syngas conditioning requirements for fuel cell, chemical production, or power generation applications. These technologies include component-selective membranes for bulk sulfur removal from the syngas, regenerable polishing sulfur removal monoliths, regenerable acidic adsorbents for  $\text{NH}_3$  removal, and inexpensive high- surface-area materials for removal of hydrogen chloride from the syngas.

The following sections provide a brief summary of the work that RTI and its collaborators carried out during the Base Program. Conclusions drawn from this work are listed, and the plans for future work are presented. Also, each section describes the challenges to be met and goals to be achieved in order to commercialize the RTI modular approach to syngas cleanup.

#### 6.1 BULK SULFUR REMOVAL

The approach that RTI and its collaborators, MEDAL and NCSU, pursued in developing the critical bulk sulfur removal technology was to develop polymer membranes engineered to specifically remove the acid gas components ( $\text{H}_2\text{S}$ ,  $\text{CO}_2$ ,  $\text{NH}_3$ , and  $\text{H}_2\text{O}$ ) of syngas. This research focused on solubility selective membranes with novel polymer compositions, an area that had received little attention in conventional commercial membrane development focused on diffusivity-selective  $\text{H}_2$ -separation membranes.

The research work on solubility-selective membranes carried out by RTI and its collaborators is described in detail in Chapter 2 of this report and is summarized here as follows:

- The research group successfully measured permeability coefficients of the rarely studied gases,  $\text{H}_2\text{S}$ ,  $\text{CO}$ ,  $\text{COS}$ , and  $\text{SO}_2$  in PDMS and confirmed that their transport behavior is consistent with the penetrant's molecular properties. Consequently,  $\text{H}_2\text{S}$ ,  $\text{COS}$ , and  $\text{SO}_2$  are more permeable than  $\text{H}_2$  in PDMS and will be selectively stripped from the raw syngas, while  $\text{CO}$  is less permeable and will be predominantly retained in the high-pressure syngas as desired.

- Mixed-gas permeation data for 14 MEDAL solubility-selective polymer samples, including recent ones with H<sub>2</sub>S/H<sub>2</sub> selectivities >30, were measured over the temperature range of 20°C (68°F) to 160°C (320°F).
- For all materials examined, a systematic decrease in acid gas/hydrogen selectivity with increasing system temperature was observed. This result illustrates the inherent difficulty in performing solubility-driven polymer separations at high temperature. Nevertheless, some of the MEDAL samples perform significantly better at elevated temperatures than PDMS. For example, at 100°C (212°F) the best performing MEDAL samples have H<sub>2</sub>S/H<sub>2</sub> selectivities of 10, as compared to approximately 2 for PDMS.
- Significant progress has been made at NCSU in preparing PEO films containing acid gas affinity salts. These so-called “solid polymer electrolytes” represent a potential breakthrough in performance for acid gas selective membranes.
- During sample screening, a previously unknown effect of polymer fluorination on H<sub>2</sub>S permeabilities was discovered. Hydrogen sulfide exhibits unexpectedly low permeability in fluorinated polymers, probably because of low solubility resulting from an unfavorable energetic interaction between the sulfur compound and the fluorinated polymer matrix. This effect causes fluorinated polymers to have unusual selectivities for CO<sub>2</sub> over H<sub>2</sub>S (as high as 10); the potential utility of this discovery is currently being explored.
- A custom membrane module simulator developed at NCSU was used to model the performance of a membrane separator having the properties of MEDAL 018 at room temperature and using the standard syngas composition and conditions. Based on these results, 80 to 90% removal of H<sub>2</sub>S from syngas is feasible without appreciable loss of H<sub>2</sub> and CO (Btu value). Various process design configurations, including use of a size-selective membrane to strip H<sub>2</sub> from the permeate stream of the solubility-selective membrane, are being considered to optimize heat integration.

In the coming year at RTI, the screening of polymer samples supplied by MEDAL and NCSU will be continued. This work will seek to improve polymer selectivity for acid gases over H<sub>2</sub> and to improve the retention of high separation factors at elevated temperatures. (The test apparatus can be operated over the range 20 to 220°C [68 to 428°F]). Additionally, MEDAL will prepare laboratory-scale membrane modules (~1-ft<sup>2</sup> surface area) out of their most promising polymer materials. These modules will undergo extended bench-scale testing with a simulated syngas at RTI’s HTHP facility. The goal of this work will be to see whether the intrinsic separation properties of the polymer translate to comparable module performance and how well the module performs over time under simulated process conditions.

## 6.2 POLISHING SULFUR REMOVAL

In the polishing sulfur removal process, RTI collaborated with Süd-Chemie Prototech, Inc., to develop regenerable ZnO-coated monoliths for removing sulfur remaining in the membrane residue from the bulk sulfur removal step to sub-ppm levels. In this research work, Prototech produced candidate ceramic monoliths washcoated with titania and top-coated with various levels of ZnO. These monoliths were screened for ability to adsorb H<sub>2</sub>S and to be activated and regenerated in the TGA and RTI's HTHP bench-scale reactor facilities. The work carried out by RTI and Prototech is described in detail in Chapter 3 of this report.

Based on the experimental studies carried out by RTI in cooperation with Prototech, the following conclusions were made:

- Titania was identified as an optimum washcoat for the ceramic honeycomb monolith base.
- Concentrations of H<sub>2</sub>S < 500 ppbv in the monolith-treated gas were achievable under selected operating conditions.
- Sulfur levels from the monolith of less than 10 ppmv were possible at monolith temperatures from 93 to 538°C (200 to 1000°F).

The work carried out on the ZnO-coated monolith during the Base Program was largely scoping tests to get an idea of what H<sub>2</sub>S removal efficiencies might be possible at various conditions. Based on process simulations described in Chapter 5 of this report, more bench-scale testing of the ZnO-coated monolith will be carried out in the future at perhaps more realistic operating conditions. Sulfur concentration in the inlet gas of 500 to 1,000 ppmv and space velocities of approximately 10,000 h<sup>-1</sup>. Other work that should be carried out in future research on the monolith sulfur polishing reactors during the proposed Option Program include the following:

- Lowering sulfur effluent concentrations by optimizing regeneration conditions to inhibit sulfate formation and by screening additives, which might inhibit sulfate formation.
- Improving low-temperature performance of the monolith reactor by screening additives to the monolith coatings to promote COS hydrolysis/removal activity and to promote basic reactivity of H<sub>2</sub>S with the monolith coatings.
- Improving low-temperature (as low as 93°C) [200°F] performance by determining optimal loadings of ZnO on the monolith.
- Investigating alternative polishing materials such as RVS-1.

Also, in future work, RTI believes it will be valuable to test the monolith and/or RVS-1 in tandem with membrane modules in RTI's HTHP bench-scale testing system.

### **6.3 HCl and NH<sub>3</sub> REMOVAL**

The development of the modular processes for HCl and NH<sub>3</sub> removal from raw syngas was carried out as a collaborative effort of RTI and SRI International.

The objective of this portion of the Base Program was to reduce the levels of chloride and ammonia vapors in hot coal gas streams to sub-ppm levels so that the coal gas can be used efficiently and under environmentally benign conditions for generating electric power using fuel cells and producing chemicals.

Theoretical analysis indicates HCl vapor could be reduced in the presence of sodium carbonate and under equilibrium conditions to desired levels by cooling the coal gas to temperatures below 350°C (662°F). Bench-scale experiments showed that moderately high surface area sorbents could be made from naturally occurring minerals such as sepiolite (hydrated magnesium silicate) and impregnated with an active ingredient such as sodium carbonate. These sorbents could be used to attain about 50-ppb levels of HCl vapor with a chloride capacity of about 7 wt% Cl. Because the chloride capacity of such sorbents is limited, the bulk of the HCl vapor needs to be removed to less than 10 ppm using nahcolite sorbents at high temperatures. The bulk removal step was developed earlier in a program sponsored by the DOE. Preliminary economic analysis indicates that the total cost of HCl vapor removal is about (1.5 mil/kWh). Of this cost, about two-thirds is for the bulk removal step and one-third is for the trace removal step.

Thermodynamic equilibrium calculations showed that thermal decomposition can reduce ammonia in syngas streams to ppm levels only at temperatures higher than 1200°C (2200°F), or below 250°C (482°F) if H<sub>2</sub> is converted to CH<sub>4</sub>. Both of these options were deemed not cost-effective. A process based on chemisorption of NH<sub>3</sub> on acidic catalysts such as molecular sieves was verified using temperature-programmed reaction apparatus. Significant levels of NH<sub>3</sub> could be adsorbed at about 225°C (437°F) and the adsorbed NH<sub>3</sub> could be recovered by increasing the sorbent temperature in a separate step. The regenerated catalyst could be cycled back to the adsorption step. The desorbed NH<sub>3</sub> can be thermally decomposed or oxidized to N<sub>2</sub> catalytically. Preliminary economic analysis indicates that the cost of the NH<sub>3</sub> removal step is about \$0.0004/kWh (0.4 mil/kWh). These results are encouraging, and the concepts should be further developed in the Option Program.

Based on the results of the bench-scale experimental work and preliminary economic analysis carried out by SRI International and RTI, the following was concluded:

- HCl vapor could be reduced to less than 50-ppb levels by using a two-step process. In the first step, conducted at about 500°C (932°F), the bulk of the HCl vapor is captured. In the second step, conducted at about 350°C (662°F), the remainder of the HCl vapor is removed.
- The bulk removal step utilizes the fast kinetics at high temperatures and high absorption capacity of the sorbent. The trace removal step takes advantage of low thermodynamic equilibrium levels for NH<sub>3</sub> at low temperatures and a high-surface-area sorbent to attain reasonable chloride capacity. The sorbents in both steps are of naturally occurring minerals or minimally modified from them.
- The cost of total HCl removal processes appears to be about \$0.0015/kWh (1.5 mil/kWh)—a reasonably low value.
- Ammonia vapor could be reduced to trace levels by adsorption onto acidic-type, high-surface-area molecular sieves. The adsorbed NH<sub>3</sub> could be desorbed at high temperatures in an inert gas stream, and the desorbed NH<sub>3</sub> can be catalytically decomposed or oxidized to N<sub>2</sub>. The catalytic decomposition is aided by the absence of H<sub>2</sub> and poisons such as H<sub>2</sub>S and high levels of H<sub>2</sub>O.
- The cost of NH<sub>3</sub> removal is estimated to be about \$0.0006/kWh (0.6 mil/kWh).

The following recommendations are made for further development of the hydrogen chloride and ammonia removal processes.

#### **HCl Removal Process:**

- Set up a bench-scale system with two fixed-bed reactors for conducting bulk and trace HCl removal experiments at 20 atm.
- Use the bulk and trace HCl removal steps sequentially for fixed-bed reactors.
- In the bulk removal step, use previously proven nahcolite-based sorbent pellets at about 500°C (932°F).
- Operate the trace HCl removal reactor at about 350°C (662°F) or lower using the high-surface-area sorbents and gas stream from the first reactor.
- Conduct parametric studies (temperature, space velocity, and gas composition) at elevated pressures (up to 20 atm).

- Complete the preliminary technical and economic evaluation of the HCl removal step for attaining ultra-low levels.

#### **Ammonia Removal Process:**

- Set up a high-pressure fluidized-bed reactor system for cyclic ammonia adsorption and desorption studies.
- Conduct a parametric study of NH<sub>3</sub> removal under fixed- and fluidized-bed conditions as a function of process parameters (gas composition, space velocity, and temperature).
- Evaluate the lifetime characteristics of selected molecular sieves under simulated coal gas conditions.
- Complete the preliminary technical and economic evaluation of the NH<sub>3</sub> removal step for attaining ultra-low levels.

### **6.4 TECHNICAL/ECONOMIC EVALUATION**

In addition to the experimental work carried out by RTI and its collaborators in support of developing novel, modular processes for sulfur, chloride, and ammonia removal from syngas, considerable technical and economic evaluations of the processes were performed in the Base Program. Evaluations of the HCl and NH<sub>3</sub> removal processes are given in detail in Chapter 4 of this report. An overall evaluation of the sulfur removal technology is presented in Chapter 5. The work reported in Chapter 5 is primarily the work of Nexant, with support from RTI. In Nexant's evaluation, separate HCl and NH<sub>3</sub> removal modules were not required because of the low temperature used in the bulk sulfur removal membrane module. The membrane temperature used (27°C [80°F]) reflected the state of the membrane development and was not exaggerated upward to obtain more favorable results from Nexant's analysis. As a result of using a low membrane temperature, the raw syngas was substantially cooled, condensing the bulk of the water, chloride, and ammonia from the raw gas prior to treatment by the membrane module. The high degree of heat integration required to cool the raw gas and reheat the membrane residue is very costly, as can be seen in Nexant's analysis in Chapter 5. This result clearly reinforces RTI's initial engineering judgment that it is critical to bring the membrane and monolith temperatures as close together as possible. Accomplishing this will be one of RTI's primary objectives in the Option Program phase of RTI's effort to develop novel technologies for gaseous contaminants control in IGCC applications.

### **6.5 OPTION PROGRAM**

As a part of RTI's original proposal to DOE to develop gaseous contaminants control technologies, an Option Program was proposed as a followup to the Base Program, which has

been the subject of this report. The Option Program will concentrate on two main areas: (1) further bench-scale testing of the bulk and polishing sulfur removal processes and additional bench-scale testing of the  $\text{NH}_3$  and HCl removal processes, and (2) market assessment and commercial applicability of the proposed concepts.

### 6.5.1 Bench-Scale Testing

This optional task is divided into three subtasks. One of the important activities under this task is to modify RTI's existing bench-scale test facility for bench-scale testing of polymer membrane micromodules and prototype commercial monoliths.

**6.5.1.1 Bulk Sulfur Removal.** In the Option Program, further development of the polymer membrane technology will continue with a systematic and structured optimization program to maximize both  $\text{H}_2\text{S}/\text{H}_2$  selectivity and the stable operating temperature of the polymer films. As discussed in Chapter 2, a number of different polymer families have properties that may allow them to selectively remove  $\text{H}_2\text{S}$ ,  $\text{H}_2\text{O}$ , and  $\text{CO}_2$  at high temperatures.

In parallel with the materials optimization program, the important technical challenges to the production of gas permeation modules for high-temperature operation will be addressed. Among these are scale-up of hollow fibers for commercial production and identification of a suitable potting material for fiber encapsulation. No insurmountable obstacles are expected to be encountered in the scale-up to commercial hollow fiber production, as this capability is one of the strengths MEDAL brings to the research team. The key objective guiding this scale-up process will be to achieve the same, if not better, acid-gas-to- $\text{H}_2$  selectivity and temperature stability as that obtained with small-scale membrane preparation.

Currently, virtually all commercial polymeric membrane modules are prepared with epoxy resins as the tubesheet encapsulant. The strength, processing simplicity, and cost make epoxy resins the material of choice for encapsulation. However, epoxy resins are not suitable for long-term performance at temperatures in excess of  $93^\circ\text{C}$  ( $200^\circ\text{F}$ ). Potential candidates for tubesheet encapsulation at the expected operating temperatures are high-temperature epoxies, polyimides, urea-formaldehydes, and other high-temperature materials.

A final effort of the membrane optimization program will be the preparation of prototype hollow-fiber membrane modules. A simple screening test using a  $\text{CO}_2/\text{H}_2$  mixture at room temperature will be used to optimize commercial-scale hollow-fiber preparation and module assembly. In a specially designed and constructed test system, assembled prototype modules will be tested at high temperatures in the presence of simulated syngas. The objective will be to collect as much technical and economic feasibility data as possible. Some of the important features are multi-component effects on selectivity, temperature effects on selectivity, and life expectancy within the operating temperature window.

This prototype module test system will utilize as much existing equipment as possible. The existing gas system from either RTI's bench-scale reactor system or the dense film permeation test apparatus will be modified to feed the prototype module test system. Gas analysis of the permeate and nonpermeate will be performed with the same Carle Series AGC 400 GC used for the dense-film permeation testing available at RTI. Because the size and configuration of the prototype modules may prohibit use of any existing furnaces, a special furnace may be required to heat the module to the desired operating temperature. Prior to analysis, condensation of steam in the permeate will be performed by a water-cooled condensation coil.

**6.5.1.2 Polishing Sulfur Removal.** Working with Prototech, RTI will continue to develop the monolith desulfurization technology. In contrast to the Base Program, TGA monolith testing in the Option Program will attempt to lower sulfidation temperature progressively while maintaining satisfactory sulfur removal performance during stable multicycle operation. Systematic lowering of the sulfidation temperature will require multiple cycles/tests to identify optimal regeneration conditions and monolith parameters. As the cycle/test time for a TGA is considerably shorter than that for a larger reactor system, many permutations can be tested in a shorter period of time. Consequently, the TGA is the most effective tool for this phase of the research.

The results collected during these TGA screening tests will include the rate of sulfur pickup during sulfidation, rate of sulfur removal during regeneration, maximum sulfur capacity, and surface area and pore size distribution. Satisfactory sulfidation performance will be identified qualitatively by both achieving an adequate weight slope at the start of sulfidation and final weight percent change at the end of a fixed sulfidation period. "Adequate" will be defined as a slope and final percent weight change greater than or equal to that for a material meeting the specified success criteria. The qualitative measure of stable multicycle performance is smaller variation in the measured variables between cycles during three to five cycle tests with no process/monolith changes. The screening process will be terminated when satisfactory sulfidation performance during stable multicycle operation cannot be achieved regardless of changes made to the regeneration conditions or monolith parameters at a given sulfidation temperature.

At this point, research efforts will shift from using the TGA to the bench-scale reactor system to optimize monolith performance. In this phase of testing, TGA will serve as gatekeeper, allowing promising candidates to advance to testing in RTI's bench-scale reactor system, but ending testing for substandard prototype monoliths. The measured values collected in the bench-scale reactor system will include sulfur leakage, sulfur capacity at breakthrough, and deactivation. Optimization with the bench-scale reactor system should be easier because required changes should be smaller, and directional effects of any change should be known from the TGA optimization process.

After any required optimization takes place, the bench-scale reactor system will be used to determine the performance effect of key process parameters, such as space velocity, sulfur

loading prior to regeneration, and steam content. Extended bench-scale testing will be used to estimate active monolith lifetimes.

McDermott Technology, Inc. (MTI), has expressed a keen interest in testing this monolith desulfurization process in conjunction with their solid-oxide fuel cell project. If the bench-scale testing results of the monolith desulfurization process appear promising, a monolith module may be built as per MTI specification for pilot plant testing in a follow-on phase of this project. The objective of the pilot tests will be to collect more accurate and real-world typical operating data. As pilot-scale testing begins, the objective criteria will shift to focus on changes that reduce the cost of the technology to be competitive with other commercial technologies.

**6.5.1.3 NH<sub>3</sub> and HCl Removal.** In the Option Program, RTI and SRI International propose to determine the operability and establish the parametric limits of the HCl removal process using SRI's bench-scale reactor system.

Additional experiments will be conducted to determine the adsorption capacities of trace metal vapors such as Hg and Cd by the HCl removal sorbents. Trace levels of these metal vapors will be mixed with the feed gas prior to exposure with the sorbent. The spent sorbents will be analyzed for the retention of these elements.

The bench-scale reactor system for NH<sub>3</sub> removal studies will allow measurement of adsorption and desorption characteristics during cyclic operation. For adsorption, the effects of temperature, space velocity, NH<sub>3</sub> concentration, and steam content will be investigated. The effects of temperature and/or pressure and space velocity on desorption of NH<sub>3</sub> will also be studied.

The sorbents for HCl removal and adsorbents for NH<sub>3</sub> removal will be characterized to understand the nature of changes occurring in them during reaction. Surface area analysis (BET method), mercury porosimetry, scanning electron microscopy, and X-ray diffraction will be used to track morphologic reaction-induced changes. Energy-dispersive X-ray fluorescence and chemical analysis will track compositional changes. Finally, crush strength and attrition testing will determine changes in mechanical strength. This information will be used to modify characteristics of the sorbents to improve their performance.

## **6.5.2 Market Assessment and Commercial Applicability**

**6.5.2.1 Polymer Membrane.** The primary objective of this task will be to critically analyze data generated to evaluate the technical feasibility of the proposed concepts. Issues to be addressed include:

- What are the upper temperature limit, reliability, and life expectancy for the polymer membranes developed for H<sub>2</sub>S and CO<sub>2</sub> separation?

- What are the challenges involved in scaling up polymer films to commercially adaptable hollow fiber membranes? What is the reliability of the potting materials? Can the laboratory-scale results with films be reproduced at pilot- and commercial-scale?

The CO<sub>2</sub> and H<sub>2</sub>S separation data will be used with software for a membrane simulation developed at NCSU (Coker and Freeman, 1997). First, the software results will be validated with results collected during mini-module membrane testing. Next, this software will be used as a design tool to maximize H<sub>2</sub>S and CO<sub>2</sub> separation while minimizing the BTU loss in the permeate stream. Once optimum process conditions are identified, MEDAL will provide a conceptual design of a commercial unit with projected costs.

**6.5.2.2 Monolith Desulfurizer Development.** The issues associated with the monolith development include the following:

- What is the lowest sulfidation temperature at which this process is capable of reducing H<sub>2</sub>S levels to sub-ppm levels? What are the effects of regeneration conditions? Can adequate sulfidation activity be maintained?
- What are the optimum conditions for regeneration to minimize loss of sulfidation activity?
- What is the stability of the ZnO coating over the long term?
- What is the maximum life of the module?

**6.5.2.3 NH<sub>3</sub> and HCl Removal.** For the NH<sub>3</sub> and HCl removal steps, SRI will use the results of bench-scale testing to update the preliminary technical and economic feasibility study reported in Chapter 4 of this report. Commercial viability of the selected chloride and NH<sub>3</sub> removal processes will be evaluated. SRI will also conduct a preliminary market assessment of the removal processes.

Process flowsheets will be developed using various optimized process modules and will be simulated using an ASPEN simulator to determine integratibility of the proposed processes into various IGCC configurations. For example, if syngas does not contain NH<sub>3</sub> and HCl, and sulfur control needs to be achieved to meet the 20-ppmv requirements, the ASPEN simulator can be used to determine the optimum process configuration to minimize capital costs and maximize the thermal efficiency. A number of system studies will be conducted to simulate IGCC/fuel cell, IGCC/chemical production, and IGCC/power production configurations.

## CHAPTER 7

### BIBLIOGRAPHY

- Anonymous, "Permeability and Other Film Properties," Plastics Design Library, New York, 1995.
- Axworthy, A. E. AICh E. Symp. Ser., **71**(148) p. 43 (1975).
- Bachovchin, D.M., et al. *A Study of High Temperature Removal of Alkali in a Pressurized Gasification System*. Report No. DOE/MC/20050 by Westinghouse Research and Development Center, October 1986.
- Baker, R. W. and J. G. Wijmans, *Membrane Separation of Organic Vapors from Gas Streams, in Polymeric Gas Separation Membranes*, D. R. Paul and Y. P. Yampol'skii (Eds.), CRC Press, Boca Raton, FL, pp. 353-397, 1994.
- Baker, R. W., N. Yoshioka, J. M. Mohr and A. J. Khan, Separation of Organic Vapors from Air, *J. Membrane Sci.*, **31**, pp. 259-271 (1987).
- Berens, A. R. and H. B. Hopfenberg, Diffusion of Organic Vapors at Low Concentrations in Glassy PVC, Polystyrene, and PMMA, *J. Membrane Sci.*, **10**, pp. 283-303 (1982).
- Bhide, B. D. and S. A. Stern. *J. Membrane Sci.*, **81**, p. 209 (1993a).
- Bhide, B. D. and S. A. Stern. *J. Membrane Sci.*, **81**, p. 239 (1993b).
- Bixler, H. J., and O. J. Sweeting in: "The Science and Technology of Polymer Films," O. J. Sweetin (Ed.), Wiley Interscience, New York, 1971, pp. 1-130.
- Bondar, V. I., B. D. Freeman, and I. Pinnau, Characterization and Analysis of the Sorption and Pure-Gas Permeation Properties of Polyether-Polyamide Block Copolymers, *Proceedings of the American Chemical Society Division of Polymeric Materials: Science and Engineering*, **77**, pp. 311-312 (1997).
- Chatterjee, G., A. A. Houde, S. A. Stern, Poly(ether urethane) and poly(ether urethane urea) membranes with high H<sub>2</sub>S/CH<sub>4</sub> selectivity, *J. Membrane Sci.*, **135**, pp. 99-106 (1997).
- Chen, S. L., M. P. Heap, D. W. Pershing, and G. B. Martin, **61** p. 1218, (1982).
- Chou, C. L. "Distribution and Forms of Chlorine in Illinois Basin Coals." In *Proceedings of International Conference on Chlorine in Coal*, J. Stringer and D. D. Banerjee (Eds.), Elsevier, pp. 11-29 (1991).
- Cicero, D. C., R. P. Gupta, B. S. Turk, J. W. Portzer, and S. K. Gangwal. *Recent Developments in Hot-Gas Desulfurization- A Critical Review*. Paper to be published in 4<sup>th</sup> International Symposium on Gas Cleaning at High-Temperatures, in Karlsruhe, Germany, September, 1999.

- Coker, D. T., and B. D. Freeman. *Stage-to-Stage Model of Multicomponent Membrane-Based Gas Separation*. Paper presented at the North American Membrane Society Meeting, Baltimore, MD, May, 1997.
- Coker, D. T., Freeman, B. D., and Fleming, G. K., *AIChE Journal*, **44**(6) (1998).
- DOE (Department of Energy). *Texaco Gasifier IGCC Base Cases*, Report No.: PED-IGCC-98-001 (Rev 1), issued by Office of Systems Engineering and Analysis, July, 1998.
- DOE (Department of Energy). VISION 21 Program Plan, April, 1999.
- Dorchak, T. P., et. al., "Method for Production Elemental Sulfur from Sulfur-Containing Gases," U.S. Patent 5,366,717, 1994.
- Freeman B. D. and I. Pinnau, Separation of Gases Using Solubility-Selective Polymers, *Trends in Polymer Science*, **5**, pp. 167-173 (1997).
- Gangwal, S.K. Hot-gas desulfurization development for IGCC. In *ICHEME Symposium Series*. No. 123. Sheffield, UK, pp. 159-170, 1991.
- Ghosal, K., and Freeman, B. D., Gas Separation Using Polymer Membranes: An Overview, *Polymers for Advanced Technologies*, **5**, pp. 673-697 (1994).
- Gluskoter, H. J. and O. W. Rees, *Chlorine In Illinois Coal*, Circular No. 372, Illinois State Geological Survey, Urbana, IL, 1964.
- Gupta, R. and S. K. Gangwal. Enhanced Durability of *Desulfurization Sorbents for Fluidized-Bed Applications: Development and Testing of Zinc Titanate Sorbents*. Topical Report to DOE/METC. Report No. DOE/MC/25006-3271. Morgantown Energy Technology Center, U.S. Department of Energy, Morgantown, WV. NTIS/DE93000247. November, 1992.
- Haldipur, G. B., D. K. Schmidt, and K. J. Smith, *A 50-month Gasifier Mechanistic Study and Downstream Unit Process Development for the Pressurized Ash-Agglomerating Fluidized-Bed Gasification System*, KRW Energy Systems Inc., DOE/MC/21063-2740, 1989.
- Hidalgo, C. A., H. Itoh, T. Hattori, M. Niwa, and Y. Murakami, Measurement of the Acidity of Various Zeolites by Temperature Programmed Desorption of Ammonia, *J. Catal.*, **85**, pp. 362-369 (1984).
- Hirschenhofer, J. H., D. B. Stauffer, and R. R. Engleman (1994). "Fuel Cells: A Handbook (Revision 3)," Report No. DOE/METC 94-1006, Morgantown Energy Technology Center, U.S. Department of Energy, Morgantown, WV.
- Jothimurugesan, K., and S. K. Gangwal, "Catalytic Decomposition of Ammonia in Coal Gas," in *High Temperature Gas Cleaning*, E. Schmidt, P. Gang, T. Pilz, and A. Dittler (Eds.), Institut für Mechanische verfahrenstechnik and Mechanik, Karlsruhe, Germany, 1996.
- Jothimurugesan, K., and Gangwal, S.K. "Regeneration of Zinc Titanate H<sub>2</sub>S Sorbents," *Industrial & Engineering Chemistry Research*, **37**, 1929-1933, (1998).

- Kawakami, M., H. Iwanaga, Y. Yamashita, M. Yamasaki, M. Iwamoto, and S. Kagawa, *Nippon Kagaku Kaishi (Japanese)*, **6**, p. 847 (1983).
- Kilpatrick, M. *Coal Gasification Environmental Data Summary: Sulfur and Nitrogen Species*, Radian Corporation, EPA/600/7-86/015b, 1986.
- Kinoshita, K., F. R. McLarnon, and E. J. Cairns, *Fuel Cells: A Handbook*, Report No. DOE/METC-88/6096, Morgantown Energy Technology Center, U.S. Department of Energy, Morgantown, WV, 1988.
- Kohl, A., and R. Nielson. *Gas Purification*. Gulf Publishing Co., Houston, TX, 1997.
- Kolb, W. B., et al. *The Coating of Monolithic Structures for the Manufacture of Catalytic Converters*. Presented at AIChE Coating Process Science and Technology Symposium, New Orleans, LA, March 30-April 2, 1992.
- Koros, W. J. and M. W. Hellums, *Transport Properties, Supplement Volume titled: Acid-Base Interactions to Vinyl Chloride Polymers*, in *Encyclopedia of Polymer Science And Engineering*, J. I. Kroschwitz, (Ed.), John Wiley & Sons, New York. p. 724, 1989.
- Krishnan, G. N. and R. P. Gupta, "Development of Disposable Sorbents for Chloride Removal from High Temperature Coal-Derived Gases," Final Report submitted to U.S. Department of Energy under contract No. DE-AC21-93MC30005 (1999).
- Krishnan, G. N., G. T. Tong, B. J. Wood, and N. Korens, "High-Temperature Coal-Gas Chloride Cleanup for MCFC Applications." Report No. DOE/ME/21167-2080, Morgantown Energy Technology Center, U.S. Department of Energy, Morgantown, WV, 1986.
- Krishnan, G. N., B. J. Wood, G. Tong, and J. G. McCarty. *Study of Ammonic Removal in Coal Gasification Processes*. Report No. DOE/MC/23087-2667. Morgantown Energy Technology Center, U.S. Department of Energy, Morgantown, WV, 1988.
- Kubek, D. J., E. Polla, and F. P. Wilcher. Purification and recovery options for gasification. In *Proceedings of Gasification Technology in Practice, Assolombarda, Milan, Italy*, February, 1997.
- Kurkela, E. and P. Ståhlberg (1992). *Fuel Processing Technol.*, **31**, p. 23.
- Lahiere, R. J., M. W. Hellums, J. G. Wijmans, and J. Kaschemekat, Membrane Vapor Separation: Recovery of Vinyl Chloride Monomer from PVC Reactor Vents, *Ind. Eng. Chem. Res.*, **32**, pp. 2236-2241 (1993).
- Leppälähti, J., T. Koljonen, M. Hupa, and P. Kilpinen, "Application of Selective Catalytic Oxidation to NH<sub>3</sub> Removal in Gasification," in *High Temperature Gas Cleaning*, E. Schmidt, P. Gang, T. Pilz, and A. Dittler (Eds.), Institut für Mechanische verfahrenstechnik and Mechanik, Karlsruhe, Germany (1996).
- Merkel, T. C., V. I. Bondar, K. Nagai, and B. D. Freeman, Gas Sorption and Transport of Perfluorocarbons in Poly(dimethylsiloxane), *J. Polym. Sci.: Polym. Phys. Ed.*, **38**, pp. 415-434 (2000).

- Merkel, T. C., R. Gupta, B. Turk and B. D. Freeman, Mixed Gas Permeation of Syngas Components in Poly(dimethylsiloxane) and Poly(1-trimethylsilyl-1-propyne) at Elevated Temperatures, *J. Membrane Sci.*, (2001).
- Morisato, A., B. D. Freeman, I. Pinnau and C. G. Casillas, Pure Hydrocarbon Sorption Properties of Poly(1-trimethylsilyl-1-propyne) [PTMSP], Poly(1-phenyl-1-propyne) [PPP], and PTMSP/PPP Blends, *J. Polym. Sci.: Polym. Phys. Ed.*, **34**, pp. 1925-1934 (1996a).
- Morisato, A., H. C. Shen, S. S. Sankar, B. D. Freeman, I. Pinnau and C. G. Casillas, Polymer Characterization and Gas Permeability of Poly(1-trimethylsilyl-1-propyne) [PTMSP], Poly(1-phenyl-1-propyne) [PPP], and PTMSP/PPP Blends, *J. Polym. Sci.: Polym. Phys. Ed.*, **34**, pp. 2209-2222 (1996b).
- Pauly, S., Permeability and Diffusion Data, in *Polymer Handbook, 3rd Edition*, J. Brandrup and E. Immergut (Eds.), John Wiley and Sons, New York, pp. VI/435-VI/449, 1989.
- Petropoulos, J. H., Mechanisms and Theories for Sorption and Diffusion of Gases in Polymers, in *Polymeric Gas Separation Membranes*, D. R. Paul and Y. P. Yampol'skii (Eds.), CRC Press, Boca Raton, pp. 17-81, 1994.
- Pinnau, I. and L. G. Toy, Transport of Organic Vapors through Poly(1-trimethylsilyl-1-propyne), *J. Membrane Sci.*, **116**, pp. 199-209 (1996).
- Pinnau, I., C. G. Casillas, A. Morisato, and B. D. Freeman, Hydrocarbon/Hydrogen Mixed-Gas Permeation in Poly(1-trimethylsilyl-1-propyne) [PTMSP], poly(1-phenyl-1-propyne) [PPP] and PTMSP/PPP Blends, *J. Polym. Sci.: Polym. Phys. Ed.*, **34**, pp. 2613-2621 (1996).
- Prasad, R., L. A. Kennedy, and E. Ruckenstein, Oxidation of Fuel Bound Nitrogen in a Transition Metal Oxide Catalytic Combustor, *Combustion Sci. and Technol.*, **27**, pp. 45-54 (1981).
- Quinn, R., D. V. Laciak, J. B. Appleby and G. P. Pez, Polyelectrolyte membranes for the separation of acid gases, United States Patent Number 5,336,298 (1994).
- Quinn, R., J. B. Appleby, and G. P. Pez, Salt hydrates: New Reversible Absorbents for Carbon Dioxide, *J. Am. Chem. Soc.*, **117**, pp. 329-335 (1995a).
- Quinn, R., J. B. Appleby, and G. P. Pez, New Facilitated Transport Membranes for the Separation of Carbon Dioxide from Hydrogen and Methane, *J. Membrane Sci.*, **104**, pp. 139-146 (1995b).
- Quinn, R. and D. V. Laciak, Polyelectrolyte membranes for acid gas separation, *J. Membrane Sci.*, **131**, pp. 49-60 (1997).
- Reid, R. C., J. M. Prausnitz, and B. E. Poling, *The Properties of Gases and Liquids*, McGraw-Hill, New York, 1987.
- Ruch R. R., H. J. Gluskoter, and N. F. Shimp. "Occurrence and Distribution of Potentially Volatile Trace Elements in Coal." Report No. EPA-650/2-74-054, U.S. Environmental Protection Agency, Washington, DC, (July 1974a).

- Ruch, R. R., H. J. Gluskoter, and N. F. Shimp. "Occurrence and Distribution of Potentially Volatile Trace Elements in Coal: A Final Report." Environmental Geology Notes No. 72, Illinois State Geological Survey, Urbana, IL, (August 1974b).
- Stannett, V. T., *Simple Gases*, in *Diffusion in Polymers*, J. Crank and G. S. Park, (Eds.), Academic Press, New York, p. 41, 1968.
- Singh, A., B. D. Freeman, and I. Pinnau, Pure and Mixed Gas Acetone/Nitrogen Permeation Properties of Polydimethylsiloxane [PDMS], *J. Polym. Sci.: Polym. Phys. Ed.*, **36**, pp. 289-301 (1998).
- Stern, S. A. Polymers for Gas Separations: The Next Decade, *J. Membrane Sci.*, **94**, pp. 1-65 (1994).
- Stern, S. A. and B. D. Bhide, *Permeability of Silicone Polymers to Ammonia and Hydrogen Sulfide*. *J. Appl. Polym. Sci.*, **38**, p. 2131-2147 (1989).
- Swisher, J. H. and K. Schwerdtfeger. Review of Metal and Binary Oxides as Sorbents for Removing Sulfur from Coal-Derived Gases, *J. Mater. Eng. Performance.*, **1**(3), pp. 399-407 (1992a).
- TRW. Monitoring Contaminants in Coal Derived Gas for Molten Carbonate Fuel Cells, Final Report to Argonne National Laboratory under contract No. 31-109-38-6108, 1981.
- Turk, B. S. and Gupta R. P. "Development and Experimental Results on RVS-1 Desulfurization Sorbent, Topical Report," DOE Contract No. DE-AC21-88MC25006, DOE/NETL, Morgantown, WV, March 2001.
- Twigg, M. *Catalyst Handbook*, Manson Publishing, London, 1996.
- Yamura, M. and T. Asabe. *Rate Constants of Chemical Reactions in the High Temperature Pyrolysis of Ammonia*, Eighteenth Symposium (International) on Combustion 1981, The Combustion Institute, Pittsburgh, Pa, p. 863, 1981.
- Van Amerongen, G. J. Diffusion in Elastomers, *Rubber Chem. Tech.*, **37**, pp. 1065-1152 (1964).
- Zolandz, R. and G. K. Fleming, Gas permeation, in *Membrane Handbook*, W. S. W. Ho and K. K. Sirkar (Eds.), Van Nostrand Reinhold, New York, p. 17, 1992.

## LIST OF ACRONYMS AND ABBREVIATIONS

ASTM	American Society for Testing and Materials	psia	Pounds per square inch atmospheric
cpai	Cells (channels) per square inch	psig	Pounds per square inch, gauge
CFB	Circulating fluidized-bed	PTMEO	Poly(tetramethylene oxide)
DOE	U.S. Department of Energy	PTMSP	Poly(1-trimethylsilyl-1-propyne)
DSC	Differential scanning calorimetry	PU	Polyurethanes
DSRP	Direct Sulfur Recovery Process	PUR	Polyureas
FPD	Flame photometric detector	PVC	Poly(vinyl chloride)
GC	Gas chromatograph	PVME	Perfluoromethyl vinyl ether
GCC	gas combined cycle	R&D	Research & Development
GHSV	Gas hourly space velocity	RTI	Research Triangle Institute
HPLC	High-pressure liquid chromatography	STP	Standard temperature and pressure
HTHP	High-temperature, high-pressure	TA	Trogamide-T
IGCC	Integrated gasification combined cycle	TCC	Total capital costs
KBR	Kellogg, Brown, and Root	TCD	Thermal conductivity detector
kW	Kilowatt	TFE	Tetrafluoroethylene
MCFC	molten carbonate fuel cell	TGA	Thermogravimetric analyzer
MDEA	Methyl di-ethyl-amine	TIC	Total installed cost
MEDAL	MEbrane DuPont Air Liquide	TPD	temperature-programmed desorption
MTI	McDermott Technology, Inc.	VOC	Volatile organic compound
MWe	megawatts electricity	XPS	X-ray photoelectron spectroscopy
NCSU	North Carolina State University		
NETL	National Energy Technology Laboratory		
PA	Polyamides		
PDMS	Poly(dimethylsiloxane)		
PE	Polyesters		
PEG	Poly(ethylene glycol)		
PEM	Proton Exchange Membrane		
PEO	Poly(ethylene oxide)		
PEOXA	Poly(2-ethyl-2-oxazoline)		
PI	Polyimides		
POx	Partial oxidation		
ppb	Parts per billion		
ppbv	Parts per billion by volume		
ppm	Parts per million		
ppmv	Parts per million by volume		
PSF	Polysulfone		